EFFECT OF PHOSPHORUS STARVATION ON METABOLISM AND SPATIAL DISTRIBUTION OF PHOSPHATIDYLCHOLINE IN *Medicago truncatula* WILD-TYPE AND *PDIL3* GENOTYPES

Dhiraj Dokwal, M.Sc

Dissertation Prepared for the Degree of

DOCTOR OF PHILOSOPHY

UNIVERSITY OF NORTH TEXAS

August 2021

APPROVED:

Rebecca Dickstein, Major Professor
Ana Paula Alonso, Co-Major Professor
Guido F. Verbeck, Committee Member
Roisin McGarry, Committee Member
Catalina I. Pislariu, Committee Member
Jyoti Shah, Chair of the Department of Biology
Pamela Padilla, Dean of the College of Science
Victor Prybutok, Dean of the Toulouse Graduate School

Dokwal, Dhiraj. *Effect of Phosphorus Starvation on Metabolism and Spatial Distribution of Phosphatidylcholine in* Medicago truncatula *Wild-Type and* PDIL3 *Genotypes*. Doctor of Philosophy (Biochemistry and Molecular Biology), August 2021, 141 pp., 2 tables, 20 figures, references, 216 titles.

Symbiotic nitrogen (N) fixation (SNF) occurs in specialized organs called nodules after successful interactions between legume hosts and rhizobia. Within nodule cells, N-fixing rhizobia are surrounded by plant-derived symbiosome membranes, through which the exchange of nutrients and ammonium occurs between bacteria and the host legume. Phosphorus (P) is an essential macronutrient, and N_2-fixing legumes have a higher requirement for P than legumes grown on mineral N. First, I investigated the impact of P deprivation on wild-type *Medicago truncatula* plants. My observations that plants had impaired SNF activity, reduced growth, and accumulated less phosphate in P-deficient tissues (leaves, roots and nodules) is consistent with those of similar previous studies. Galactolipids decreased with increase in phospholipids in all P-starved organs. Matrix-assisted laser desorption/ionization–mass spectrometry imaging (MALDI-MSI) of phosphatidylcholine (PC) species in nodules showed that under low P environments distributions of some PC species changed, indicating that membrane lipid remodeling during P stress is not uniform across the nodule. Secondly, a metabolomics study was carried out to test the alterations in the metabolic profile of the nodules in P-stress. GC-MS based untargeted metabolomics showed increased levels of amino acids and sugars and decline in amounts of organic acids in P deprived nodules. Subsequently, LC-MS/MS was used to quantify these compounds including phosphorylated metabolites in whole plant. My findings showed strong drop in levels of organic acids and phosphorylated compounds in P deprived leaves with moderate reduction in P deprived roots and

nodules. Moreover, sugars and amino acids were elevated in whole plant under P deprivation.

Finally, the last project of my thesis involved studying the response of *PDIL3* (*Phosphate Deficiency-Induced LncRNA-3*), a long non-coding RNA (lncRNA) mutant, under severe P stress. *PDIL3* is known to regulate Pi-deficiency signaling and transport in *M. truncatula*. My results confirmed that in P starvation, *pdil3* plants showed better shoot growth, accumulated more phosphate in shoots, had impaired SNF and less rhizobial occupancy in nodules than WT. Subsequently, MALDI–MS imaging was used to spatially map and compare the distribution of phosphatidylcholine (PC) species in nodules of *pdil3* and WT in P-replete and P-depleted conditions. Several PC species showed changes in distributions in *pdil3* nodules compared to WT in both P sufficient and P deprived conditions. These data suggest that *PDIL3*'s role is not just suppression of the Pi transporter, but it may also influence P partitioning between shoots and nodulated roots, meriting further investigation.

ACKNOWLEDGEMENTS

I would like to thank my major professor Dr. Rebecca Dickstein for giving me this opportunity to work on this project. Initially, my experience in the field of analytical chemistry, plant biochemistry and physiology were very minimal. It has been a long journey since then and I am thankful for her continuous advice, inspiration, support, and endless patience during this learning process. I would like to specially thank my co-major professor Dr. Ana Paula Alonso for her constant motivation and constructive criticism that taught me to think and formulate scientific argument. I would also like to thank my committee members, Dr. Guido Verbeck, Dr. Roisin McGarry, and Dr. Catalina Pislariu for their mentoring and advice. This voyage would not have been possible without the help and support of all Dickstein, Alonso and Verbeck lab members past and present. Thank you to the Toulouse Graduate School and Department of Biological Sciences at UNT for the various scholarships provided that supported my scientific endeavors. I sincerely appreciate the timely guidance and help from Christophe Cocuron, Dr. Cintia Arias, Dr. Trevor Romsdahl, Dr. Dan Kunz, Dr. Umesh Yadav and Dr. Fernanda Castro-Moretti. Thank you to the members and staff of all labs at UNT for their invaluable support. Thanks to Subhayu Nayek for being a good friend. I dedicate all my success I received to my inspiring parents Omprakash and ManjuDevi Dokwal whose care, love and guidance shaped me to face various challenges in my life. I also extend my gratitude to my brother and sister, Amit Dokwal and Raksha Nerurkar, for their support in every aspect of my life. I am very proud of my wife, Neha Iyer for being supportive throughout my PhD.

TABLE OF CONTENTS

Page

LIST OF TABLES

Page

LIST OF FIGURES

Page

ABBREVIATIONS

ANOVA	Analysis of variance
ARA	Acetylene reduction assay
BNF	Biological nitrogen fixation
C	Carbon
DGDG	Digalactosyldiacylglycerol
DHB	2,5-Dihydroxybenzoic acid
DPI	Days post inoculation
DW	Dry weight
ESI-MS	Electrospray ionization - mass spectrometry
FC	Fold change
FLC	Flowering Locus C
FW	Fresh weight
GC-MS	Gas chromatography–mass spectrometry
GL	Galactolipid
LC-MS	Liquid chromatography–mass spectrometry
LncRNA	Long non-coding RNA
LincRNA	Long intergenic non-coding RNA
MALDI-MSI	Matrix-assisted laser desorption/ionization - mass spectrometry imaging
MGDG	Monogalactosyldiacylglycerol
MSTFA	N-methyl-N-trimethylsilytrifluoroacetamide
N	Nitrogen
NIST	National Institute of Standards and Technology
OPPP	Oxidative pentose phosphate pathway
P	Phosphorus
PA	Phosphatidic acid
PC	Phosphatidylcholine
PCA	Principal component analysis
PDIL	Phosphate deficiency-induced LncRNA
PE	Phosphatidylethanolamine
PEP	Phosphoenolpyruvate

PEPC	Phosphoenolpyruvate carboxylase
PG	Phosphatidylglycerol
PHO2	PHOSPHATE2
PHR1	Phosphate starvation response 1
Pi	Inorganic phosphate
PI	Phosphatidylinositol
PL	Phospholipid
PLS-DA	Partial least squares discriminant analysis
PPi	Inorganic pyrophosphate
PS	Phosphatidylserine
RT	Room temperature
SD	Standard deviation
SM	Symbiosome membrane
SNF	Symbiotic nitrogen fixation
Sym	Symbiosome
SymM	Sym membrane
TCA	Tricarboxylic acid cycle
TMCS	Trimethylchlorosilane
VIP	Variable importance in projection
WT	Wild-type

CHAPTER 1

INTRODUCTION

1.1 Importance of Nitrogen (N) Fixation

Nitrogen (N) is a key element that is essential for the normal growth and development of the plants and animals. About 78% of the atmosphere is composed of N_2, which animals, plants, and most of the prokaryotes cannot utilize. Because N_2 exists with a triple bond, a huge amount of energy is required to break it, reducing it or oxidizing it in the process. Plants can utilize the nitrogen in the form of ammonium (NH_4^+) or nitrate (NO_3^-), or other N sources, such as urea or amino acids. N is crucial for life because it is necessary for biosynthesis of DNA, RNA, and amino acids, which are building blocks of living cells. It is also found in smaller amounts in the other major biomolecules in the carbohydrate and lipid classes. N fixation is the process where atmospheric N_2 is converted to ammonium by reduction processes.

1.2 Industrial N Fixation

Chemically synthesized ‘fixed’ N is available in fertilizers that either contain ammonium and/or nitrate. In early 1900s, German scientist Fritz Haber invented the method for chemically synthesized N using N_2 and H_2 gases, which are converted into ammonia. It was later modified to become an industrial process to make fertilizers by Carl Bosch and is commonly known as the Haber-Bosch process. This process is not only expensive and non-sustainable but also has led to an increase in water and soil pollution (Nosengo, 2003).

1.3 Biological N Fixation

Biological N fixation (BNF) is another process through which atmospheric N_2 is converted to bioavailable N. BNF is carried out by certain prokaryotic bacteria (Postgate, 1982). Soil bacteria belonging to genera including *Rhizobium*, *Bradyrhizobium*, *Sinorhizhobium* and *Mesorhizobium* form symbiotic relationships with legumes and inhabit nodules formed on the roots of these plants to fix N (Denarie et al., 1992; de Lajudie et al., 1998; van Berkum et al., 1998). Bacteria of the genera *Sinorhizhobium* and *Rhizobium* nodulate roots of temperate legumes like *Medicago truncatula*, *Pisum sativa* (pea) and *Medicago sativa* (alfalfa) whereas, tropical legumes like *Glycine max* (soybean) and *Phaseolus vulgaris* (bean) are nodulated by *Bradyrhizobium* and other species.

1.4 Symbiotic N Fixation

The process of symbiotic N fixation (SNF) occurs between a legume and a soil bacterium when bioavailable N in the soil is low. The process occurs after an exchange of molecular signals between plants and rhizobia, which leads to the growth of nodules on the plant's root containing rhizobia that have become intracellular, that are celled bacteroids to distinguish them from free-living forms. This process is known as nodulation. The rhizobia are only able to fix N once they are within the plant cells. Specifically, SNF occurs in the N fixation zone within the nodules of the temperate legumes that mostly develop indeterminate nodules, such as *M. truncatula*, used as model legume (Barker et al., 1990; Cook, 1999; Peoples et al., 2009; Cannon, 2013). Determinate nodules are formed by mostly tropical legumes, exemplified by the model legume *Lotus japonicus.* Determinate nodules lack a persistent meristem compared to the indeterminate ones. In determinate nodules, the rhizobia in the invaded cells are all at a similar developmental

stage (Ferguson et al., 2010), while indeterminate nodules are elongated because of a persistent apical meristem that leads to the formation of different developmental stages or zones, which contain rhizobia and bacteroids at different stages of nodulation and fixation development (Vasse et al., 1990; Roux et al., 2014).

1.5 *M. truncatula* as a Model Legume

M. truncatula (barrel medic) was proposed as a model legume in 1990 (Barker et al., 1990) and by the early 2000s was fully accepted as a model by the legume community (Cook, 1999; Cannon, 2013). *M. truncatula* is a close relative to other important legumes like *M. sativa* and *Pisum sativum,* both economically important crops. The soil bacterium *Sinorhizobium meliloti* is the symbiotic partner of *M. truncatula* and is itself well-studied; the *S. meliloti-M. truncatula* symbiosis is well established as a model for symbiotic nitrogen fixation (Long, 1996; Roy et al., 2020). *M. truncatula* is a self-fertile, diploid (2n = 16) with a relatively small genome size. Its genome had been sequenced (Young et al., 2011; Tang et al., 2014; Pecrix et al., 2018). It is convenient to genetically transform *M. truncatula* by *Agrobacterium tumefaciens* (Boisson-Dernier et al., 2001). Because *M. truncatula* is very closely related to other economically important legumes, knowledge gained in the *M. truncatula* model can be easily exploited to increase agricultural productivity in those crops (Young and Udvardi, 2009).

1.6 Nodule Morphogenesis

The successful establishment of rhizobia-legume symbiosis involves the formation of unique organs called nodules on the plant's roots. A molecular dialog in the form of biochemical signal exchange takes place between the host plant and the rhizobia before the establishment of the symbiotic relationship (Oldroyd, 2013). Plant roots secrete

flavonoids; in return, bacteria respond by producing Nod factors. Once the host perceives the Nod factor in the root cells, curling of the epidermal root hair cells take place. Cell division occurs in the root cortical cells initiating the formation of the nodule primordia. Rhizobia enter the root hair and the underlying cells through the infection threads after which they are released into the cortical cells via a process resembling endocytosis. This series of events results in a unique cytoplasmic organelle called the symbiosome that contains the rhizobia surrounded by a membrane of plant origin called the symbiosome membrane (SM) or peribacteroid membrane (PBM) (Verma and Hong, 1996). Rhizobia and plant cells then start a differentiation process that culminates in induction of the N fixation genes in the rhizobia and a fully grown functional pink nodule (Vasse et al., 1990; Jones et al., 2007; Roy et al., 2020).

1.7 Phosphorus, an Important Plant Nutrient

Phosphorus (P) is an essential macronutrient for plant growth and development, usually available as phosphate, Pi. P is unevenly distributed and relatively immobile in the soils. This has resulted in a decrease in crop yield by 30% to 40% over last four decades due to limited P availability (Vance et al., 2003). N-fixing legumes are known to require more P than legumes that grow on mineral N (Israel, 1987; Schulze et al., 2006; Hernandez et al., 2009). Thus, widespread P deficiency is of a major concern not only for SNF as an N fertilizer alternative, but also for legume crop productivity. In legume plants, nodules act as a P sink under P deprivation which is poorly understood mechanism. For example, P concentration in nodules can be increased up to three times compared to that of leaves and roots under P deprivation (Sa and Israel, 1991; Schulze et al., 2006).

Nodulation is accompanied by reprogramming of plant metabolism. The plant

provides bacteria with reduced carbon and other nutrients and a significant amount of lipid remodeling occurs. This includes lipid remodeling for the synthesis of SM that surrounds the bacteroids during endocytosis as well as other processes. It is already known that the SM lipids are primarily rich in phospholipids followed by glycolipids (Hernández and Cooke, 1996; Whitehead and Day, 1997; Gaude et al., 2004; Si et al., 2019), which originate in the endoplasmic reticulum, where their synthesis takes place and later, they are transported to the SM via the Golgi apparatus (Brewin, 2012). Plastids are the major sites for *de novo* fatty acid synthesis (Ohlrogge and Jaworski, 1997). Acetyl-CoA, ATP, and NAD(P)H are required as substrates for fatty acid synthesis (Jin et al., 1990). After synthesis, fatty acids are exported to the endoplasmic reticulum and incorporated into lipids that are later redistributed to specific organs in plants (Holzl and Dormann, 2019). Extraplastidial membranes of roots are rich in phosphatidylcholine (PC) while chloroplasts are abundant in galactolipids like monogalactosyldiacylglycerol (MGDG) and digalactosyldiacylglycerol (DGDG) (Dormann and Benning, 2002; Tjellstrom et al., 2008).

To adapt to P-stress, plants modify metabolic processes to reprioritize utilization of internal Pi and increase acquisition of external Pi in low Pi environments (Vance et al., 2003). Plants increase lateral root surface area to enable exploration of more soil volume under P deficiency (Niu et al., 2013). Furthermore, P-deficient plants optimize mobilization of P from internal resources through the modification of metabolic processes, and hydrolysis of P-containing metabolites like nucleic acids, phospholipids, and small phosphorylated metabolites (Poirier and Bucher, 2002; Plaxton, 2004; Cruz-Ramirez et al., 2006). Plants secrete organic acids through roots in the rhizosphere and enzymes to

increase P availability, and simultaneously synthesize more Pi transporter proteins in the plasma membrane of root epidermal cells for higher Pi uptake capacity (Lopez-Bucio et al., 2000; Vance et al., 2003). Transcriptomic analyses of leaves in Arabidopsis and rice have shown that changes in the expression of several hundred genes takes place in P-stressed plants (Muchhal and Raghothama, 1999). These genes are involved in various metabolic pathways, such as photosynthesis, carbon metabolism, nitrogen assimilation and synthesis of protein and nucleic acids that lead to adaptive changes in metabolite profiles (Uhde-Stone et al., 2003; Wu et al., 2003; Misson et al., 2005; Morcuende et al., 2007). Legumes also have evolved strategies at morphological and physiological levels to adapt to P deficiency. Metabolic profiling of P-starved non-nodulated roots of common bean showed elevated levels of most amino acids, polyols, sugars, and few organic acids namely succinate and shikimate (Hernandez et al., 2007). A follow-up GC-MS study on P-starved nodulated roots of common bean revealed decreases in the amounts of amino acids and metabolites involved in N metabolism, suggesting that lack of P in the medium strongly reduced N_2-fixation (Hernandez et al., 2009). Lack of P in the medium also resulted in elevated levels of amino acids like asparagine, glutamine, and phenylalanine in the phloem of *M. truncatula* (Sulieman et al., 2013; Sulieman and Tran, 2013).

1.8 Use of Mass Spectrometry

The most conventional way of analyzing lipids from tissues or seeds has been achieved through bulk extraction followed by analysis by mass spectrometry. Extraction of lipids from whole plants is an easy and a convenient process performed using 1:1 mixture of $CHCl_3$:Methanol. Extracted lipids are introduced to the mass spectrometer by direct infusion, usually performed on a triple quadrupole mass spectrometer. For direct

infusion, the sample is loaded into the syringe pump and later ionized using an electrospray ionization source (Brugger et al., 1997). Precursor and neutral loss scans are performed for specific lipid detection and quantification (Shiva et al., 2013). Use of standards are recommended to quantify lipids in the biological sample using direct infusion mass spectrometry (Shiva et al., 2013). Recent advances in the mass spectrometry field like high chemical resolution (Hu et al., 2005), ion mobility coupled (Kalapothakis and Barran, 2013) to chromatographic techniques (Salazar et al., 2017) have improved chemical coverage and sensitivity enabling researchers to analyze lipids even in complex biological samples. The biggest problem with these types of analyses is the information on the spatial distribution of where these lipid metabolites originated are lost during their extraction process (Sturtevant et al., 2016). Thus, imaging mass spectrometers like Matrix-assisted laser desorption ionization - mass spectrometry imaging (MALDI-MSI) are of particular importance for analysis of membrane lipids in plant tissues. At this point, amongst membrane lipids, PC species are amenable for MALDI-MSI due to their abundance and positively charged quaternary ammonia group (Horn et al., 2012; Horn and Chapman, 2014; Dokwal et al., 2021). The MALDI has significant advantages like high resolution leading to accurate mass measurements of the metabolites which are very critical for studies involving metabolomics (Gemperline et al., 2015).

Analysis of large number of metabolites/compounds from a sample is now possible, due to recent advances in analytical technologies like gas and liquid chromatography coupled to mass spectrometry (GC-MS and LC-MS) (Kopka, 2006). Such global metabolite profiling provides a broader view of the systematic adjustments

that occur in metabolic processes revealing new insights in metabolism. Metabolite profiling studies on nutrient deficiencies, including N, sulfate, iron, and P have been performed in green alga (Bolling and Fiehn, 2005), Arabidopsis (Hirai et al., 2004) and common bean (Nikiforova et al., 2004; Hernandez et al., 2007). Despite the agronomic importance of legumes, little information is available for metabolite changes in response to severe P deficiency. As Pi homeostasis is regulated at the whole-plant level from shoots to roots (roots+nodules) under P limiting conditions, it is necessary to determine alterations at a deeper level in shoots, roots, and nodules to increase our understanding of biochemical mechanisms underlying legume adaptation to low P environments while maintain optimal SNF.

1.9 LncRNAs

The noncoding RNAs have been categorized based on their length into small RNAs and long non-coding RNAs (lncRNAs) (Brosnan and Voinnet, 2009; Kim et al., 2011). LncRNAs, also sometimes referred as long intergenic non-coding RNA (lincRNA), have a length of more than 200 nucleotides and constitute the biggest class of noncoding RNAs. Some of their features include: little or no protein coding capacity; transcription by RNA polymerase II; tissue-specific expression (Wilusz et al., 2009); and occurrence in the genome at different locations, like intronic and intergenic, and, directionality, as, sense, antisense and bidirectional with respect to genes in the close proximity (Ponting et al., 2009). For many years lncRNAs have been mostly ignored and regarded as transcriptional ‘noise’ either due to their low expression or low protein-coding potential. In the past decade, extensive research has been reported showing involvement of lncRNAs in transcriptional interference, chromatin remodeling repression and epigenetic silencing.

For instance – *AUXIN REGULATED PROMOTER LOOP (APOLO)* and *ALTERNATIVE SPLICING COMPETITOR* (*ASCO)* were reported to regulate root development in *A. thaliana* (Ariel et al., 2014). Two lncRNAs called *COLD INDUCED LONG ANTISENSE INTRAGENIC RNA* (*COOLAIR),* transcribed from the antisense strand of *FLOWERING LOCUS C* (*FLC)* and were involved in regulation of flowering by silencing the expression of *FLC* (Swiezewski et al., 2009). A recent study in *M. truncatula* implicated three lncRNAs, *PHOSPHATE DEFICIENCY-INDUCED LncRNA* (*PDIL1, 2* and *3)* involved in regulation of P deficiency responses in shoot and root tissues of the plants (Wang et al., 2017).

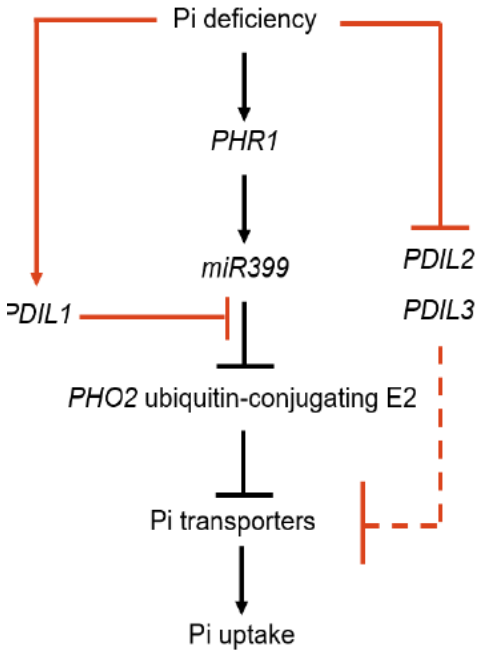

Figure 1.1: **A model for Pi signaling involving *PHR1*, *miR399*, *PHO2*, *PDIL1*, *PDIL2,* and *PDIL3* in *M. truncatula*.**

(Adapted from Wang et al., 2017). The red lines represent pathways identified in Wang et al., 2017. Arrows indicate upregulation or positive effects, whereas lines ending in a short bar indicates downregulation or negative effects.

A model was proposed in Wang et al., 2017 describing the involvement of three lncRNAs, *PDLI1*, *PDIL*, and *PDIL3* in the regulation of Pi-deficient signaling in *M.*

truncatula. *PHOSPHATE STARVATION RESPONSE 1 (PHR1)*, *miR399* and *PHOSPHATE STARVATION2* (*PHO2),* a ubiquitin-conjugating E2 enzyme, have been established as playing a central role in the regulation of P acquisition (Bari et al., 2006). In P-deficient medium, *PHR1* and *miR399* are upregulated consecutively. *PHO2,* a target of miR399, is downregulated by miR399 under low P environments. PHO2 is involved in degradation of the Pi transporters via the ubiquitination pathway; thus *PHO2*'s silenced mediated by miR399 results in increased P acquisition by upregulated Pi transporters in P-stress. *PDIL1* expression is evoked in absence of P and it shares a conserved motif with *PHO2* that is identified by miR399. Hence, in WT plants *PDIL1* competitively binds to *miR399* as a target mimic preventing degradation of *PHO2*, thereby regulating expression of Pi transporters and inhibiting superfluous accumulation of P (Wang et al., 2017). *pdil1* mutants have no expression of *PDIL1* due to presence of a *Tnt* insert (Wang et al., 2017). In P stress, expression of *PHO2* is lowered by *miR399* compared to WT and Pi transporters are upregulated leading in P uptake. Wang et al., 2017, predicted that *PDIL2* and *PDIL3* negatively regulate the expression of the Pi transporter gene *Medtr1g074930* through sequence complementarity. In WT *M. truncatula* plants, *PDIL2* and *PDIL3* were somewhat downregulated by P-starvation, enhancing the expression of Pi transporter gene leading in P uptake. However, *pdil2* and *pdil3* mutants lack expression of their respective lncRNAs due to the presence of a *Tnt* insert, resulting in more upregulation of Pi transporter gene, thereby enhancing P uptake compared to WT (Wang et al., 2017).

1.10 Objective of the Research

M. truncatula-S. meliloti is an excellent model to study N-fixation. Until now, only a

few studies have investigated and identified some metabolites that influence this symbiotic relationship (Gaude et al., 2004; Gemperline et al., 2015). Moreover, the composition of SM housing the bacteroids is not yet fully known. SM is the interface between the host plant and the bacteria and acts as the structural and functional communication channel. Metabolite and lipid composition have not been studied extensively in the model *M. truncatula-S. meliloti* symbiotic system (Sulieman et al., 2013; Sulieman et al., 2013; Sulieman and Tran, 2013, 2015; Wang et al., 2017).

In starting this research, we hypothesized that legumes have evolved nodule specific lipid and metabolite remodeling machinery that is critical for establishment of a successful *M. truncatula-S. meliloti* symbiotic relationship under P deprivation (Si et al., 2019; Zhang et al., 2020). We also hypothesize that *M. truncatula* plants that have defects in their responses to P deprivation will show differences in lipid and metabolite remodeling during P starvation. This would set the stage for future studies in *M. truncatula* plants that will take advantage of the wealth of molecular genetic resources available in this model legume.

To address these hypotheses, the first objective of this research was to establish and quantify the membrane lipids (galactolipids and phospholipids) to study the changes in their molecular species under phosphorus deprivation in leaves, root, and nodules of wild-type (WT) *M. truncatula,* followed by their in-depth spatial characterization across the cross-section of nodules. This analysis was expected to reveal insights on lipid metabolites' distribution in different zones of the nodules and whether it changes under P stress. Once this was established, we investigated the impact of P-stress on growth, development, symbiotic efficiency, and distribution of PC species in nodules of *pdil3*

mutant in comparison with WT. Finally, a global metabolic profiling study covering wide range of metabolites; sugars/sugar alcohols, amino acids, phosphorylated compounds, and organic acids was carried out in leaves, roots, and nodules of WT *M. truncatula* under P starvation. This study was intended to fill gaps integrating shoot, root, and nodule response of P deficient plants and gather a better understanding of how *M. truncatula* plants undergo metabolic changes in various organs to sustain survival and N_2 fixing nodule functioning under P stress.

CHAPTER 2

PHOSPHORUS DEPRIVATION AFFECTS COMPOSITION AND SPATIAL DISTRIBUTION OF MEMBRANE LIPIDS IN LEGUME NODULES*

2.1 Abstract

In legumes, symbiotic nitrogen (N) fixation (SNF) occurs in specialized organs called nodules after successful interactions between legume hosts and rhizobia. In a nodule, N-fixing rhizobia are surrounded by symbiosome membranes, through which the exchange of nutrients and ammonium occurs between bacteria and the host legume. Phosphorus (P) is an essential macronutrient, and N_2-fixing legumes have a higher requirement for P than legumes grown on mineral N. As in the previous studies, in P deficiency, barrel medic *(Medicago truncatula)* plants had impaired SNF activity, reduced growth, and accumulated less phosphate in leaves, roots, and nodules compared with the plants grown in P sufficient conditions. Membrane lipids in *M. truncatula* tissues were assessed using electrospray ionization–mass spectrometry. Galactolipids were found to increase in P deficiency, with declines in phospholipids (PL), especially in leaves. Lower PL losses were found in roots and nodules. Subsequently, matrix-assisted laser desorption/ionization–mass spectrometry imaging was used to spatially map the distribution of the positively charged phosphatidylcholine (PC) species in nodules in both P-replete and P-deficient conditions. Our results reveal heterogeneous distribution of several PC species in nodules, with homogeneous distribution of other PC classes. In P poor conditions, some PC species distributions were observed to change. The results

* This entire chapter is reproduced from Dhiraj Dokwal, Trevor B Romsdahl, Daniel A Kunz, Ana Paula Alonso, Rebecca Dickstein, Phosphorus deprivation affects composition and spatial distribution of membrane lipids in legume nodules, Plant Physiology, 2021;, kiaa115, https://doi.org/10.1093/plphys/kiaa115, with permission from Oxford University Press.

suggest that specific PC species may be differentially important in diverse nodule zones and cell types, and that membrane lipid remodeling during P stress is not uniform across the nodule.

2.2 Introduction

Legumes have the distinctive ability to interact with symbiotic nitrogen (N)-fixing soil bacteria called rhizobia. A mature interaction culminates in the formation of nodules, specialized plant structures on legume roots. With nodules, symbiotic N fixation (SNF) takes place in the internalized rhizobia, which biosynthesize ammonia from atmospheric N. Rhizobia exchange the ammonia for photosynthate-derived carbon from the plant in complex processes (Fuchs et al., 2010; Udvardi and Poole, 2013; Flores-Tinoco et al., 2020). In N deficiency, a molecular signal exchange between the host plant and appropriate rhizobial species initiates nodule development (Oldroyd, 2013). Plant roots secrete flavonoids and rhizobia responds by producing Nod factors. Nod factor perception leads to curling of the epidermal root hair cells in the plant. Plant cell division in the root cortical cells initiates the formation of the nodule primordia, leading to the development of a nodule meristem. Concomitantly, rhizobia enter root hairs enclosed in plant-derived infection threads (ITs) that bring them into the underlying dividing root cells. There they are released into symbiosomes (Syms), organelle-like structures containing the rhizobia, now called bacteroids, enclosed in a plant-derived Sym membrane (SymM), also called the peribacteroid membrane (Verma and Hong, 1996). Bacteroids and plant cells then start a differentiation process that culminates in induction of SNF genes in the rhizobia and a mature functional leghemoglobin-containing pink nodule.

Tropical legumes like soybean *(Glycine max)*, and birdsfoot trefoil *(Lotus*

japonicus) forms determinate nodules that contain one symbiotic state at a time (HIRSCH, 1992). In contrast, temperate legumes like barrel medic *(Medicago truncatula)*, and pea *(Pisum sativum)*, form indeterminate nodules. Indeterminate nodules are elongated because of a persistent apical meristem that leads to the formation of different developmental stages or zones (Vasse et al., 1990; Roux et al., 2014). Zone I (ZI) is the rhizobia-free meristematic region, containing mostly non-differentiated dividing cells. Zone II (ZII) corresponds to the infection zone, comprising the pre-infection zone with non-infected differentiating cells and cells releasing rhizobia from ITs into Syms with rhizobia enclosed within the SymM; the proximal ZII includes the area where plant and bacterial cells differentiate and enlarge through endoreduplication (Cebolla et al., 1999). Zone III (ZIII) comprise large cells containing N-fixing, Sym-enclosed bacteroids interspersed with uninfected plant cells. Between ZII and III is Interzone II–III (IZII–III), a region several cell layers wide. The senescent zone, Zone IV (ZIV), gradually develops in the proximal part of the nodule and becomes apparent after several weeks (Perez Guerra et al., 2010). These cells are contained within the epidermal, outer cortical, vascular, and inner cortical cells of the nodule.

Most agricultural fields lack sufficient phosphorus (P) for maximum crop yields. Legumes are especially affected because they are typically grown symbiotically, and it has been shown that legumes reliant on SNF require higher P compared to legumes grown with N fertilizer. Studies in diverse legumes have shown growth parameters and symbiotic responses are improved by P fertilization (Israel, 1987; Itoh, 1987; Pereira and Bliss, 1989; Al-Niemi et al., 1997; Vance, 2001; Vance et al., 2003; Schulze and Drevon, 2005; Hernandez et al., 2009; Liu et al., 2018). Legume nodules act as a P sink in P

deprivation, with nodule P concentration increased up to three times compared to that of leaves and roots (Sa and Israel, 1991; Schulze and Drevon, 2005). Nodulation is accompanied by reprogramming of both plant and bacterial metabolism including membrane biosynthesis required for division and differentiation of both rhizobial and plant cells, organelle function, and formation and development of SymMs. These membrane lipids are among the P sinks in nodules and are typically rich in phospholipids (PLs) primarily followed by galactolipids (GLs) (Hernández and Cooke, 1996; Whitehead and Day, 1997; Gaude et al., 2004). The major PLs present in nodules are phosphatidylcholine (PC) and phosphatidylethanolamine (PE), while phosphatidylglycerol (PG), phosphatidylinositol (PI), phosphatidylserine (PS), and phosphatidic acid (PA) are low in abundance (Gaude et al., 2004). The major GLs reported in nodules are monogalactosyldiacylglycerol (MGDG) and digalactosyldiacylglycerol (DGDG) where they are found in the SymM and likely other plant membranes (Gaude et al., 2004).

Because nodules are symbiotic organs, bacteroid membrane lipids are also present (de Rudder et al., 1999; Lopez-Lara et al., 2003; López-Lara et al., 2005). Rhiziobial membrane lipid composition has been extensively studied in *Bradyrhizobium* and *Sinorhizobium meliloti* spp. in cell cultures (Miller et al., 1990; de Rudder et al., 1997) and has been found to contain PG, cardiolipin and PE as major membrane lipids, followed by PC in substantial amounts. Under P limiting cell culture conditions, rhizobial membrane PLs serve as a pool of metabolizable phosphate (Pi) for the synthesis of P-free lipids such as sulfoquinovosyl diacylglycerol, an ornithine containing lipid and diacylglyceryl trimethylhomoserine (Zavaleta-Pastor et al., 2010). The composition and changes in bacteroid membrane lipids in absence of P have been studied in the large determinate

nodules formed by *G. max*– *Bradyrhizobium japonicum* (Gaude et al., 2004).

The conventional way of analyzing lipids from plant tissues or seeds is through organic extraction followed by analysis by mass spectrometry (Narasimhan et al., 2013). The extracted lipids are typically introduced in the mass spectrometer by direct infusion using an electrospray ionization (ESI) source (Brugger et al., 1997). Precursor and neutral loss scans are performed for specific lipid detection and quantification, with standards (Shiva et al., 2013). The biggest problem with this type of analyses is the information on the spatial distribution of where these lipid metabolites originated is lost during their extraction processes (Sturtevant et al., 2016; Sturtevant et al., 2017). Imaging techniques using genetically encoded biosensors have been developed and used to reveal tissue and subcellular spatial differences in specific membrane lipid classes; however, these biosensors cannot discriminate degree of lipid unsaturation and can be difficult to use quantitatively (Colin and Jaillais, 2020). Semiquantitative matrix-assisted laser desorption ionization– mass spectrometry (MALDI–MS) imaging has emerged as a promising alternative to analyze the spatial distribution of plant membrane lipids (Horn et al., 2012; Duenas et al., 2017; Woodfield et al., 2017). MALDI–MS imaging (MALDI– MSI) has the advantages of high resolution leading to accurate mass measurements of the metabolites which are critical for imaging studies (Gemperline et al., 2015). Among membrane lipids, PC species are amenable for MALDI–MSI because of their abundance and positively charged quaternary ammonia group. In addition, MALDI–MSI allows determination of PC lipid unsaturation.

Inspired by reports showing spatial differences in PC species distribution in seed tissues (Sturtevant et al., 2017; Woodfield et al., 2017), we wondered whether PC

distribution would be evenly across nodule zones that have distinct physiological functions in indeterminate nodules. Further, we were curious about whether PC species distribution would change in P deprivation. In this study, we investigated membrane lipid composition in nodulated *M. truncatula* plants that were P deprived compared to controls. We analyzed the spatial distribution of PC in nodules from both P starved and control plants. Our findings showed expected changes in membrane lipid composition during P deprivation and present insights of PC distribution and remodeling in nodule development, in SNF, and those processes during P deprivation.

2.3 Materials and Methods

2.3.1 Seed Collection, Surface Sterilization, and Germination

Medicago truncatula R108 wild type (WT) pods were crushed to release their seeds. Seeds were scarified with concentrated H_2SO_4 for 5 min, rinsed in sterile water, surface sterilized with 6% (v/v) sodium hypochlorite for 1.5 min and rinsed with sterile water. The seeds were then imbibed in sterile water for 3 days at 4 °C in the dark. Seeds were subsequently placed on 1% water agar petri dishes for germination. The plates were inverted and kept in the dark at room temperature (RT) for 2 days to allow seeds to germinate.

2.3.2 Plant Growth in Aeroponic Systems

Germinated seedlings were grown using aeroponic chamber systems prepared similarly as those described in the Medicago handbook (Barker et al., 2006) and previously (Veereshlingam et al., 2004). Briefly, our aeroponic chamber is a 20 gal. trashcan (Rubbermaid, Atlanta, GA, USA) modified with a black Plexiglas lid containing 4 mm holes to accommodate seedlings. It is powered by a misting humidifier (Defensor

505; Texas Air Systems, Irving, TX, USA) sealed with silicone sealant. Plants were grown in two aeroponics chambers side by side. Lullien's medium was used for growth (Lullien et al., 1987). Lullien's medium contains 5 mM NH_4NO_3, 0.52 mM K_2SO_4, 0.25 mM $MgSO_4$, 1 mM $CaCl_2$, 50 mM Na_2EDTA, 30 mM H_3BO_3, 10 mM $MnSO_4$, 0.7 mM $ZnSO_4$, 0.2 mM $CuSO_4$, 0.1 mM Na_2MoO_4, 0.04 mM $CoCl_2$, 23.7 mM $FeSO_4$, 33.2 mM $FeCl_2$, and 5.5 mM potassium Pi buffer at pH 6.9. Seedlings were grown in full Lullien's medium for 5 days to encourage robust growth, then in Lullien's medium without 5 mM $NH4NO_3$ for 5 days to induce N starvation. Then media was changed to fresh Lullien's medium without 5 mM NH_4NO_3 for +P plants. For the –P plants, fresh Lullien's medium without 5 mM NH_4NO_3 and without potassium Pi buffer was used. 1 M KOH was added as a potassium source and to adjust the pH to 6.9. Plants were inoculated with *S. meliloti* Rm41 and grown for 4 weeks.

2.3.3 Plant Phenotypes

Plants were phenotyped at 28 DPI. Plant fresh and DW were measured. Plants and nodules were photographed by camera (Canon model PC1562; Canon USA, Huntington NY, USA) and microscopically (Leica dissection microscope, MSV269; Buffalo Grove, IL, USA). Nodule length and width were measured, and lateral roots were enumerated. The

ARA was used to measure nitrogenase activity (Dilworth, 1966). Glass bottles (38 mL) were preloaded with 1 mL of Lullien's medium with Pi and without Pi in order to maintain the consistency of the growth conditions for +P and – P plants, respectively. The bottles were sealed with gas-tight rubber cap. Immediately, 3.7 mL gas was withdrawn from the bottle with a gas-tight syringe and 3.7 mL of acetylene was introduced back in

the bottle. Plants in acetylene contained bottles were maintained at RT and after 2 h 300 µL of gas was removed from the bottle and injected into a gas chromatograph–flame ionization detector (Shimadzu GC-14A Gas Chromatograph, Dallas, TX, USA) to quantitate the amount of acetylene reduced to ethylene. Haysep T80/100 column (*6’ x 1/8" stainless steel) from Alltech (Maynooth, Ireland) was used. Helium was used as the carrier gas. The GC conditions were as follows: injection temperature 120 °C, constant isothermal column temperature at 55 °C, and detector temperature 120 °C. Fifteen plants were randomly sampled from +P and –P treatment conditions for determining plant fresh weight, DW, lateral root number, and nodule number. Fifteen individual nodules were arbitrarily picked from plant subjected or not to P stress for estimating nodule length, nodule width, nodule fresh weight, and nodule DW. For ARA five replicates from each growth conditions were used. One-way analysis of variance (ANOVA) was used to determine the statistical significance. Data from at least two independent experiments were used for this and all following experiments.

2.3.4 Total P and Inorganic Pi Quantitation

Fifteen to 30 mg of tissues were collected, frozen, and ground to a fine powder in liquid N. The ground tissues were suspended in 1% glacial acetic acid and vortexed thoroughly. Cellular debris was separated by a brief centrifugation and aliquots of the solution were assayed for Pi using a phosphomolybdate colorimetric assay as described previously (Chiou et al., 2006). For total P quantification, tissues were ashed, hydrolyzed, and subjected to colorimetric assay (Chiou et al., 2006). One milliliter of media was collected daily for 28 days from +P and –P growth conditions to assay amount of Pi in the growth media using colorimetric assay described in (Chiou et al., 2006). Six replicates of

each growth conditions for each tissue type (leaves, roots, and nodules) were processed and analyzed. One-way ANOVA test was used to determine the statistical significance. Data from two independent experiments were used for inorganic Pi and total P experiments.

2.3.5 Lipid Extraction and Profiling

Leaves, roots, nodules, and nodules sections sliced with razor blades from 28 DPI *M. truncatula* plants were lyophilized at –80 °C. Lipids were extracted from the tissues as described in (Shiva et al., 2013). Briefly, lyophilized tissues were homogenized in hot (75 °C) isopropanol with 0.01% butylated hydroxytoluene and incubated at 75°C for 15 min to inactivate endogenous phospholipases. After incubation, a stream of N was used to evaporate the extract. The dry extract was dissolved in 1 mL $CHCl_3$ and stored at –20°C. Lipid samples were analyzed using an ESI triple quadrupole mass spectrometer (ABI 3000; Applied Biosystems, Foster City, CA, USA). Internal standards were used for quantification of PL and GL species. The internal standards for GLs were 1.665 nmol 16:0–18:0-MGDG, 1.405 nmol di18:0-MGDG, 0.44 nmol 16:0–18:0-DGDG, and 1.48 nmol di18:0-DGDG, purchased from the Kansas Lipidomics Research Center (Manhattan, KS, USA). The internal standards for PLs were 0.6 nmol di14:0-PC, 0.6 nmol di24:1-PC, 0.3 nmol di14:0-PE, 0.3 nmol di24:1-PE, 0.3 nmol di14:0-PG, 0.3 nmol di24:1-PG, 0.3 nmol di14:0-PA, 0.3 nmol di20:0 (phytanoyl)-PA, 0.2 nmol di14:0-PS, 0.2 nmol di20:0 (phytanoyl)-PS, 0.287 nmol 16:0–18:0-PI, and 0.105 nmol di18:0-PI. We used the previously determined limit of detection (0.002 nmol) to filter lipids for analysis (Devaiah et al., 2006). The quantity of each lipid was determined after normalizing with the amount of the internal standard added and later expressed in per milligram DW of tissue. Five

replicates of each treatment for each tissue type (leaves, roots, and nodules) were processed and analyzed. One-way ANOVA test was used to determine the statistical significance. Data from two independent experiments were used for lipidomic analysis.

2.3.6 MALDI–MSI

Twenty eight DPI nodules were fixed under vacuum with 4% paraformaldehyde in 50mM piperazine-N,N'-bis(2-ethanesulfonic acid) (PIPES)-NaOH, pH 7.2 buffer for 15–45 min at RT. Nodules were rinsed 3 times with 50 mM PIPES-NaOH pH 7.2 for 10 min each rinse, replacing the buffer after each wash. A 10% (w/v) porcine gelatin solution in deionized water was prepared and equilibrated in a 37°C water bath with shaking for 2 h. Fixed nodules were embedded in the gelatin solution, flash frozen at –80°C at least overnight, and then were transferred to –20°C for 48 h prior to sectioning. Embedded nodules were sectioned at 25 µm tissue thickness using a cryo-microtome (Leica CM1950, Leica Microsystems, Buffalo Grove, IL, USA). Sections were collected using forceps and then placed on Superfrost microscope slides (Fisherbrand, 12-544-7). Slides with the thaw-mounted sections were lyophilized for 3 h, then used immediately for MALDI–MSI. All MALDI–MSI occurred within 12 h of cryosectioning. Bright-field images were taken of all sections used for MALDI–MSI using Leica microscope MSV269.

For MALDI–MSI, the matrix 2,5 dihydroxybenzoic acid (DHB) was used for analysis of PLs and GLs (MGDG and DGDG). DHB was applied by sublimation using an adapted method developed from (Hankin et al., 2007). MALDI–MSI data were collected on a hybrid MALDI-LTQ-Orbitrap XL mass spectrometer (Thermo Scientific, Waltham, MA, USA). The instrument laser was equipped with an N laser with a spot size of ~40 µm. MALDI–MSI data acquisition conditions were as follows: laser energy was 16-µJ/pulse, a

raster step size of 40 µm, 10 laser shots per raster step with zero sweepshot. Data were acquired using the Orbitrap mass analyzer with a resolution of 60,000, between an m/z scan range of 700–1,200. Raw mass spectra were processed into MALDI–MS images using ImageQuest software (Thermo Scientific). Images were generated using Metabolite Imager software (Horn and Chapman, 2014) and plotted as mol% on a color scale of green (low mol%) to red (high mol%). Imaging of PC molecular species are sums of intensities of [M + H]+ adducts. Each nodule image was carefully dissected virtually using the Metabolite Imager filter into distal, central, and proximal zones (Fig. 2.4B) and in order to determine the amount of PC content for the zonal profiling study. Five individual nodules from different plants grown in +P and –P conditions were used for MALDI–MSI. One-way ANOVA was used to calculate the statistical differences. One independent experiment was done for MALDI–MSI.

2.4 Results

2.4.1 P Deficiency has Differing Effects on *M. truncatula* Membrane Lipid Composition in Leaves, Roots, and Nodules

To induce P deprivation, we grew plants in aeroponics chambers to control the growth medium conditions. R108 genotype plants were grown for 5 d in N and P replete media, starved for N for 5 d while receiving full P, and subsequently starved for P at the same time as they were inoculated with *Sinorhizobium melliloti* (–P). In these conditions, nodules started to develop at the onset of P starvation. Control plants were grown side-by-side in replete P conditions (+P). Media was assessed daily for P concentrations (Supp. Table S2.1). After 4 weeks, –P plants were assessed for P deprivation characteristics (Li et al., 2001; Williamson et al., 2001; Schulze et al., 2006; Hernandez et al., 2007; Morcuende et al., 2007; Hernandez et al., 2009; Sulieman et al., 2013;

Sulieman et al., 2013; Ding et al., 2021). *Medicago truncatula* –P plants showed impaired growth compared to those in +P, with lower fresh and dry weights (DWs) and lower inorganic Pi and total P in leaves, roots, and nodules (Supp. Fig. S2.1, A–E). The nodulated root systems from –P plants were found to have higher numbers of lateral roots and fewer and smaller nodules than those from +P plants (Supp. Fig. S2.2, A–H). Plants had reduced nitrogenase activity, as revealed by the acetylene reduction assay (ARA; Supp. Fig. S2.2I). This confirmed that our –P conditions were effective in inducing P deprivation.

To gain insight into membrane lipid composition changes under P deprivation versus sufficiency, lipid profiling using ESI–MS was carried out to determine the polar membrane glycerolipid composition of leaves, roots, and nodules, including PLs and GLs. In leaves, in +P conditions, the GLs MGDG and DGDG were found to be highly abundant, comprising almost 75% of total glycerolipids measured (Fig. 2.1A). In –P leaves, the composition of GLs increased to 90% of total membrane lipids (Fig. 2.1B). In both +P and –P, MGDG species were found to be more abundant than DGDG species, with increases in DGDG species higher than MGDG in –P as compared to +P (Fig. 2.1, A and B). MGDG and DGDG species of 36:6 fatty acid composition predominated in both +P and –P leaves (Fig. 2.1, A and B). In –P, DGDG 36:3 species were found to increase markedly compared to +P, although their levels were found to be ~10-fold lower than those of DGDG 36:6 species (Supp. Fig. S2.3A). MGDG and DGDG 36:6 and DGDG 36:3 species accumulated close to two-fold higher in –P leaves (Supp. Fig. S2.3, A and B), accounting for most of the GL increases observed (Fig. 2.1, A and B). In +P leaves, PLs were found to comprise only ~25% of total membrane glycerolipids measured, with PC and PG

species encompassing 75% and 14% of the total PLs, respectively (Fig. 2.1A). Smaller contributions to total PL were made by PE (1.67%), PI (0.91%), PS (0.17%), and PA (0.04%; Fig. 2.1A). In –P leaves, PLs comprised only 10% of the total glycerolipids, with a significant decrease observed in quantities of PC (7.24%) and PG (1.17%; Fig. 2.1, A and B). PC species with fatty acid compositions 34:3, 34:2, 36:6, 36:5, 36:4, and 36:3 were markedly reduced in –P (Supp. Fig. S2.3C). Levels of PE species with fatty acids compositions 34:3, 34:2, 36:5, and 36:4 were lower in –P leaves (Supp. Fig. S2.3D). PG 34:4 significantly contributed to decrease in the PG species (Supp. Fig. S2.3E) as it was reduced almost by two-fold in –P leaves. No significant difference in PA and PI species was observed between +P and –P leaves (Supp. Fig. S2.3, F and H). Two PS species with fatty acid composition 40:3 and 42:3 were reduced in –P leaves (Supp. Fig. S2.3G).

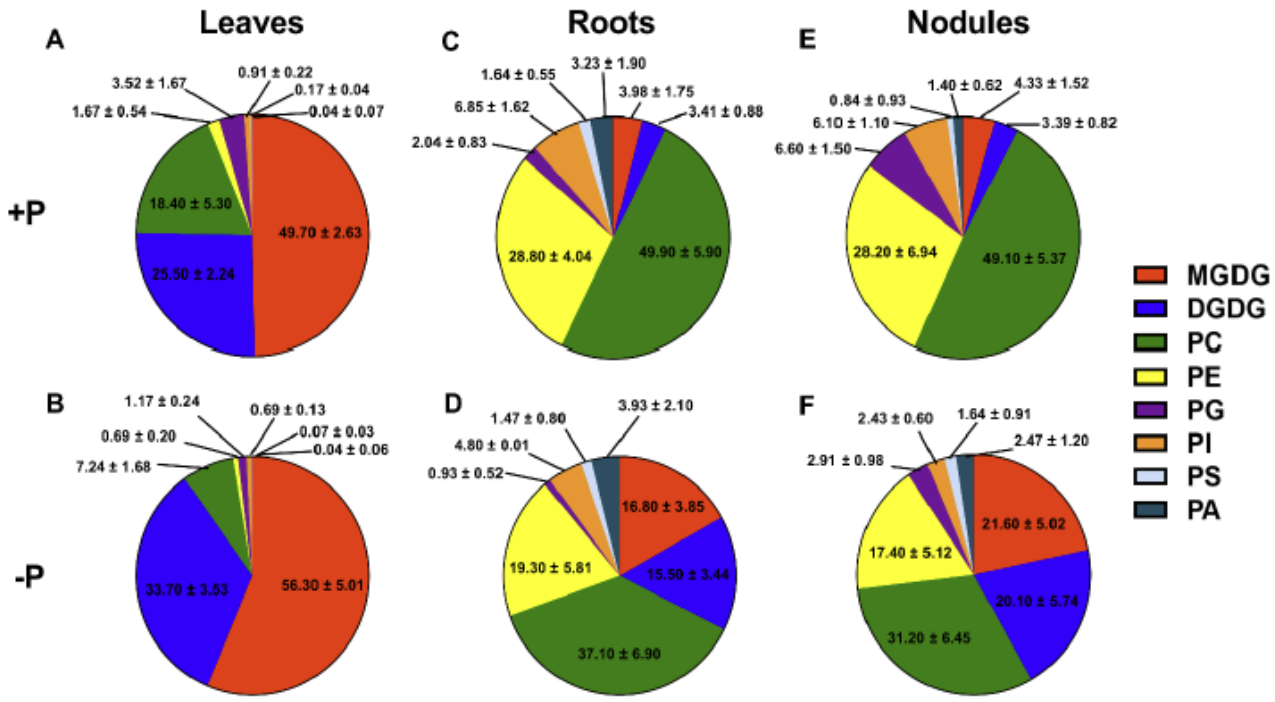

Figure 2.1: **Total lipid composition for leaves, roots, and nodules in mol%.**

A and B, represent total lipid composition in leaves. A, +P; B –P. C and D, represent total lipid composition in roots. C, +P; D –P. E and F, represent total lipid composition in nodules. E, +P; F –P. The values are mean ± standard deviation (SD).

In roots, contrasting differences in the membrane composition were observed in +P versus –P compared to leaves. PL species contributed 92% to the total glycerolipids in +P roots and showed a decline to 68% in –P (Fig. 2.1, C and D). PC species were the most abundant membrane lipids encompassing 50% of the total lipids in roots in +P which decreased to 37% in –P roots, respectively (Fig. 2.1, C and D). Relatively abundant PC species with fatty acid compositions of 34:3, 34:2, 36:5, 36:6, 36:4, 36:3, and 36:2 showed a significant reduction in –P (Supp. Fig. S2.4A). In +P roots, lower contributions to total lipid composition were made by PE (28.80%), PG (2.04%), PI (6.85%), PS (1.64%), and PA (3.23%; Fig. 2.1C). P deprivation resulted in lower concentrations of root PE (19.30%), PG (0.93%), and PI (4.80%), while PS (1.47%) and PA did not significantly change (3.93%; Fig. 2.1D). Like PC, 34- and 36-carbon containing PE species (34:3, 34:2, 36:6, 36:5, 36:3, and 36:2) were reduced in –P roots (Supp. Fig. S2.4B). PG 32:0, 34:2, and 34:3 and PI 34:3 and 34:2 were also found to be decreased in –P roots (Supp. Fig. S2.4, C and D). Most of the PS and PA species showed no significant difference between +P and –P roots, except PS 40:2 and 42:2 which decreased in –P (Supp. Fig. S2.4, E and F). In +P roots, the GLs MGDG and DGDG comprised only 7.39% of the total glycerolipid composition, with 3.98% and 3.41%, respectively (Fig. 2.1C). In –P roots, the GL content increased to 32.30% of total glycerolipids, with MGDG comprising 16.80% and DGDG 15.50% of the total (Fig. 2.1D). Similar to leaves, the 36:6 fatty acid moieties of both MGDG and DGDG were found to predominate in +P and –P roots (Supp. Fig. S2.4, G and H). MGDG 36:6 was relatively more abundant compared to DGDG 36:6 in roots in –P conditions (Supp. Fig. S2.4, G and H). Levels of most 34- and 36-carbon species of DGDG and 36-carbon species of MGDG (including 34:3) were increased in –P roots in

(Supp. Fig. S2.4, G and H).

We found that nodules had a similar membrane glycerolipids profile to roots, with PLs most abundant. In +P nodules, PC (49.10%) species comprised the most abundant class of membrane lipids, with PE (28.20%) second in abundance of the total glycerolipids (Fig. 2.1E). In –P nodules, PC species remained the most abundant class of membrane glycerolipids (31.20%). Major PC species that showed decreases in –P nodules included those of 34:3, 34:2 34:1, 36:6, 36:5, 36:4, 36:3, and 36:2 compositions (Supp. Fig. S2.5A). PE species were reduced to 17.40% in –P nodules (Fig. 2.1F), with the 34- and 36-carbon fatty acid containing species showing the most significant changes (Supp. Fig. S2.5B). Other PL species in nodules that showed changes in their levels between the two different growth conditions were PG (6.60% in +P to 2.91% in –P) and PI (6.10% in +P to 2.43% in –P; Fig. 2.1, E and F). Similar to PC and PE, the 34- and 36-carbon containing fatty acid species of PG and PI showed the largest changes in –P nodules (Supp. Fig. S2.5, C and D). No significant differences were observed in PS and PA species in –P nodules compared to +P nodules (Fig. 2.1, E and F; Supp. Fig. S2.5, E and F). In +P nodules, the GLs MGDG (4.33%) and DGDG (3.39%) comprised 7.72% of the total glycerolipid composition (Fig. 2.1E), similar to that of roots. In –P nodules, MGDG (21.60%) and DGDG (20.10%) increased to 41.70% of the total glycerolipids in nodules, noticeably (8%) higher than that observed in –P roots (Fig. 2.1, D and F). The 36:6 fatty acid species were the most abundant species of GLs in nodules regardless of the growth conditions (Supp. Fig. S2.5, G and H). DGDG 36:6 accumulated approximately four-fold in –P nodules and MGDG 36:6 showed a three-fold increase (Supp. Fig. S2.5, G and H). Most 34- and 36-carbon species of DGDG and 36-carbon species of MGDG (including 34:3) showed

increased levels in nodules in P deficiency (Supp. Fig. S2.5, G and H).

2.4.2 MALDI–MSI Shows PC Species are Non-Uniformly Distributed in *M. truncatula* Nodules

MALDI–MSI is a semi-quantitative technique that permits mapping of metabolites in biological sections, yielding a spatial metabolic context (Chen et al., 2009; Fuchs et al., 2010; Gemperline et al., 2015; Sturtevant et al., 2016; Lu et al., 2018). With this technique, matrix-coated nodule sections are subjected to laser rastering in a series of points, collected as x–y coordinates. The laser-excited metabolite ions enter a mass spectrometer where their m/z values are measured. Subsequently, metabolites are identified and used to show individual metabolite intensity at each x–y coordinate via false-color images (Fig. 2.2).

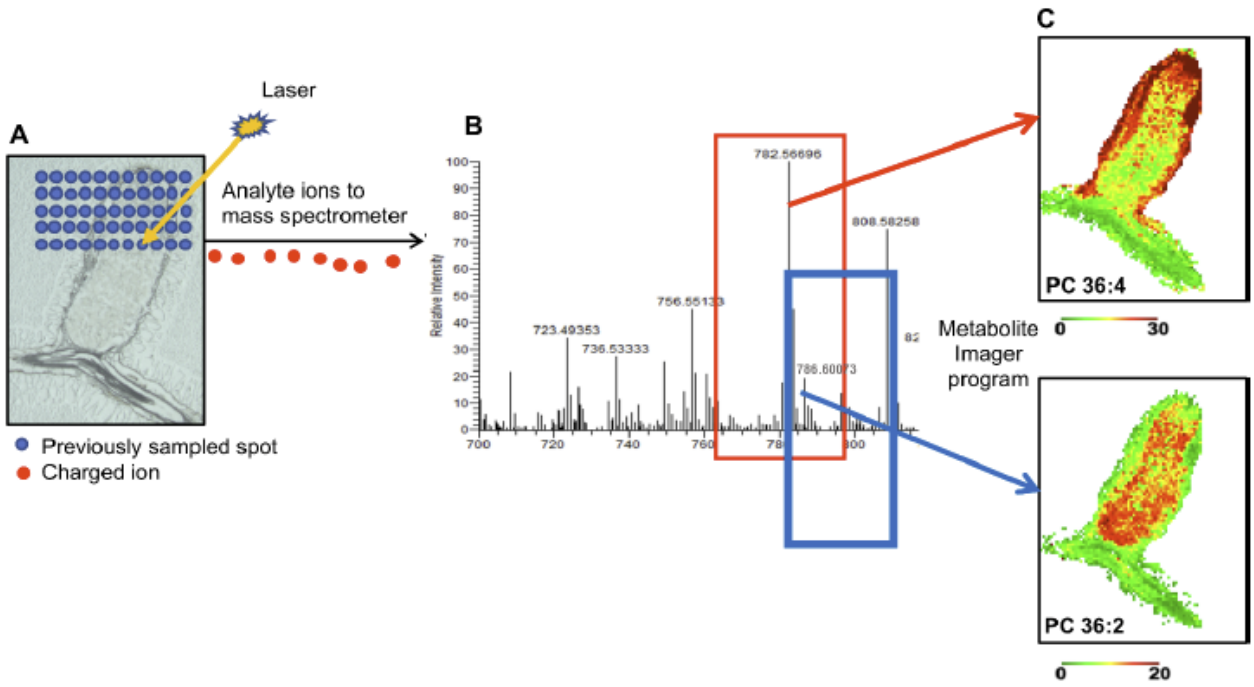

Figure 2.2: **Schematic showing the MALDI–MSI method.**

A, A laser is rastered over a DHB-coated nodule cross-section in a series of spot points with a given x–y coordinate. The example shown is a nodule cross-section of *M. truncatula* R108 (25 µm). B, The analyte ions produced are directed to a mass spectrometer, where their m/z values

are measured. C, Metabolites are identified, and images are generated using Metabolite Imager. For example, PC 36:4 and PC 36:2 as shown.

Among the membrane glycerolipids, PC species are abundant and contain a quaternary ammonia group with a permanent positive charge and are thus detectable in tissue sections. MALDI–MSI has been used to investigate PC species distribution in animal tissues (Jackson et al., 2007; Chen et al., 2009; Fuchs et al., 2010). Among plants, barley germinating seeds and *Brassica napus* developing seeds have been subjected to MALDI–MSI for PC distribution (Gorzolka et al., 2016; Woodfield et al., 2017; Lu et al., 2018; Colin and Jaillais, 2020). We sought to bring MALDI–MSI to indeterminate *M. truncatula* nodules to examine PC species distribution, the most abundant membrane glycerolipid type found there (Fig. 2.1, E and F). The instrument we used had 40 μm resolution, capable of analyses at the tissue scale.

To examine nodule PC species distribution, we first evaluated the PC distribution in +P nodules (Fig. 2.3, A and B; Supp. Fig. S2.6, A and B). Figure 2.3A and Supplemental Figure S2.6A show false-color image maps where all the species are shown at the same intensity scale (40 mol%), revealing the absolute abundance of each PC, allowing comparison of PC species abundance to one another. For example, this analysis shows that PC species 34:1, 36:2, 36:5, and 38:5 are more abundant in nodules, and for 36:4 in the surrounding root tissue, in comparison with other species (Fig. 2.3A; Supp. Fig. S2.6A). Overall, it can be seen that the PC species abundance determined by semi-quantitative MALDI–MSI agrees reasonably well with results obtained via the more quantitative ESI–MS (Supp. Fig. S2.5A) where PC species 34:1, 36:2, 36:4, and 36:5 were abundantly present in nodules, as has been similarly shown in seed studies where PC species have been imaged by MALDI–MS (Woodfield et al., 2017). The disadvantage

of fixed value false-color MALDI–MS images is that the spatial distribution of lipid molecular species is difficult to see for species with high or low amounts in tissues: either overexposed in brown/dark red for high levels or all green for low levels. To surmount this, we adjusted the scale for in each MALDI–MS image and created a relative distribution profile, so that the maximum ion intensity (in mol%) was brown/dark red to show the distribution of particular lipid molecular species in each nodule section (Fig. 2.3B; Supp. Fig. S2.6B).

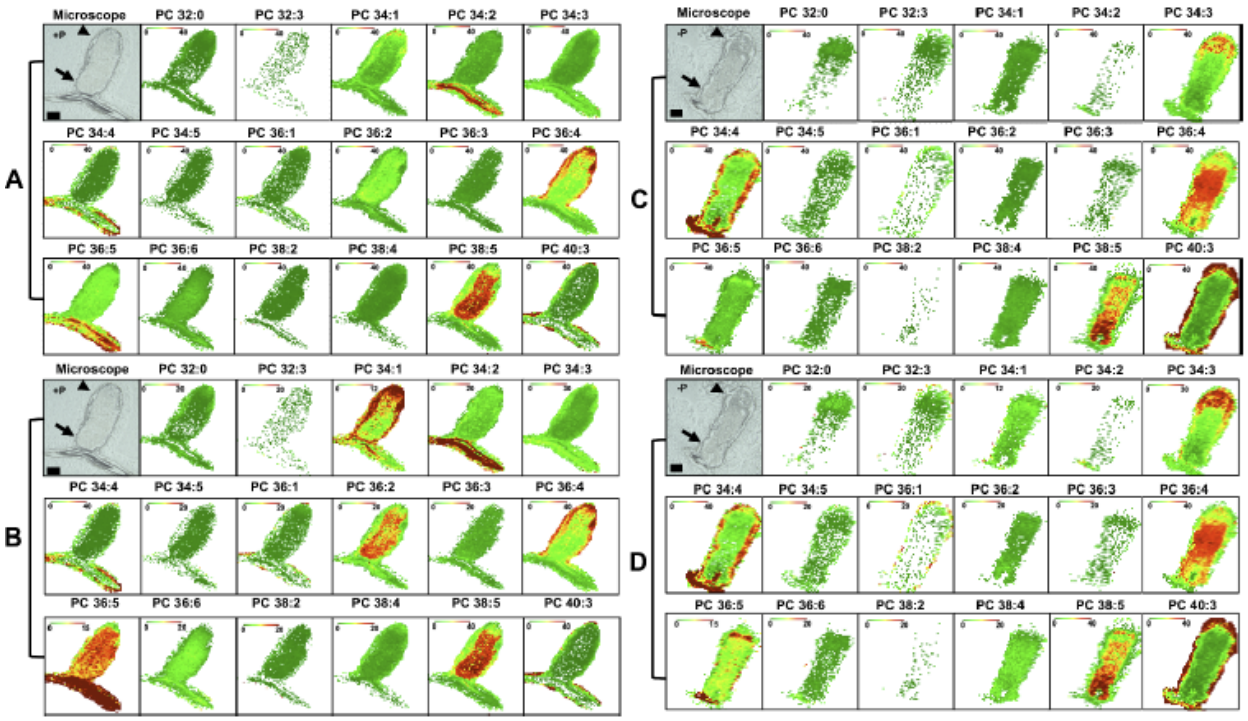

Figure 2.3: **MALDI–MSI of PC metabolites in *M. truncatula* nodules.**

A and B, Bright-field images of nodule cross-section (25 µm) before coating with DHB matrix grown under +P. C and D, Bright-field images of nodules cross-section (25 µm) before coating with DHB matrix grown under –P is shown on the left. A and C, Distributions of selected PC molecular species are shown with fixed mol% to show absolute distribution profiles. B and D, Adjusted mol% to show relative distribution profiles. Bars = 500 mm. Proximal zone is indicated by arrowhead and distal zone by arrow. MALDI scale shows mol% with green and red representing low and high levels, respectively. Representative images of N = 5 each for +P and –P.

The adjusted image maps reveal dramatic differences in distributions of PC species in +P nodules (Fig. 2.3B; Supp. Fig. S2.6B). For example, PC 34:2 and 36:5 have high distribution in the root tissue attached to the nodule, while PC 36:5 shows fairly high distribution in the central parts of the nodule (Fig. 2.3B). In contrast, PC 36:2 and 38:5 have a similar distribution in nodules but are not as abundant in root tissue. PC 36:2 and 38:5 species are not found as distally in nodules as 36:5. Other PC species, for example, PC 34:1 and 36:4, show higher abundance in the nodule epidermal, parenchymal, and vascular regions, with lower accumulations in the nodule's central region (Fig. 2.3B). Other species, for example, PC 36:3 and 36:6 show a relatively uniform distribution across the nodule (Fig. 2.3B; Supp. Fig. S2.6B). Thus, these data show that in *M. truncatula* +P nodules, PC species differentially accumulate in different regions of nodules.

2.4.3 Different Nodule PC Species Show Differential Spatial Changes in P Stress

We sought to determine changes in PC distribution in –P nodules as compared to +P nodules using MALDI–MSI (Fig. 2.3, C and D; Supp. Fig. S2.6, C and D). Maps created at the same intensity scale showed that most PC species declined in abundance in –P nodules, in agreement with the quantitative results determined by the ESI–MS analysis (Fig. 2.3C; Supp. Fig. S2.5A). To compare whether there were changes in distribution of particular PC species in –P nodules compared with +P nodules, we used image maps for –P nodules that were scaled to the same mol% values used in +P nodules (compare Fig. 2.3, B and D; Supp. Fig. S2.6, B and D). These data revealed that many PC species changed distribution in response to P stress. For instance, PC 34:2, 36:2, 36:5, and 38:5 species were found in lower abundance across the nodule in –P

conditions. These PCs were also found to be consistently lower in the ESI–MS lipidomic analysis (Supp. Fig. S2.5A). Curiously, PC species 34:3 had higher distributions in the distal part of nodule zone II in –P conditions. PC species 34:1 and 36:4 showed relatively similar localization pattern with higher abundance in the peripheral tissues of +P nodules, PC 34:1 was less abundant in –P nodules and PC 36:4 was found at higher abundance in the central part of –P nodules (Fig. 2.3, B and D). In a similar vein, PC 36:2 and 38:5 species, which were both abundant in the central parts of +P nodules, were both observed to have lower distribution in –P nodules, but PC 38:5 had fairly high abundance in the proximal parts of the –P nodule (Fig. 2.3, B and D). PC 36:5 also had lower abundance in –P nodules compared to +P (Fig. 2.3, B and D). Some PC species did not show major changes in spatial distribution in –P nodules compared to +P nodules; their image maps are shown in Supp. Fig. S2.6. Unfortunately, we were not able to image the non-P containing GLs (MGDG and DGDG) in nodule sections. This is likely because of ion suppression caused by PC (Supp. Fig. S2.7; Supplemental Dataset 2.1). The phenomenon of ion suppression caused by PC has been observed previously (Petkovic et al., 2001; Fuchs et al., 2009; Emerson et al., 2010; Fuchs et al., 2010; Horn et al., 2012; Woodfield et al., 2017; Stopka et al., 2018; Colin and Jaillais, 2020).

2.4.4 Validation of the Differences in PC Distribution in Dissected Nodules

There are known limitations of the MALDI–MSI technique, which include ion suppression, lack of absolute quantitation (Horn et al., 2012; Woodfield et al., 2017), and the observation that a longitudinal section does not represent the entire nodule in three dimensions. To address this, we used a second approach to compare and validate the differences in spatial distributions observed by MALDI–MSI. Twenty-eight days post-

inoculation (DPI) nodules from plants grown in +P and in –P conditions were dissected into distal (approximately ZI to ZII), central (IZII/III and ZIII), and proximal (proximal zone III–IV) sections (Fig. 2.4A). We extracted lipids from the separated nodule sections and subjected them to ESI–MS to determine the PC species composition of each. The resulting data were compared to those obtained from nodule MALDI–MS images that were “virtually” sectioned (Fig. 2.4B), followed by a computational determination of the intensity of PC species in each virtual section (Fig. 2.4B).

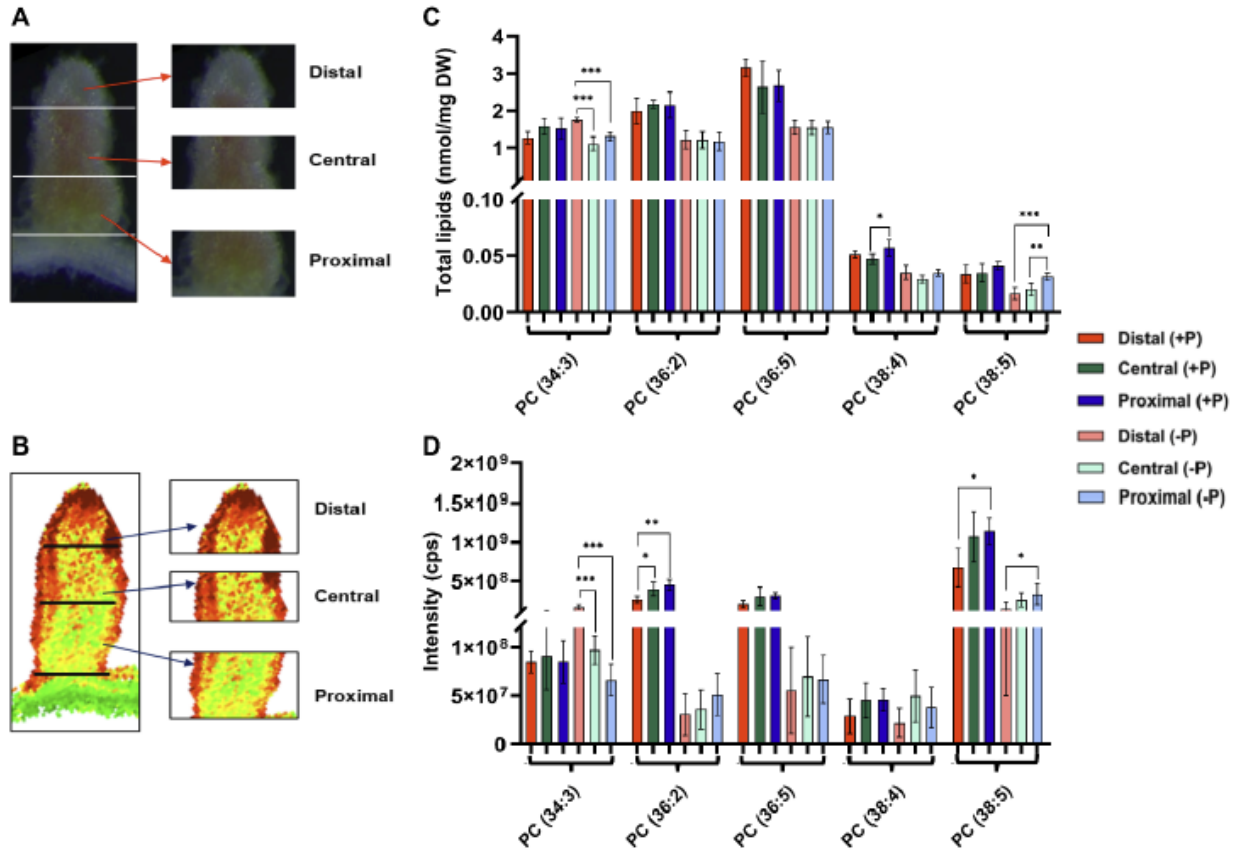

Figure 2.4: **Comparison of ESI–MS and MALDI–MSI results for PC species in different sections of dissected nodules.**

A, Bright-field image of a nodule dissected into distal, central, and proximal sections used for ESI–MS analysis. B, Virtually dissected nodule into distal, central, and proximal sections used for MALDI–MSI analysis. C, Quantitative data of representative PC species obtained from distal, central, and proximal nodules sections using ESI–MS. Values are expressed as total lipids (nmol/mg DW of tissue) after normalizing with the amount of respective standards. D, Representative PC species obtained from distal, central, and proximal nodules sections using MALDI–MSI are expressed in intensities count per second; values are mean ± SD (N = 5). Error

bars indicate SD. Asterisks indicate a significant difference between the control plants (+P) and test plants (–P), as determined using one-way ANOVA analysis; *P ≤ 0.05; **P ≤ 0.01; ***P ≤ 0.001.

Comparison of the ESI–MS to MALDI–MS results showed reasonable agreement with each other. Our results showed that PC 34:3 was similarly abundant in all nodule zones in +P nodules. In –P nodules statistically significant differences were found similarly when comparing distal to central and distal to proximal areas in both ESI–MS and MALDI analyses (Fig. 2.4, C and D). Differences between central and proximal regions in –P were not significantly different. For PC 36:2 ESI–MS analysis showed relatively uniform concentrations of this PL in all three nodule areas. In contrast, MALDI results showed statistically significant differences in +P conditions when comparing distal to central and distal to proximal areas of the nodule (Fig. 2.4, C and D). PC 36:5 and PC 38:4 were found at similar abundance in +P and –P nodules with one exception, PC 38:4 was found to be significantly lower in the central area of the nodule compared to the proximal area of the nodule in ESI results; in comparison MALDI showed a similar distribution of PC 38:4 in these zones (Fig. 2.4, C and D). PC 38:5 was found to be similarly distributed in –P nodules by each analysis with the highest abundance in the proximal part (Fig. 2.4, C and D). However, it was significantly lower in distal compared to the proximal part of +P nodules by MALDI–MSI. Similar differences in trend between ESI–MS and MALDI–MS were also observed for PG 34:4 in a study on maize leaf (Duenas et al., 2017).

2.5 Discussion

P deficiency is one of the limiting factors adversely affecting worldwide legume growth and productivity (Tesfaye et al., 2007). Legumes that are nodulated and fixing N_2 are known to have a higher demand for P than those grown on mineral N (Graham, 1981;

Vance et al., 2003; Sulieman and Tran, 2015). Processes that contribute to N_2-fixing legumes' high P requirement include the high energy required for nitrogenase to function at a high level, signal transduction/enzyme regulation particularly those pathways regulated by protein phosphorylation, nucleic acid biosynthesis, and membrane lipid biosynthesis and homeostasis (Graham and Vance, 2000).

This study focused on membrane lipid homeostasis in *M. truncatula* plants undergoing severe P deficiency. We confirmed that *M. truncatula* growth was impaired in P deprivation compared to control P replete (+P) plants in our aeroponic growth system (Supp. Figs. S2.1 and S2.2), showing that *M. truncatula* plants were stressed similarly to those in previous studies on P deprivation in *M. truncatula* (Sulieman et al., 2013; Sulieman et al., 2013), *M. sativa* (Sulieman et al., 2013; Sulieman et al., 2013), rice (Li et al., 2001), *A. thaliana* (Williamson et al., 2001; Morcuende et al., 2007), common bean (Hernandez et al., 2007; Hernandez et al., 2009), white lupin (Schulze et al., 2006), and switchgrass (Ding et al., 2021).

The glycerolipid composition of *Sinorhizobium*-nodulated *M. truncatula* leaves and roots (Fig. 2.1, A and C; Supp. Figs. S2.3 and S2.4) was found to be similar to that observed in *Bradyrhizobium*-nodulated soybean leaves and roots (Gaude et al., 2004; Narasimhan et al., 2013) with plastidial DGDG and MGDG species found in highest abundance in leaves, and PC and PE species in highest amounts in roots. *M. truncatula* nodule glycerolipid content was also found to be similar to that of soybean (Gaude et al., 2004), with a similar profile as roots, but with more PG found in nodules as compared to roots (Fig. 2.1E). As a symbiotic organ, a fraction of the glycerolipid content in nodules comes from the internalized bacteroids, which in the larger, determinate *Bradyrhizobium*-

soybean nodules contain predominantly PE, PC, PG, and PI in their membranes (Gaude et al., 2004). To our knowledge, the polar lipid composition of the bacteroids from *S. meliloti-M. truncatula* nodules has not yet been assessed, but since PG is a prominent lipid found in free-living *S. meliloti* (López-Lara et al., 2005), the increased PG found in nodules compared to roots may come from the bacteroid component of nodules. The lipid profiling results reported here show higher content of PC than PE in roots and nodules (Fig. 2.1, C and E). This differs from lipid compositions found in soybean (Gaude et al., 2004) and in a previous *M. truncatula* study in genotype A17 (Si et al., 2019), who observed more PE than PC in roots and nodules. The differences might be attributable to the different growth conditions employed in the different studies and the different species and *M. truncatula* genotypes studied.

In P deprived *M. truncatula*, we observed changes in glycerolipids composition that were overall similar to those observed previously in soybean (Gaude et al., 2004) and *M. truncatula* (Si et al., 2019). Leaves, roots, and nodules showed increases in GLs MGDG and DGDG, as anticipated (Fig. 2.1, B, D, and F), although PC still comprised the largest single class of glycerolipid in roots and nodules (Fig. 2.1, D and F). The increases in the non-P-containing GLs during P stress in the roots and nodules instead of PLs is likely necessary to conserve P for other essential biological processes like biosynthesis of nucleic acids, phosphorylated sugars, and signaling by phosphorylated proteins. In –P nodules, similar to +P nodules, PL species detected in our study could originate from bacteroid membranes. We note that *S. meliloti* possesses three Pi transport systems each of which is sufficient for SNF in alfalfa, *M. truncatula's* close relative, in normal +P

conditions (Yuan et al., 2006). It is not yet known how these are regulated in internalized bacteroids of nodulated plants when P is depleted from the environment.

One of the advantages of studying the effect of P deprivation on membrane lipids in *M. truncatula* is that its indeterminate nodules make it possible to examine whether specific PLs change abundance at different stages of symbiotic development using the developmental gradient found in the continually differentiating nodules. MALDI–MSI, a

semi-quantitative technique allows visualization of metabolites at the tissue level with fairly high resolution (Gemperline et al., 2015). For membrane lipids, MALDI–MSI is currently limited to abundant and well-ionizable PLs and has the advantage of being able to discriminate their degree of unsaturation. PC is the most abundant membrane lipid in nodules and possesses a quaternary ammonia group containing a permanent positive charge (Fuchs et al., 2010; Horn et al., 2012; Woodfield et al., 2017). Therefore, detection of PC species is sensitively detected in complex lipid mixtures or tissue sections than other less abundant or poorly ionizable molecular species (Petkovic et al., 2001; Emerson et al., 2010; Fuchs et al., 2010; Horn et al., 2012; Woodfield et al., 2017; Stopka et al., 2018; Colin and Jaillais, 2020). To address the question of PC distribution in nodules, we used this technique. Our results (Fig. 2.3, A and B) showed spatial heterogeneity of many PC species in nodules that are obscured when using regular analytical extraction-based techniques. The differences in spatial distribution of PC species observed here open the possibility that there may be cell- and tissue-specific regulation of membrane lipid metabolism during nodule development. We then used MALDI–MSI to address PC distribution in –P nodules, with our results showing a markedly different spatial heterogeneity for many PCs from patterns observed in +P nodules (Fig.

2.3). Traditional organic extractions of membrane lipids of dissected nodule sections followed by with ESI–MS analysis of PC content for selected PC species showed strong associations with virtual MALDI–MSI sections (Fig. 2.4), validating the comparison. For example, the MALDI–MSI results show that PC 38:5 abundant in +P inner nodule tissues changes localization to several cell layers at the distal end of –P nodules (compare Fig. 2.3, B with D). In contrast PC 36:4, different from PC 36:5 by one desaturation step each, is found in peripheral nodule cells in +P conditions, while in –P nodules was found as an abundant species in the central nodule zones. These data suggest that other membrane lipid species in addition to PC, particular fatty acid biosynthetic enzymes, and specific desaturases may be differentially regulated in nodule cells at different stages of nodule cell maturation and in +P versus –P environmental conditions. Another possibility is that different PC species may be better substrates for MGDG and DGDG synthetases (Si et al., 2019), which may themselves be heterogeneously distributed spatially in nodules.

PC species are abundant membrane lipids that are mostly thought of as structural lipids as compared to less abundant PLs, like PI species, that have additional well-established signaling roles (Boss and Im, 2012; Noack and Jaillais, 2020). When one considers PC in structural roles, our results suggest the possibility that modifying plants to engineer higher abundance of PC species to favor those species found in higher amounts in the N-fixing zones of nodules could result in altered, perhaps increased, SNF efficiency. The distinction between structural and signaling roles for PCs are becoming blurred, with the finding that flowering time in Arabidopsis is influenced by PC content and that florigen FLOWERING LOCUS T binds preferentially to PC species with 18:3 fatty acids in vitro (Nakamura et al., 2014). Plants that are engineered to contain higher 18:3

fatty acid have been shown to flower later than controls (Arondel et al., 1992). Together these data suggest that specific PC species or their metabolites could have signaling roles (Colin and Jaillais, 2020). Thus, we speculate that in nodules, different PC species may have specific roles, signaling as well as structural, in different zones of *M. truncatula* nodules and that these roles may change in P deprivation. We further suggest that other membrane lipids, such as GLs and other PL species are likely to demonstrate non-homogeneous spatial distribution in nodules and this is likely to be of functional importance. Because of the technical challenges in localizing these molecules spatially, especially at the subcellular level, it is not possible to speculate about function. It is known that altering the GL composition by modifying DGDG abundance in nodules alters nodule function (Si et al., 2019), but the mechanism by which nodules are functionally altered, or which intracellular membranes are affected, is not yet clear. Further work to investigate whether manipulating the membrane lipid composition in nodules could alter nodule function and/or P deprivation effects on N fixation will address issues about particular membrane lipids and function.

2.6 Supplemental Data for Chapter 2

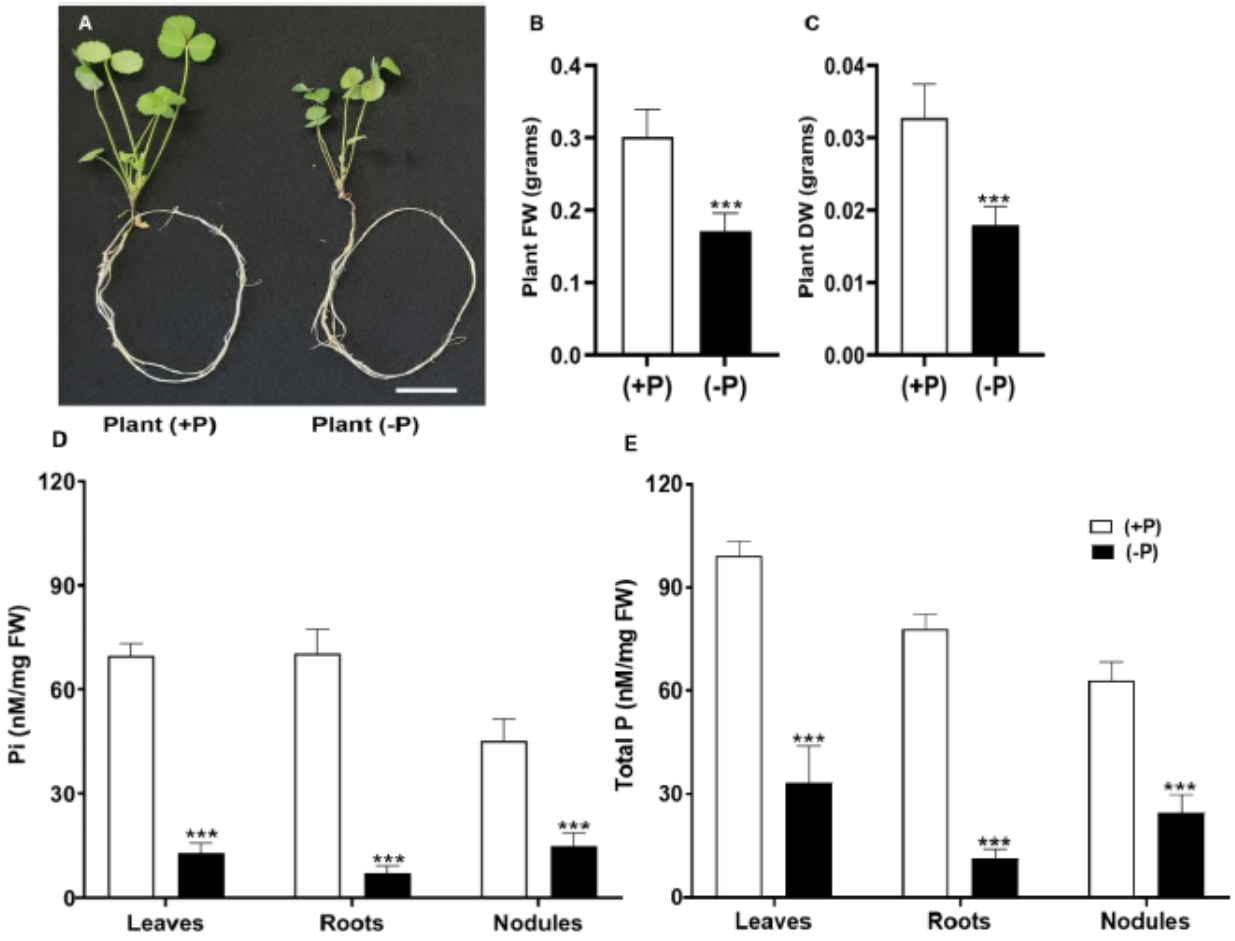

Supplemental Figure S2.1 Characteristics of *Medicago truncatula* in phosphorus (P) depleted conditions.

A. Appearance of wild-type R108 under sufficient phosphorus (+P) and absence of phosphorus (–P) after 28 days post inoculation (DPI) with *Sinorhizobium meliloti* Rm 41. Scale bar 2cm; B. Average Fresh weight (FW); C. Average Dry weight (DW). N = 15 for B and C. D. Inorganic Phosphate (Pi); E. Total P in leaves, roots and nodules of plants grown under +P and –P conditions, N=6. The values are mean ± SD. Asterisks indicate a significant difference between the control plants (+P) and test plants (-P), as determined using one-way ANOVA analysis; ***, $P \leq 0.001$.

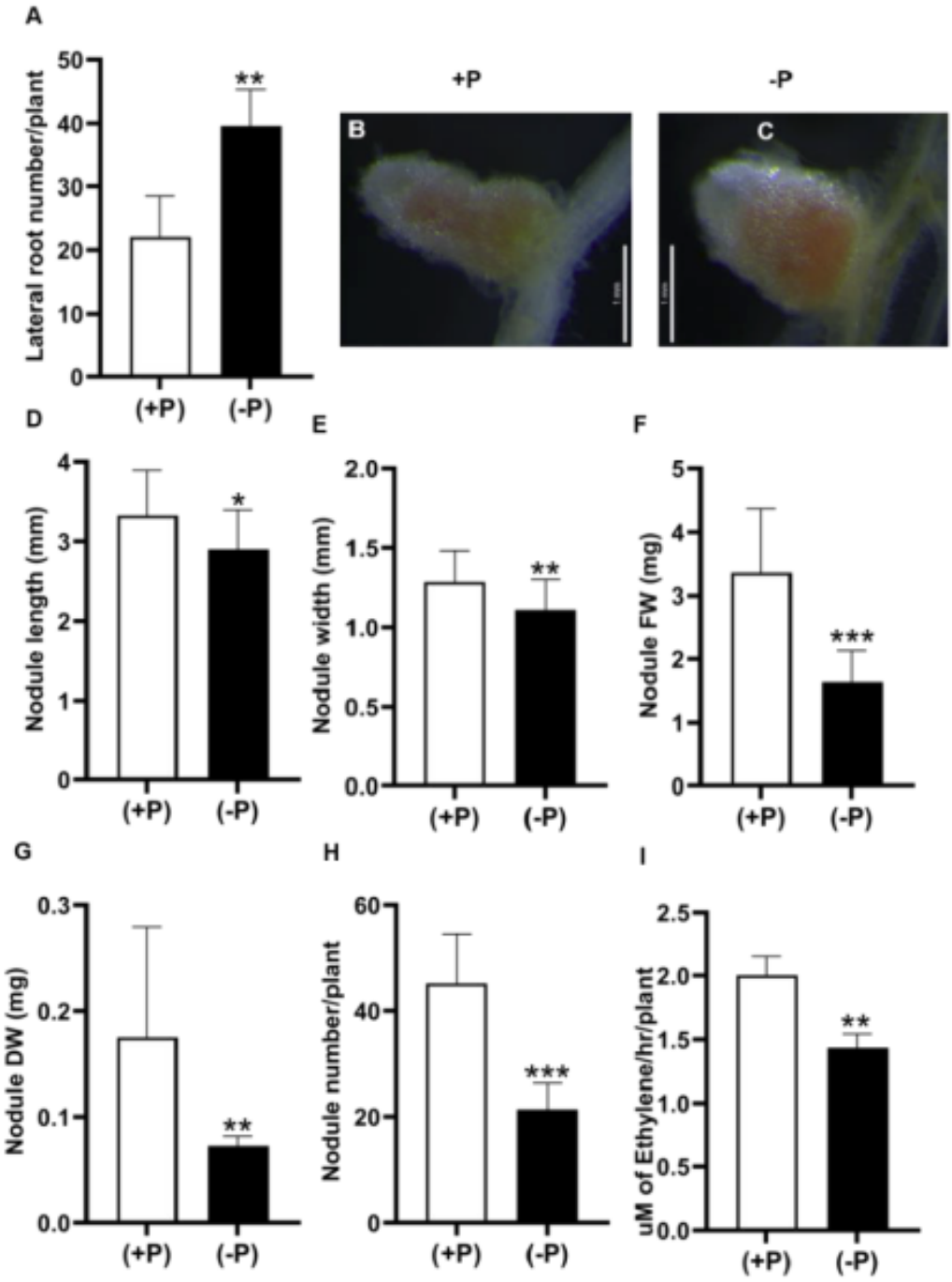

Supplemental Figure S2.2 Characteristics of nodulated root system of *Medicago truncatula* R108 in phosphorus (P) depleted conditions.

A. Lateral root number; B and C. Images of nodules from plants grown under sufficient phosphorus (+P) and absence of phosphorus (–P) conditions respectively, scale bar - 1mm; D. Nodule length; E. Nodule width; F. Nodule fresh weight (FW); G. Nodule dry weight (DW); H. Nodule number. N = 15 for figures A, D, E, F, G and H. I. Acetylene reduction activity assayed using whole plant 28 DPI with *Sinorhizobium meliloti* Rm41; N=5. The values are mean ± SD. Asterisks indicate a significant difference between the control plants (+P) and test plants (-P), as determined using one-way ANOVA analysis; *, $P \leq 0.05$; **, $P \leq 0.01$; ***, $P \leq 0.001$.

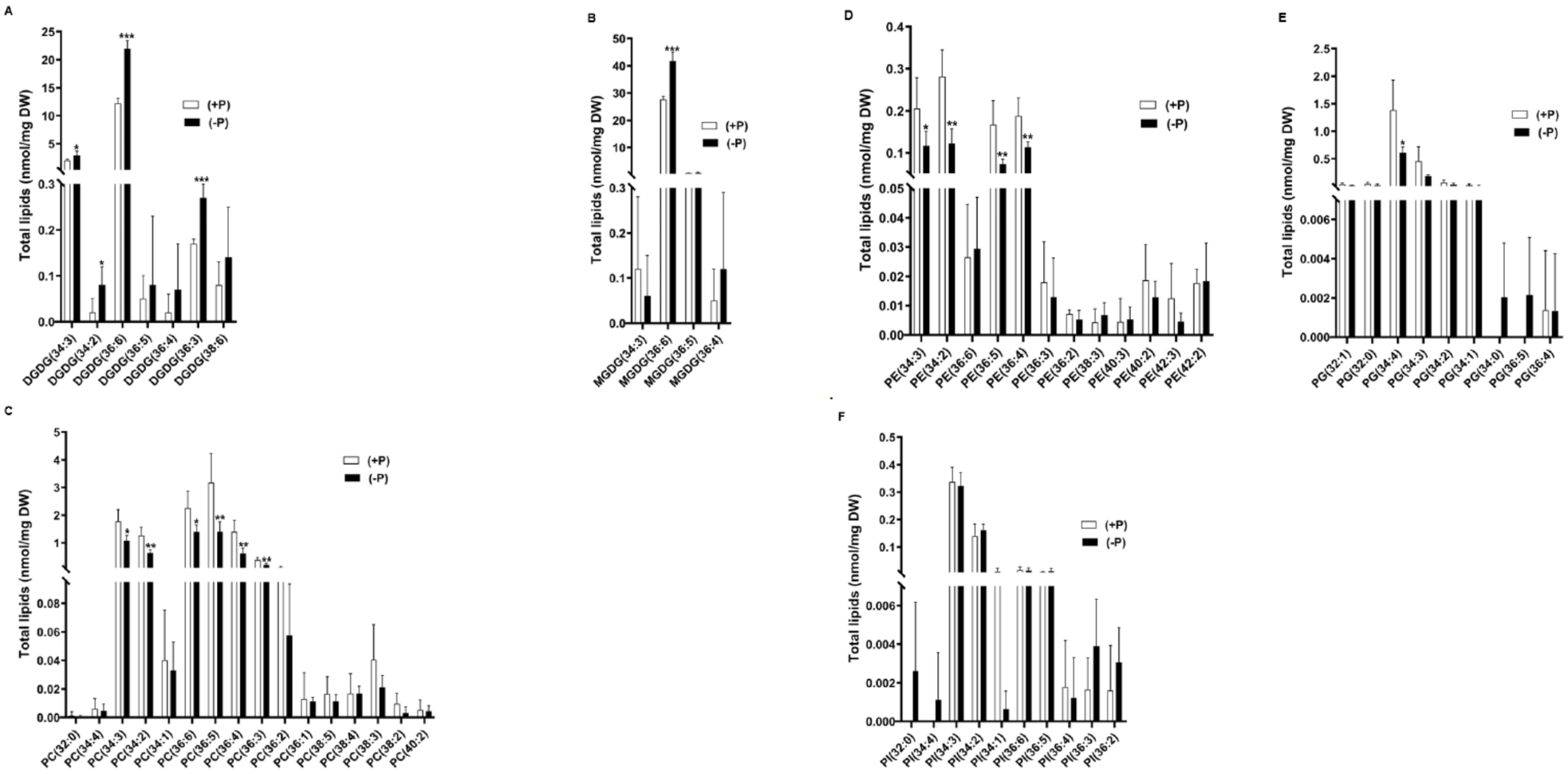

A. Digalactosyldiacylglycerol (DGDG); B. Monogalactosyldiacylglycerol (MGDG); C. Phosphatidylcholine (PC); D. Phosphatidylethanolamine (PE); E. Phosphatidylglycerol (PG); F. Phosphatidylinositol (PI).

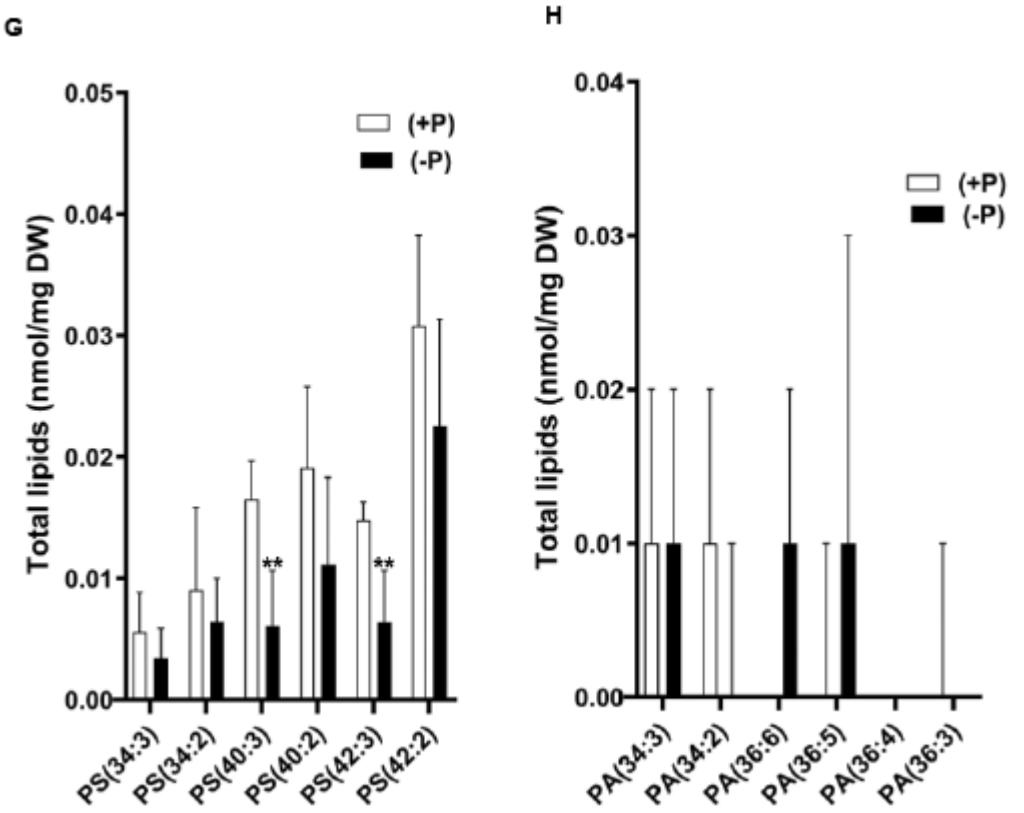

G. Phosphatidylserine (PS); H. Phosphatidic acid (PA).

Supplemental Figure S2.3 Total polar glycerolipids from leaves of *Medicago truncatula* R108 plants.

Plants were grown under sufficient phosphorus (+P) and absence of phosphorus (–P) conditions for 28 days after inoculation with *Sinorhizobium meliloti* Rm41. Values are expressed as total lipids (nmol/mg dry weight (DW) of tissue) after normalizing with the amount of respective standards. The values are mean ± SD (N =5). Asterisks indicate a significant difference between the control plants (+P) and test plants (-P), as determined using one-way ANOVA analysis; *, $P \leq 0.05$; **, $P \leq 0.01$; ***, $P \leq 0.001$.

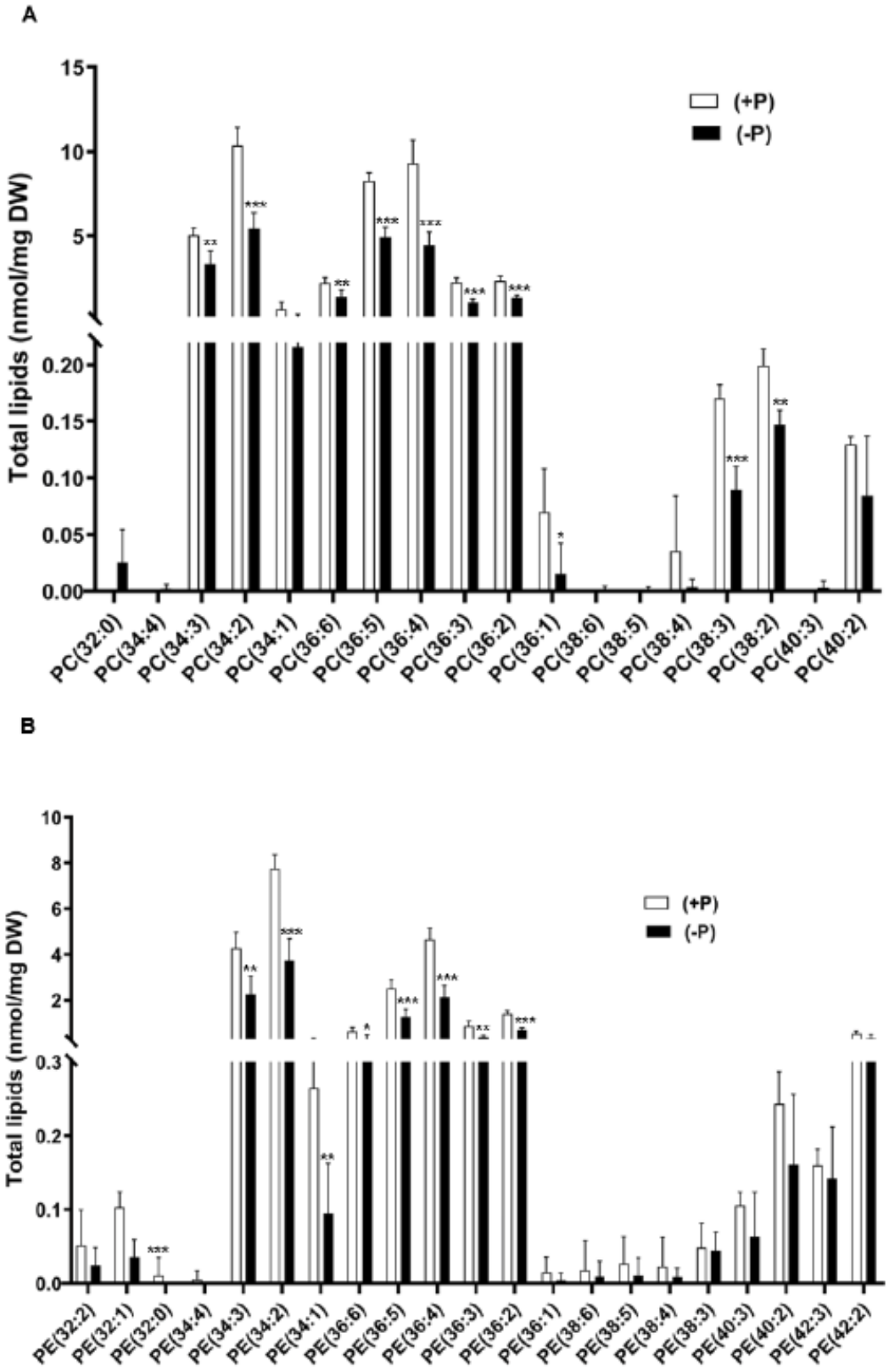

A. Phosphatidylcholine (PC); B. Phosphatidylethanolamine (PE).

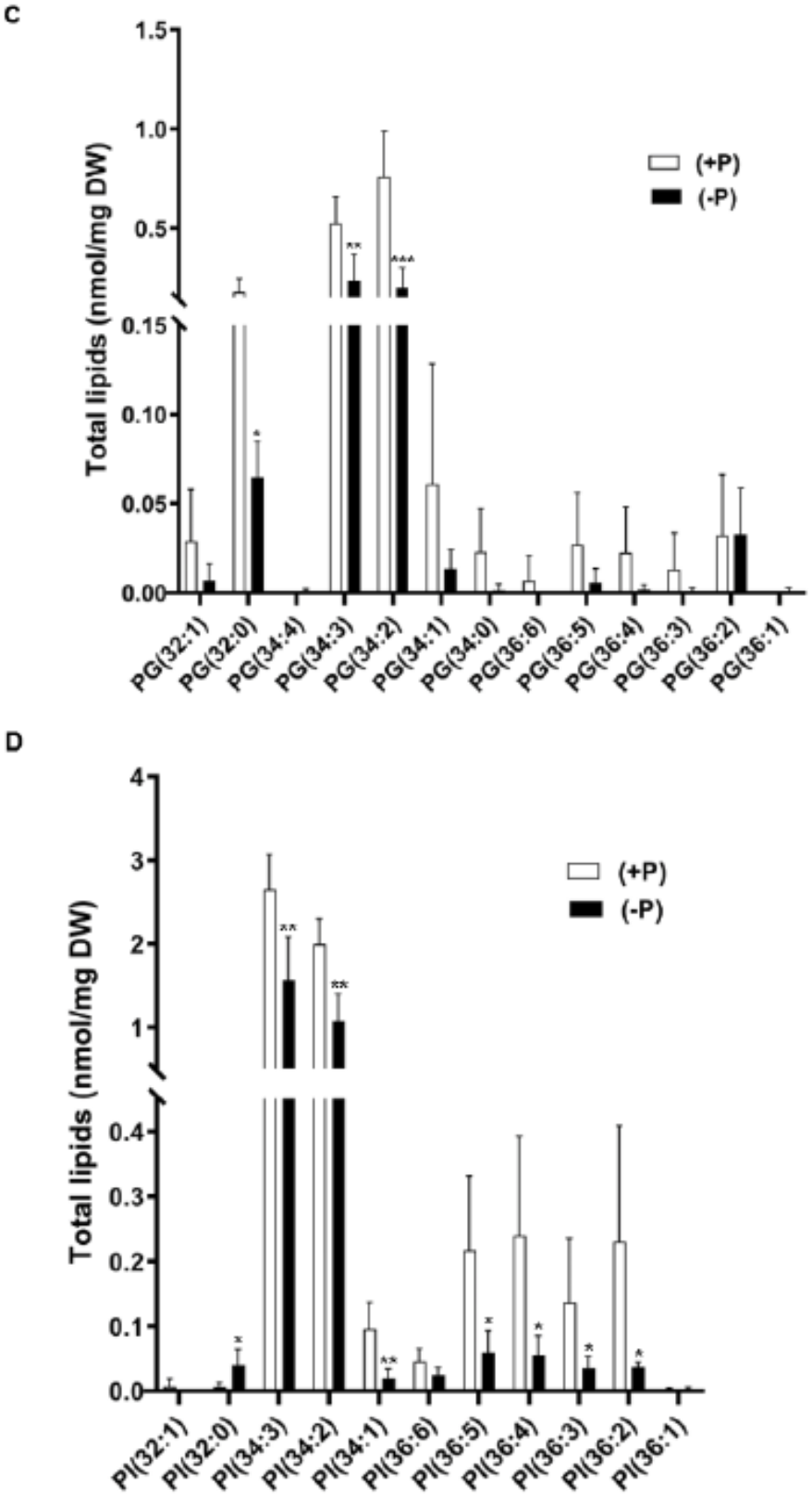

C. Phosphatidylglycerol (PG); D. Phosphatidylinositol (PI).

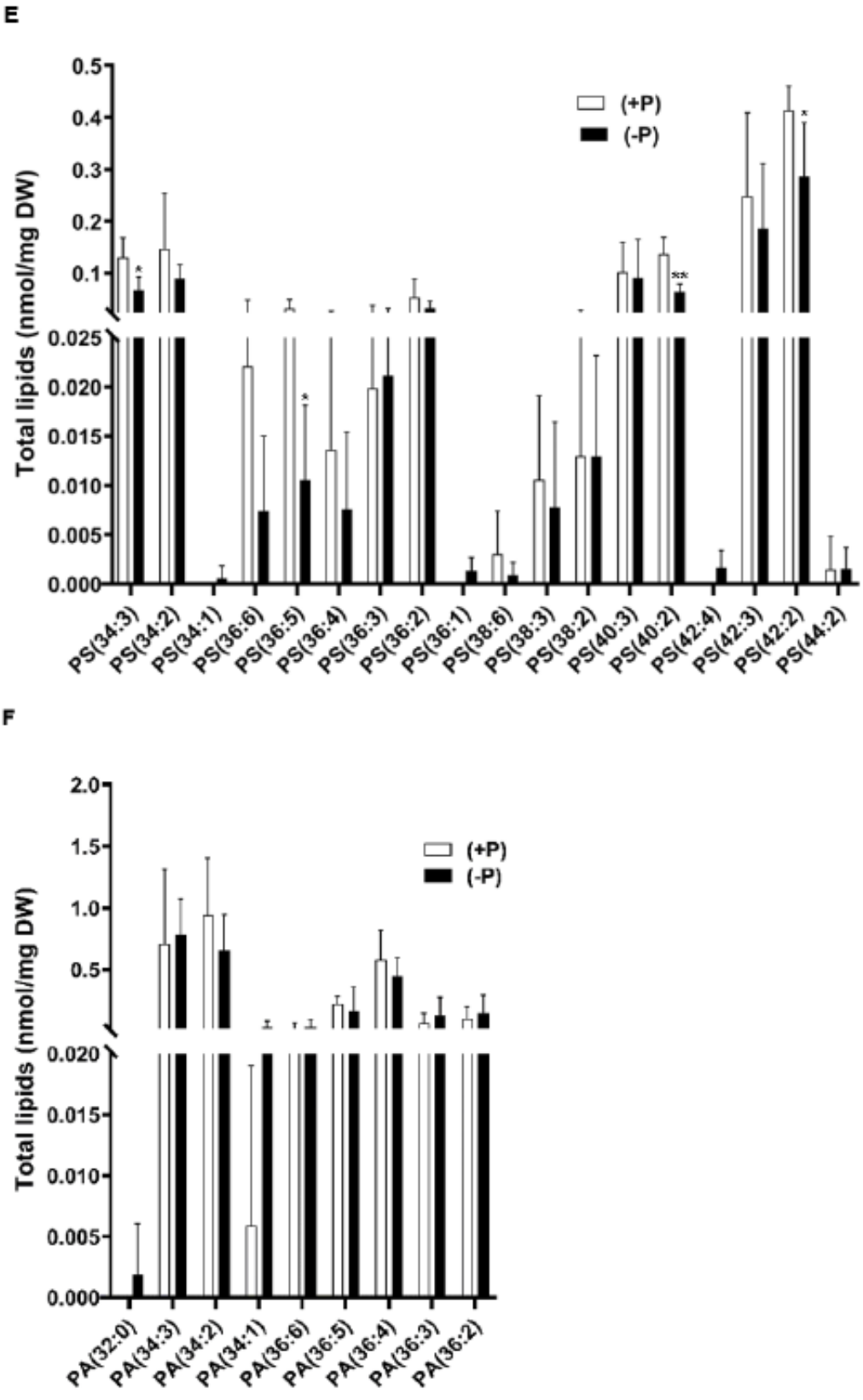

E. Phosphatidylserine (PS); F. Phosphatidic acid (PA).

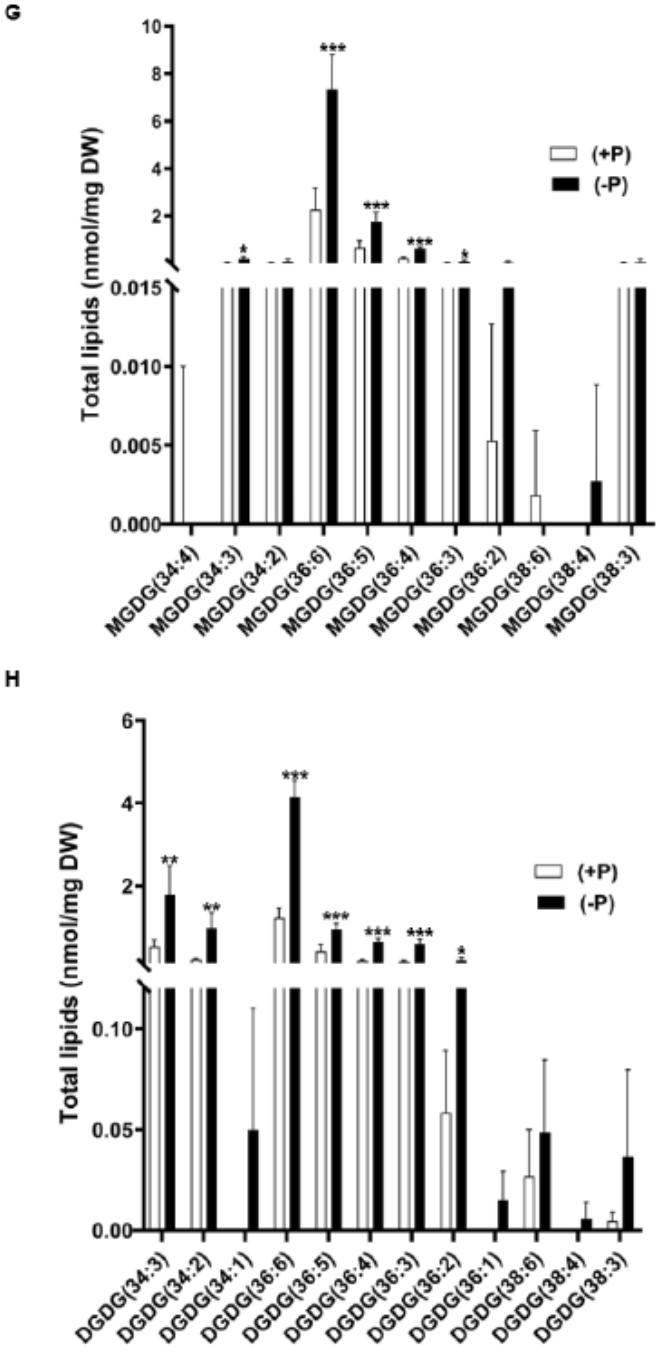

G. Monogalactosyldiacylglycerol (MGDG); H. Digalactosyldiacylglycerol (DGDG).

Supplemental Figure S2.4 Total polar glycerolipids from roots of *Medicago truncatula* R108 plants.

Plants were grown under sufficient phosphorus (+P) and absence of phosphorus (–P) conditions for 28 days after inoculation with *Sinorhizobium meliloti* Rm41. Values are expressed as total lipids (nmol/mg dry weight (DW) of tissue) after normalizing with the amount of respective standards. The values are mean ± SD (N =5). Asterisks indicate a significant difference between the control plants (+P) and test plants (-P), as determined using one-way ANOVA analysis; *, P ≤ 0.05; **, P ≤ 0.01; ***, P ≤ 0.001.

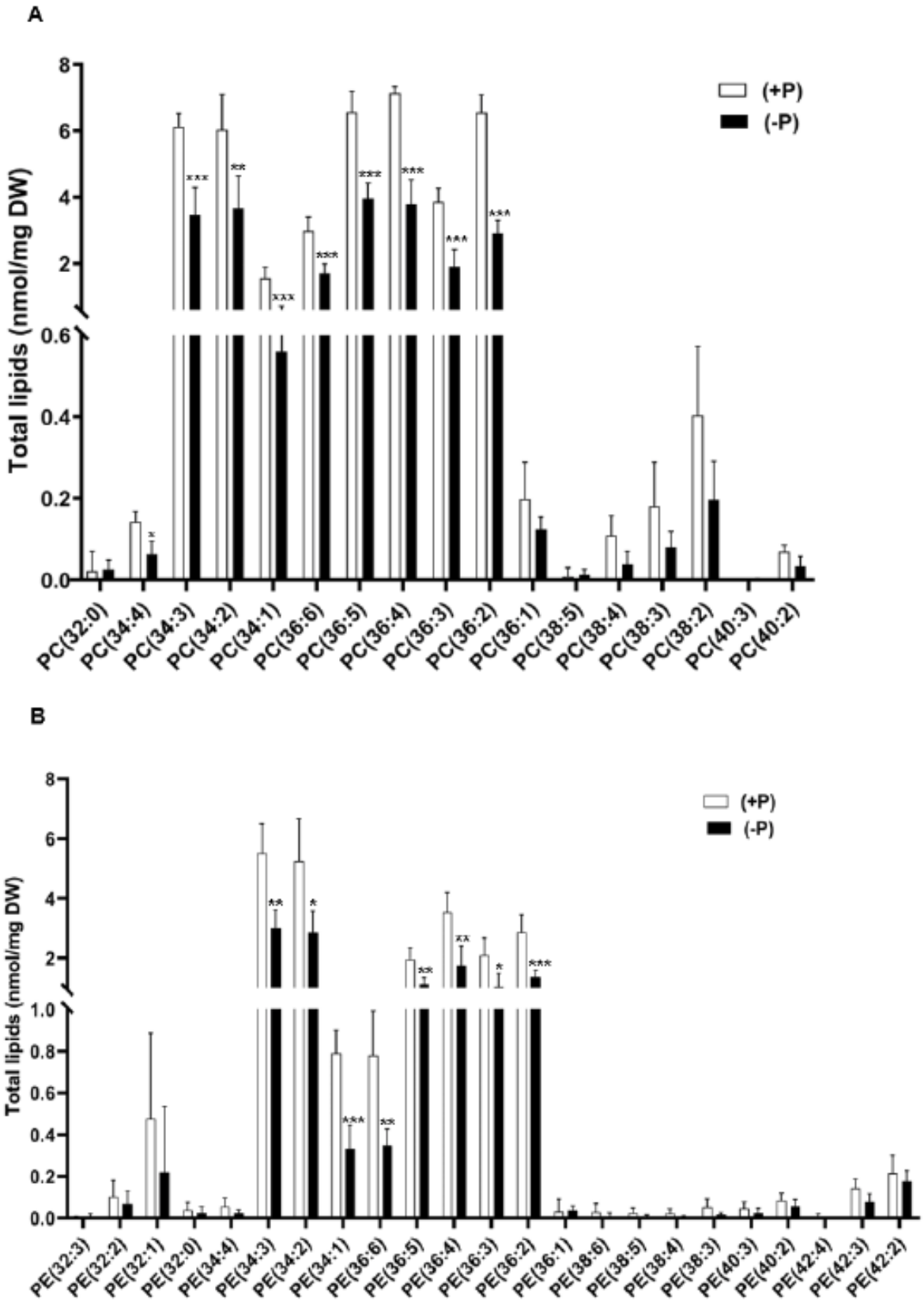

A. Phosphatidylcholine (PC); B. Phosphatidylethanolamine (PE).

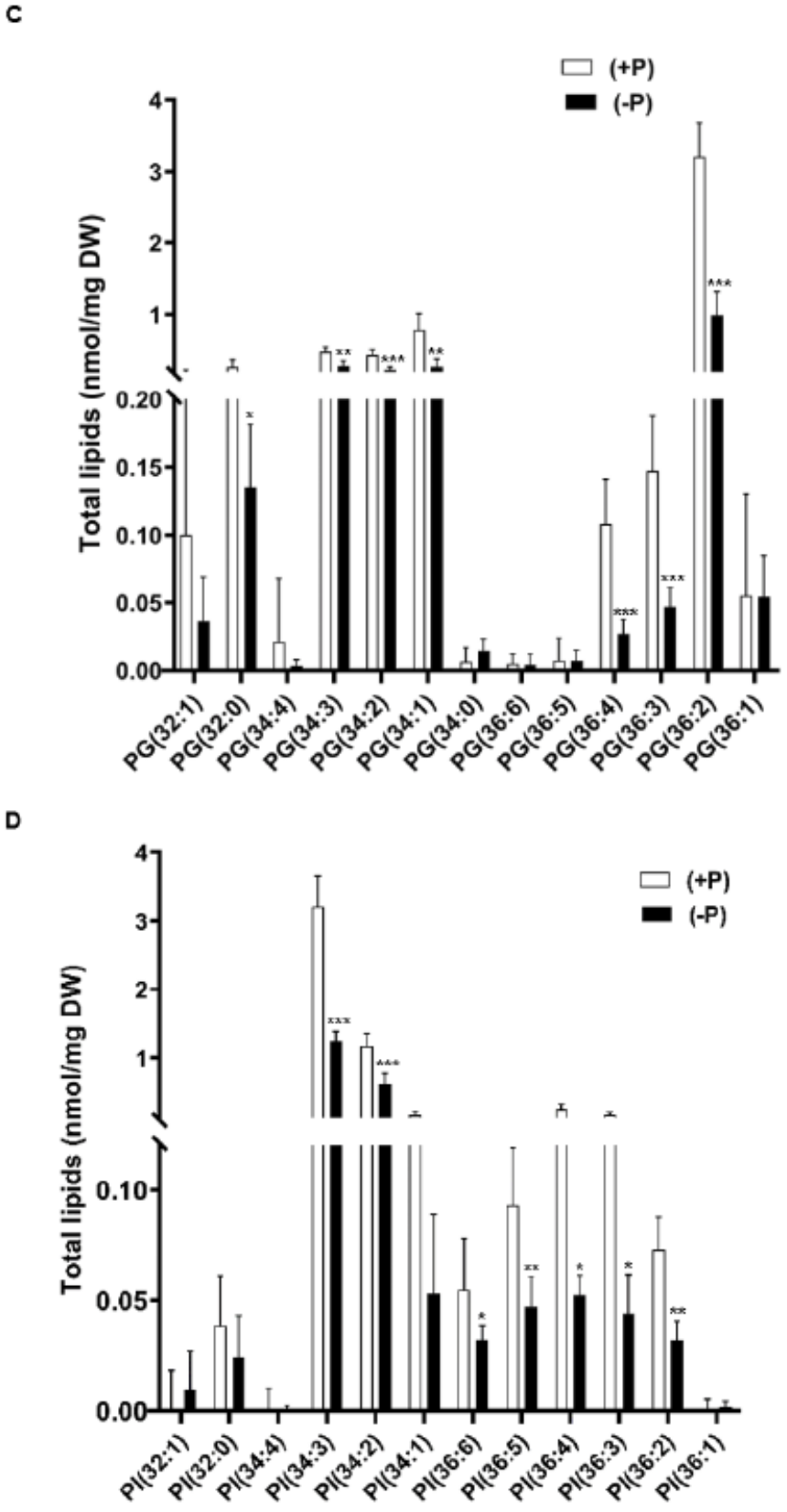

C. Phosphatidylglycerol (PG); D. Phosphatidylinositol (PI).

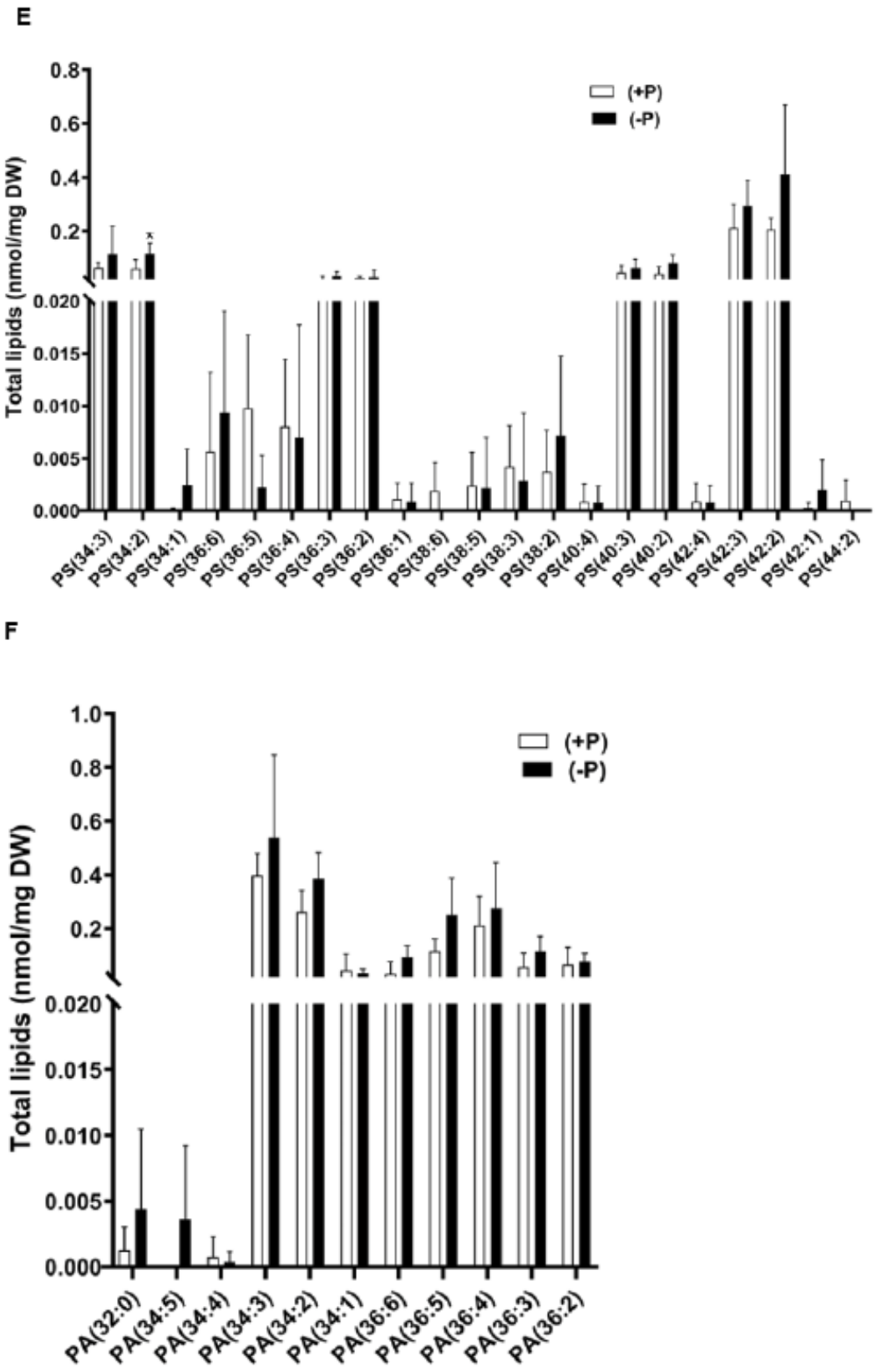

E. Phosphatidylserine (PS); F. Phosphatidic acid (PA).

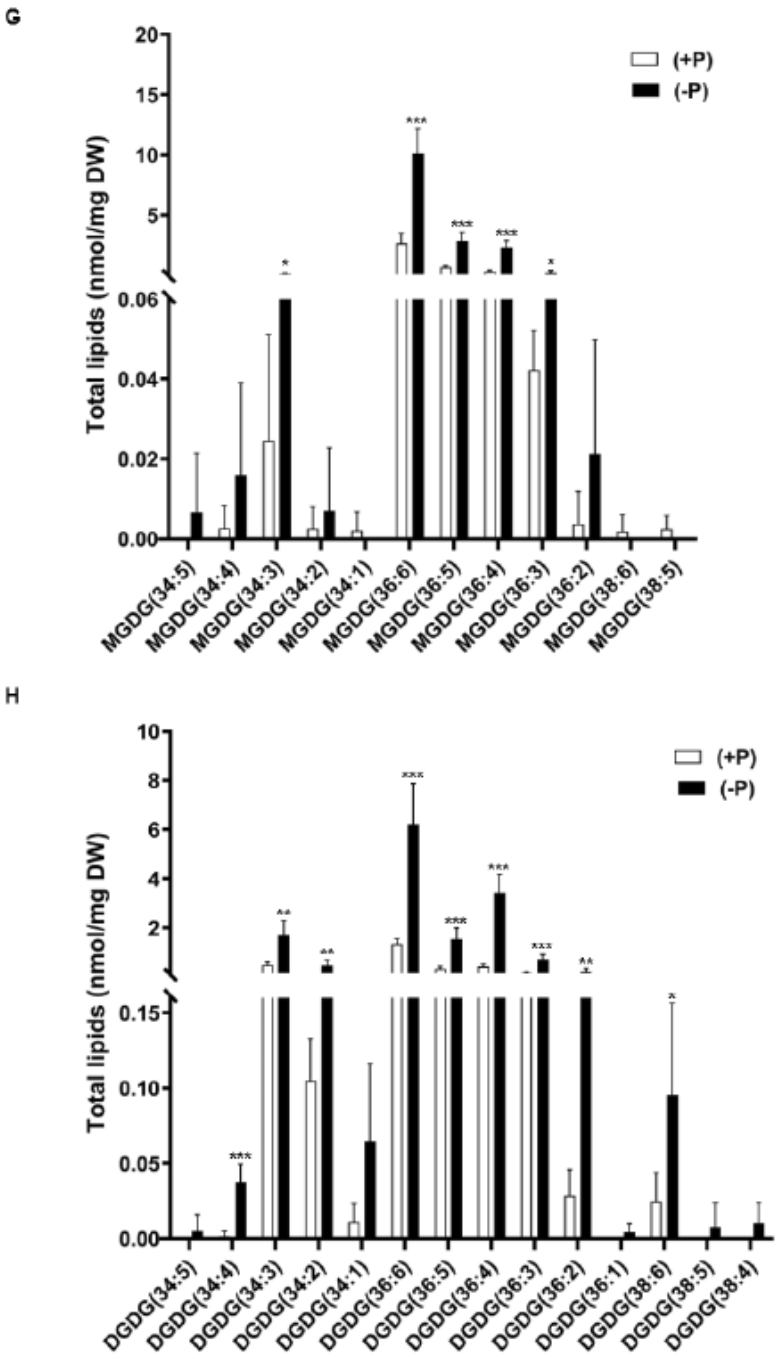

G. Monogalactosyldiacylglycerol (MGDG); H. Digalactosyldiacylglycerol (DGDG).

Supplemental Figure S2.5 Total polar glycerolipids from nodules of *Medicago truncatula* R108 plants.

Plants were grown under sufficient phosphorus (+P) and absence of phosphorus (–P) conditions for 28 days after inoculation with *Sinorhizobium. meliloti* Rm41. Values are expressed as total lipids (nmol/mg dry weight (DW) of tissue) after normalizing with the amount of respective standards. The values are mean ± SD (N =5). Asterisks indicate a significant difference between the control plants (+P) and test plants (-P), as determined using one-way ANOVA analysis; *, P ≤ 0.05; **, P ≤ 0.01; ***, P ≤ 0.001.

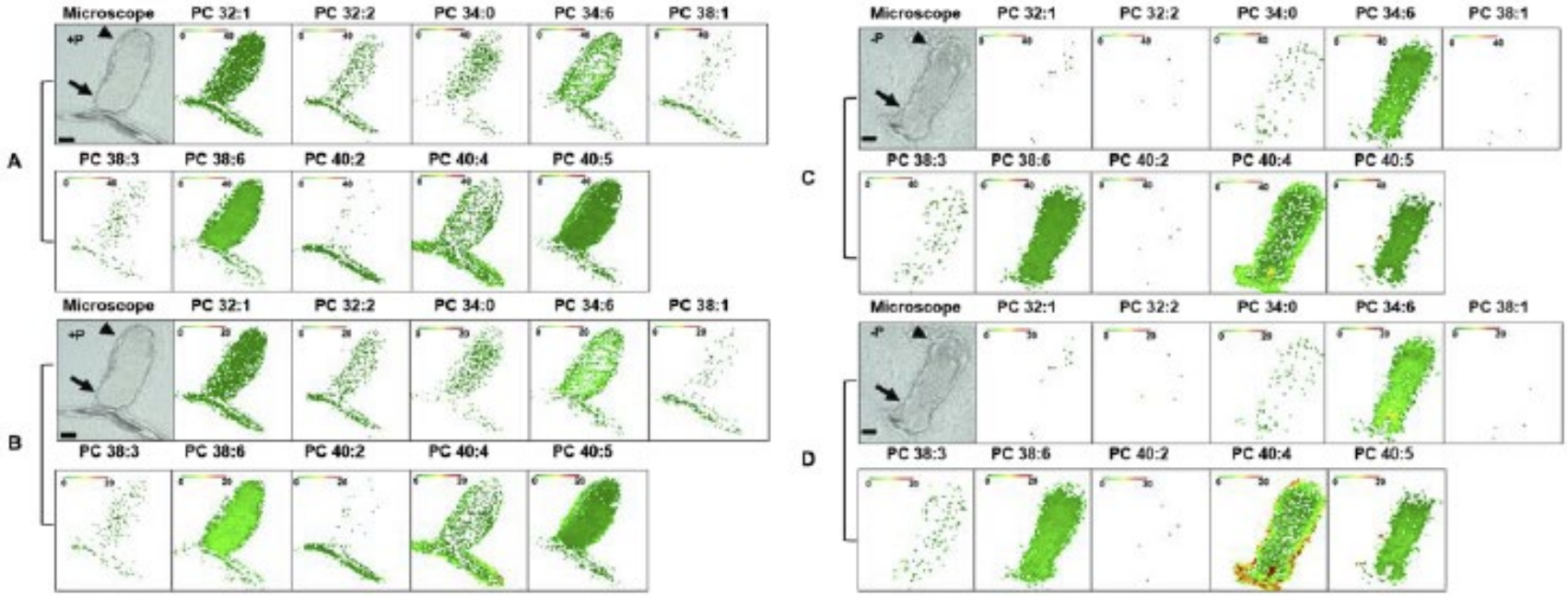

Supplemental Figure S2.6 MALDI-MS imaging of phosphatidylcholine (PC) metabolites in *Medicago truncatula* nodules.

Bright field images of nodules cross section (25µm thick) before coating with DHB matrix grown under sufficient phosphorus (+P); A, B, and absence of phosphorus (–P); C, D are shown on the left. The distributions of selected PC molecular species are shown with fixed mol % to show absolute distribution profiles; A, C and adjusted mol % to show relative distribution profiles; B, D. Bars = 500µm. Proximal zone is indicated by arrowhead and distal zone by arrow. MALDI scale shows mol% with green and red representing low and high levels, respectively. Representative images of N = 5 each for +P and –P.

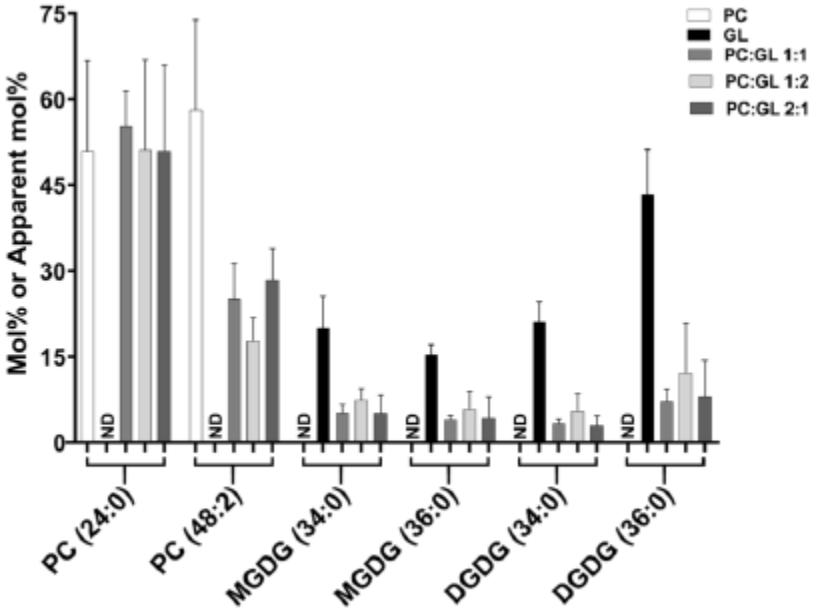

Supplemental Figure S2.7 Suppression of galactolipids by phosphatidylcholine (PC) in matrix-assisted laser desorption/ionization (MALDI).

Phosphatidylcholine (PC) standards (PC 24:0 and PC 48:2) and galactolipid (GL) standards containing monogalactosyldiacylglycerol (MGDG) and digalactosyldiacylglycerol (DGDG); (MGDG 34:0, MGDG 36:0, DGDG 34:0 and DGDG 36:0) were spotted on a slide. Standards were spotted individually and in different ratios as follows: PC, GL, PC/GL 1/1, PL/GL, 1:2 and PL/GL 2/1. The mol% and apparent mol% in PL/GL mixtures were determined by MALDI-MS. N=4. ND=not detected. The values are mean ± SD.

Supplemental Table S2.1 Phosphate (Pi) levels in media during *Medicago truncatula* growth.

DPI*	Total phosphate levels		DPI*	Total phosphate levels	
	Replete, µM	Deprived, µM		Replete, µM	Deprived, µM
1	53.2 ± 4.4	0.0 ± 0.3	15	45.2 ± 1.7	0.0 ± 0.6
2	51.2 ± 1.3	0.6 ± 0.1	16	45.5 ± 0.2	0.1 ± 0.3
3	51.9 ± 3.6	0.1 ± 0.3	17	40.5 ± 1.7	0.2 ± 0.6
4	51.5 ± 3.7	0.0 ± 0.3	18	42.4 ± 2.5	0.0 ± 0.3
5	55.1 ± 7.6	0.4 ± 1.2	19	44.5 ± 4.6	0.2 ± 0.3
6	48.9 ± 3.7	0.0 ± 0.3	20	45.1 ± 1.5	0.0 ± 0.0
7	45.7 ± 1.7	0.2 ± 0.6	21	44.2 ± 3.7	0.1 ± 0.6
8	47.4 ± 2.0	0.1 ± 1.3	22	55.5 ± 8.8	0.2 ± 1.1

(table continues)

DPI*	Total phosphate levels		DPI*	Total phosphate levels	
	Replete, µM	Deprived, µM		Replete, µM	Deprived, µM
9	50.5 ± 5.1	0.0 ± 0.1	23	49.7 ± 3.1	0.2 ± 0.6
10	44.4 ± 2.2	0.2 ± 0.3	24	49.7 ± 2.6	0.4 ± 0.7
11	47.4 ± 3.0	0.4 ± 0.7	25	43.4 ± 5.1	0.1 ± 1.1
12	46.2 ± 0.0	0.6 ± 0.1	26	42.5 ± 1.6	1.7 ± 2.1
13	47.1 ± 3.0	0.4 ± 0.7	27	46.7 ± 1.8	0.3 ± 0.3
14	41.9 ± 1.1	0.1 ± 0.7	28	44.2 ± 2.2	0.6 ± 0.6

*DPI = Days post-inoculation. Phosphate (Pi) levels were assayed daily in aeroponic chambers in Pi replete and Pi deprived growth media. Data are mean values +/- SD. N=3.

Supplemental Dataset S2.1: Suppression Study of Phosphatidylcholine (PC) on Galactolipid Detection in Matrix-Assisted Laser Desorption/Ionization (MALDI).

2.6.1 Results

To address the phenomenon of ion suppression of galactolipids by phosphatidylcholine (PC), we used similar parameters to those employed for imaging the nodule cross sections by MALDI-MS imaging. We observed lower intensities of galactolipids (MGDG 34:0, 36:0 and DGDG 34:0, 36:0) as reported by MALDI-MS when galactolipid standards were spotted in different ratios with PC compared to galactolipid standards alone (Fig. S2.7). When the galactolipid mixture was individually spotted on a MALDI slide, MGDG 34:0 and 36:0 comprised 20 and 15 mol%, while DGDG 34:0 and 36:0 was 20 and 45 mol%, respectively. When this galactolipid standard mix was spotted with PC standard in 1:1 ratio, MGDG 34:0 and 36:0 decreased to an apparent 5 and 4 mol% and DGDG 34:0 and 36:0 to an apparent 3 and 7 mol% respectively (Fig. S2.7). The recovery of MGDG and DGDG 34:0 and 36:0 signal in mol% was negligible when galactolipid and PC standard mixes were spotted in a 2:1 ratio. Further suppression of galactolipids by PC was observed when spotted in a 1:2 ratio. In that case DGDG 34:0 had the lowest apparent abundance of 3 mol% (Fig. S2.7). In contrast, the PC 24:0 signal

showed no ion suppression by galactolipids, while PC 48:2 showed moderate suppression by galactolipids, but not nearly as severe as the suppressive effect of PC on galactolipid (Fig. S2.7).

2.6.2 Discussion

In an effort to evaluate the suppression phenomenon of PC on galactolipids (MGDG and DGDG), we carried out a study using similar parameters that were used for imaging nodule cross sections in MALDI-MS imaging. As shown in Figure S2.7, we observed lower intensities of galactolipids when spotted in different ratios with phospholipids compared to when galactolipids were spotted alone. The reduction in galactolipid signal was at least 75% when spotted along with PC standards compared to being spotted without PCs. This study also evaluated the suppression of PC species by galactolipids in MALD-MS imaging. We found PC 24:0 was not suppressed while PC 48:2 showed moderate suppression by galactolipids, but the amount of suppression was independent of the ratio of PC to galactolipids in the spot sampled by MALDI-MS. We interpret this to mean that if galactolipids are induced in nodules in all parts of the nodule but in varying amounts depending on developmental stage, they will not interfere with PC imaging results. PC has previously been shown to cause ion suppression in MALDI-MS imaging of cotton embryos triacylglycerols (Horn et al., 2012) other phospholipids (PS, PE, PI) from a mixture (Petkovic et al., 2001), tripalmitin from beef and egg yolk (Emerson et al., 2010) and various other studies (Fuchs et al., 2009; Fuchs et al., 2010; Woodfield et al., 2017). The reduction of apparent intensities of other lipids including galactolipids in MALDI-MS imaging by PC thereby makes it difficult to make qualitative or quantitative conclusions. Technological improvements in metabolite and lipid imaging (Stopka et al.,

2018; Colin and Jaillais, 2020) will likely improve our understanding of glycerolipid distribution in nodules beyond.

2.6.3 Materials and Methods

Galactolipids (GL) and phospholipids (PL) standards that were obtained from KLRC were spotted individually and together in different ratios (1:1 PL/GL, 1:2 PL/GL and 2:1 PL/GL) on slides. Matrix (DHB) was sublimed on slides containing the spotted standards and subjected to MALDI-MS imaging as described in the main manuscript methods section.

CHAPTER 3

RESPONSE OF *pdil3* MUTANT TO PHOSPHORUS STARVATION

3.1 Abstract

Phosphorus (P) deficiency in soil in the form of inorganic phosphate (Pi) affects plant growth widely across natural and agricultural ecosystems. Recent reports indicate that long non-coding RNAs (lncRNAs) play a key role in the regulation of various biological processes, including plant response to nutrient stress. One such lncRNA is *PDIL3,* which was first identified and characterized in *Medicago truncatula* by Wang et al., (2017). Studies with *PDIL3* transiently expressed in *Nicotiana benthamiana* suggest a role for this lncRNA in regulating Pi-deficiency signaling and transport (Wang et al., 2017). We investigated impacts of prolonged P stress on growth and development of *pdil3* under symbiotic conditions in comparison with the wild-type (WT) plants. In P starvation, *pdil3* plants showed better shoot growth, accumulated more phosphate in shoots, and had impaired nitrogen fixation activity and less rhizobial occupancy in nodules than WT. Subsequently, matrix-assisted laser desorption/ionization–mass spectrometry (MALDI–MS) imaging was used to spatially map and compare the distribution of phosphatidylcholine (PC) species in nodules of *pdil3* and WT in P-replete and P-deplete conditions. Several PC species showed changes in distributions in *pdil3* nodules compared to WT in both +P and -P conditions.

3.2 Introduction

Recent improvements in high-throughput sequencing technology have shown that more than 90% of the genome in eukaryotes generates huge numbers of non-coding RNAs (ncRNAs) (Chekanova et al., 2007). Based on their length, these ncRNAs are

categorized into small RNAs and long non-coding RNAs (lncRNAs) (Brosnan and Voinnet, 2009; Kim et al., 2011). LncRNAs have more than 200 nucleotides, less protein capacity, and comprise the largest class of ncRNAs (Rinn and Chang, 2012; Chekanova, 2015). The majority of the lncRNAs are transcribed by RNA polymerase II and are expressed in tissue-specific manners (Wilusz et al., 2009). Based on their location in the genome, they can be grouped into sense, intronic, antisense, bidirectional, and intergenic lncRNAs in relative to protein-coding genes (Ponting et al., 2009). Due to their low expression and non- or low-protein-coding potential, lncRNAs were ignored and often regarded as transcriptional noise (Ponting et al., 2009) . LncRNAs are now known to modulate biological processes by regulating their targets' RNA or DNA in either a *cis*-acting or *trans*-acting manner by sequence complementarity (Kornienko et al., 2013). LncRNAs have been identified in Arabidopsis (Ben Amor et al., 2009; Liu et al., 2012; Zhu et al., 2014), rice (Liu et al., 2013; Xu et al., 2016), and poplar (Shuai et al., 2014). Studying lncRNAs in *Medicago truncatula* started gaining traction in the last decade (Wang et al., 2015; Wang et al., 2017; Zhao et al., 2020).

Legumes account for one-third of the world's primary crop production, and often suffer from abiotic stresses (Benedito et al., 2008). Osmotic and salt stress-responsive lncRNAs were reported to play role in biological processes such as signal transduction and detoxification in *M. truncatula* (Wang et al., 2015). Phosphorus (P) is one of the essential nutrients required for plant growth and development. N_2-fixing legumes have a higher demand for P than those grown on mineral N (Sa and Israel, 1991; Schulze et al., 2006). To cope with P deficiency, plants have evolved numerous strategies at morphological, physiological, and molecular levels (Ding et al., 2016; Nath and Tuteja,

2016). Under P-deficient conditions a *PHR1-* (Phosphate Starvation Response 1), miR399-, and *PHO2- (PHOSPHATE 2)* dependent pathway has been established to play a central role in P acquisition (Bari et al., 2006). Lack of P in the medium upregulates *PHR1* and miR399. The expression of *PHO2*, a ubiquitin-conjugating E2 enzyme, a target of miR399 is suppressed by miR399, thereby preventing the degradation of Pi transporters by the ubiquitination pathway resulting in P acquisition (Fig. 3.1) (Burleigh and Harrison, 1997; Shin et al., 2006; Franco-Zorrilla et al., 2007). Many microRNAs and protein-coding genes involved in sensing and responding to P starvation have been identified in plants (Plaxton and Tran, 2011). One such lncRNA, *Phosphate Deficiency-Induced LncRNA* (*PDIL3)* was found to play a role in P starvation in *M. truncatula* via the *PHR1*-miR399-*PHO2* pathway (Fig. 3.1) (Wang et al., 2017).

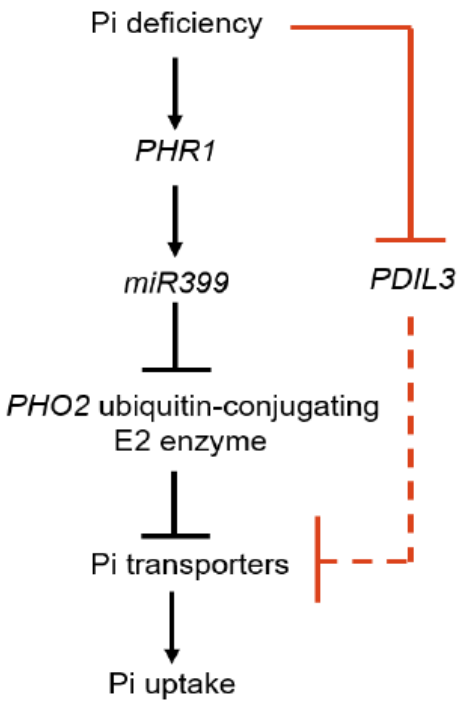

Figure 3.1: **A model for Pi signaling involving *PHR1*, *miR399*, *PHO2* and *PDIL3* in *M. truncatula*.**

Adapted from Wang et al., 2017). The red lines represent pathways identified in Wang et al., 2017. Arrows indicate upregulation or positive effects, whereas lines ending in a short bar indicates downregulation or negative effects.

In the Wang et al. (2017) study, plants were exposed to P stress for up to 48 hours in non-symbiotic conditions (Wang et al., 2017). Wang et al., 2017 showed sequence complementarity between *PDIL3* and phosphate transporter genes and suggested that *PDIL3* negatively regulated the expression of Pi transporter gene by a mechanism that depends on complementarity (Wang et al., 2017). The absence of *PDIL3* in *pdil3* mutants thus upregulates the transcript of Pi transporter gene in roots of *M. truncatula,* thus resulting in higher accumulation of P in the mutant's shoot compared to the wild-type (Fig. 3.1) (Wang et al., 2017).

We recently reported a detailed study investigating the growth of *M. truncatula* wild type plants under prolonged periods of starvation for four weeks post nodulation in aeroponic conditions (Dokwal et al., 2021). In this study, P starved plants had decreased SNF, impaired growth, and lowered phosphate in leaves, roots, and nodules than P sufficient plants. Additionally, results showed changes in membrane lipid composition and spatial distributions of phosphatidylcholine (PC) in nodules from both P starved and control plants, providing insights on membrane lipid remodeling in developed SNF nodules during P stress were reported (Dokwal et al., 2021). We hypothesize that *pdil3* mutants would show distinct differences in lipid remodeling during P deprivation compared to WT. In this chapter, I first investigated the phenotype of the *pdil3* plants compared to wild type when grown under nodulated conditions in absence of P for four weeks for comparison to previous work. Second, we addressed whether PC species distribution would change in different growth conditions using MALDI-MS imaging.

3.3 Materials and Methods

3.3.1 Identification and Confirmation of Homozygotic *pdil3* Mutants

M. truncatula seeds were obtained from the Noble Research Institute (Ardmore, OK) that contained a known *Tnt1* insert in the *PDIL3* gene (Wang et al. 2017). The seeds were from a bulked population that contained both homozygous and heterozygous plants (J. Wen, personal communication). To identify homozygotic *pdil3* mutants (Wang et al., 2017), seeds of line NF21369 were germinated and grown to maturity. Genomic DNA from *M. truncatula* WT and *pdil3* mutant was isolated from leaves for PCR genotyping as described in (Veerappan et al., 2016). Homozygotes were identified using two sets of PCR primers (Wang et al., 2017) as follows: (PDIL3- F+PDIL3-R and PDIL3-F+TNT1-R). Primers used for the identification of homozygous *pdil3* mutants are listed below in Table 3.1. Identified *pdil3* homozygous mutants were propagated for further study.

Table 3.1: Sequences of primers used for identification of homozygous *pdil3* plants

Primers	Sequence (5'-3')
PDIL3-I-F	GCGTGGCTTGTTACTTGA
PDIL3-I-R	AAATCTTCTGTTGGCATA
TNT1-I-F	ACAGTGCTACCTCCTCTGGATG
TNT1-I-R	CAGTGAACGAGCAGAACCTGTG

3.3.2 Seed Collection, Surface Sterilization and Germination

M. truncatula R108 (WT) and NF21369 *(pdil3)* pods were crushed for seed collection. Concentrated H_2SO_4 and 6 % (v/v) sodium hypochlorite were used for seed scarification and sterilization, respectively. After which seeds were germinated in 1 % w/v agar petri dishes as described in (Dokwal et al., 2021).

3.3.3 Plant Growth in Aeroponic System

Germinated seedlings were grown in aeroponic chambers as previously described (Veereshlingam et al., 2004; Barker et al., 2006). WT and *pdil3* plants were grown

simultaneously in two aeroponic chambers with Lullien's medium and inoculated with *S. meliloti* Rm41 carrying the *hemA:lacZ* reporter (Lullien et al., 1987) as described previously in +P and -P conditions (Dokwal et al., 2021).

3.3.4 Plant Phenotypes and X-Gal Staining

Plants were phenotyped at 28 DPI. Plants and nodules were photographed by camera (Canon model PC1562; Canon USA, Huntington NY, USA) and microscopically (Leica dissection microscope, MSV269; Buffalo Grove, IL, USA). Shoot and root (root and nodule) fresh and dry weights were measured. Nodule length and width were measured, and lateral roots were enumerated. The acetylene reduction assay (ARA) was used to measure nitrogenase activity as previously used in (Dilworth, 1966; Dokwal et al., 2021). Nodules were fixed and stained with X-Gal as described (Veereshlingam et al., 2004). Nodule sections, 50 µm thick were obtained using a 1000 Plus model vibratome (Vibratome, St. Louis, MO). Sections were observed and documented under an Olympus BX50 microscope using bright-field settings. One-way ANOVA tests were used to determine statistical significance.

3.3.5 Total Phosphorus and Inorganic Phosphate Quantitation

Twenty to thirty mg of tissues were collected, frozen and ground to fine powder in liquid nitrogen. Total phosphorus and inorganic phosphate were quantified from WT and *pdil3* plants using the colorimetric assay described in (Chiou et al., 2006; Dokwal et al., 2021). Six replicates of each growth condition for each tissue type (leaves, roots, and nodules) were processed and analyzed. One-way ANOVA tests were used to determine statistical significance.

3.3.6 MALDI MS Imaging

Twenty eight DPI nodules were fixed, embedded in gelatin, and sectioned (25 µm thick) using a cryotome (Leica CM1950, Leica Microsystems, Buffalo Grove, IL, USA) as previously described in (Dokwal et al., 2021). DBH (2,5 dihydroxybenzoic acid) was used as a matrix and applied by sublimation (Hankin et al., 2007) prior to imaging of PC. DHB coated nodules were imaged on hybrid MALDI-LTQ-Orbitrap XL mass spectrometer and images for PC molecular species ([M+H]+ adducts) were generated using metabolite imager as detailed in (Horn and Chapman, 2014; Dokwal et al., 2021). Five individual nodules from different plants grown in +P and -P conditions were used for MALDI-MS imaging.

3.4 Results

3.4.1 P Deficiency has Varying Impact on Growth, Biomass, and Symbiotic Phenotype of *pdil3* Compared to R108

Genotyping analysis using primers specific to *PDIL3* (PDIL3- F+PDIL3-R and PDIL3-F+TNT1-R) was carried to identify homozygous individuals with *Tnt1* insertions from a subpopulation of seeds obtained from the Noble Research Institute harboring a known *Tnt1* insert in *PDIL3* (Wang et al. 2017). If the first reaction was negative (PDIL3-F and PDIL3-R) and the second was positive (PDIL3-F and TNT1-R), this indicates that the plant was a homozygote (Fig. 3.2 A and B). Homozygous plants were propagated for seeds and later used in the study.

To induce P deprivation, *pdil3* and R108 (WT) plants were grown side by side in aeroponics chambers for five days in N and P replete media, then starved for N for five days in presence of full P. The plants were subsequently starved for P at the same time as they were inoculated with *Sinorhizobium meliloti* Rm41. Plants in controlled conditions

were grown in parallel in P replete conditions (+P). After 4 weeks, -P plants were evaluated for P deficiency characteristics and compared to those grown side-by-side in P replete conditions as in Chapter 2. In -P conditions, *pdil3* plants showed less impaired growth compared to WT, with an increased shoot fresh and dry weight. No significant difference in root system (root + nodule) fresh weight and no significant difference in dry weight were noted between *pdil3* and WT irrespective of the growth conditions (Fig. 3.2 C-G).

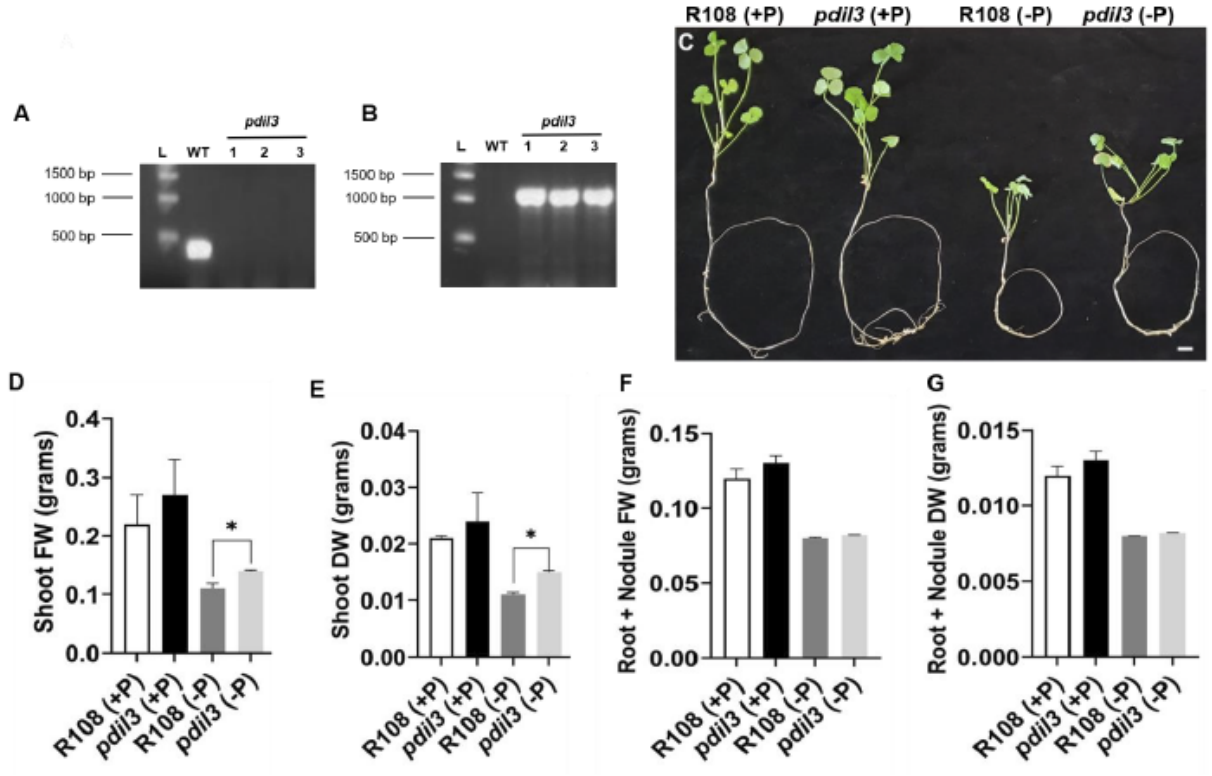

Figure 3.2: **Identification and characterization of homozygous *pdil3* plants in phosphorus (P) depleted conditions.**

A and B Identification of homozygotic *pdil3* mutants using two sets of primers. A. *PDIL3*-F+*PDIL3*-R; B. *PDIL3*-F+*TNT1*-R. C. Appearance of wild-type R108 and *pdil3* under sufficient phosphorus (+P) and absence of phosphorus (–P) after 28 days post inoculation (DPI) with *Sinorhizobium meliloti* Rm 41. Scale bar 2 cm; D. Average Shoot Fresh weight (FW); E. Average Shoot Dry weight (DW); F. Average Root+Nodule Fresh weight (FW); G. Average Root+Nodule Dry weight (DW). N=20 for D, E, F, and G. The values are mean ± SD. Asterisks indicate a significant difference between WT and *pdil3*, as determined using one-way ANOVA analysis; *, P ≤ 0.05.

Nodules of WT and *pdil3* were pink, regardless of the growth conditions (Fig. 3.3 A-D). The symbiotic phenotypes of the *pdil3* were assessed in the presence and absence of P, using *S. meliloti* strain Rm 41 carrying a *hemA:lacZ* reporter gene.

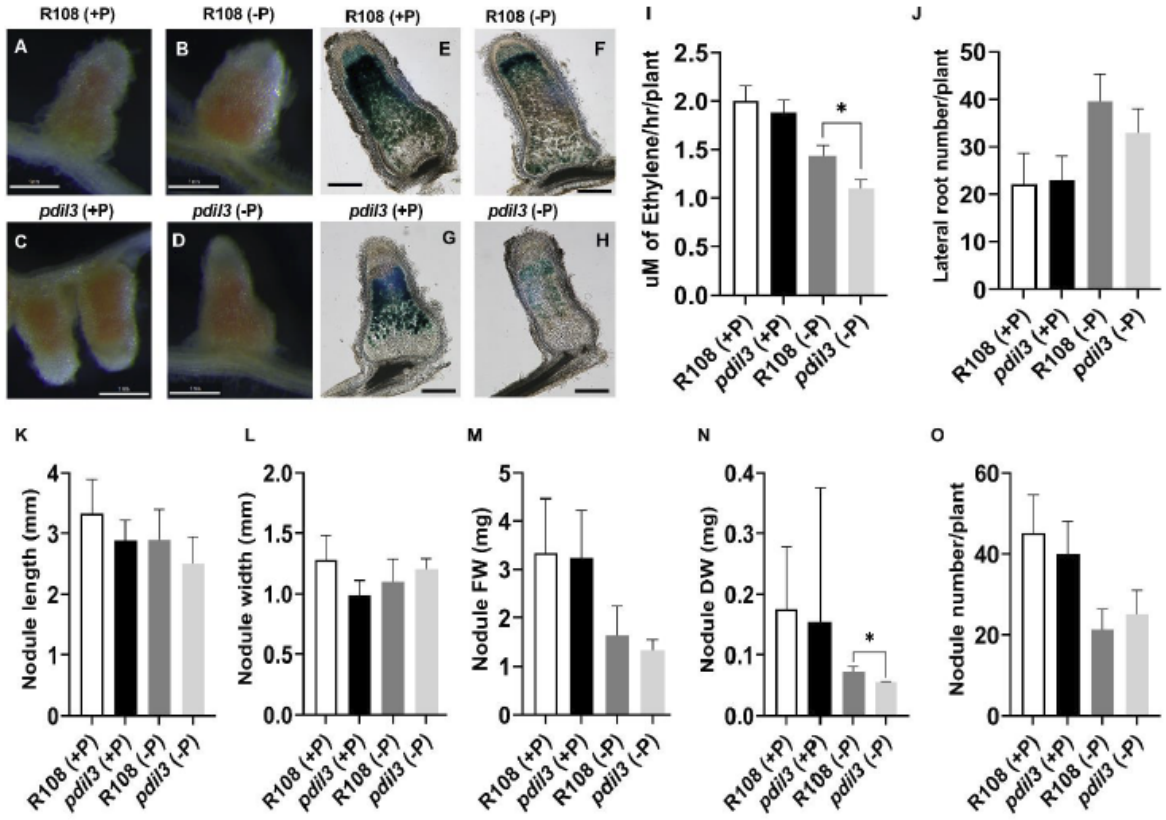

Figure 3.3: **Characteristics of nodulated root system of *pdil3* and R108 in phosphorus (P) depleted conditions.**

A and B. Images of nodules from R108 plants; C and D. Images of nodules from *pdil3* grown under sufficient phosphorus (+P) and absence of phosphorus (–P) conditions respectively, scale bar – 1 mm. E and F. Histochemical staining of *Sinorhizobium meliloti* Rm41 carrying *hemA:lacZ* reporter from R108 nodules, G and H from *pdil3* grown under +P and –P conditions respectively, scale bar – 0.5mm. I. Acetylene reduction activity assayed using whole plant after 28 DPI with *Sinorhizobium meliloti* Rm41; N=5. J. Lateral root number; K. Nodule length; L. Nodule width; M. Nodule fresh weight (FW); N. Nodule dry weight (DW); O. Nodule number. N = 20 for figures J, K, L, M, N and O. The values are mean ± SD. Asterisks indicate a significant difference between the R108 and *pdil3*, as determined using one-way ANOVA analysis; *, P ≤ 0.05.

The intensity of the 5-bromo-4-chloro-3-indolyl-β-D-galactopyranoside staining of *lacZ*-expressing rhizobia revealed that nodules from WT and *pdil3* harbored fewer rhizobia in -P conditions, with *pdil3* -P nodules showing lower rhizobial occupancy in zone II and

interzone II-III than WT -P nodule (Fig. 3.3 E-H). In +P conditions, *pdil3* plants had no significant differences from WT. In -P conditions, *pdil3* plants had reduced nitrogenase activity compared to WT as showed by acetylene reduction assay (ARA) (Fig. 3.3 I). The nodulated root systems of *pdil3* were found to have higher lateral root numbers like WT in P starvation (Fig. 3.3 J). No differences were observed in nodule length, width, fresh weight, and nodule number between *pdil3* and WT in +P and -P environments, while -P nodule dry weight for *pdil3* decreased significantly compared to -P WT (Fig. 3.3 K-O). Leaves from *pdil3* plants in -P conditions had higher inorganic phosphate (Pi) and total P content, while roots and nodules showed reduced levels of Pi and total P than WT under P stress (Fig. 3.4 A-F).

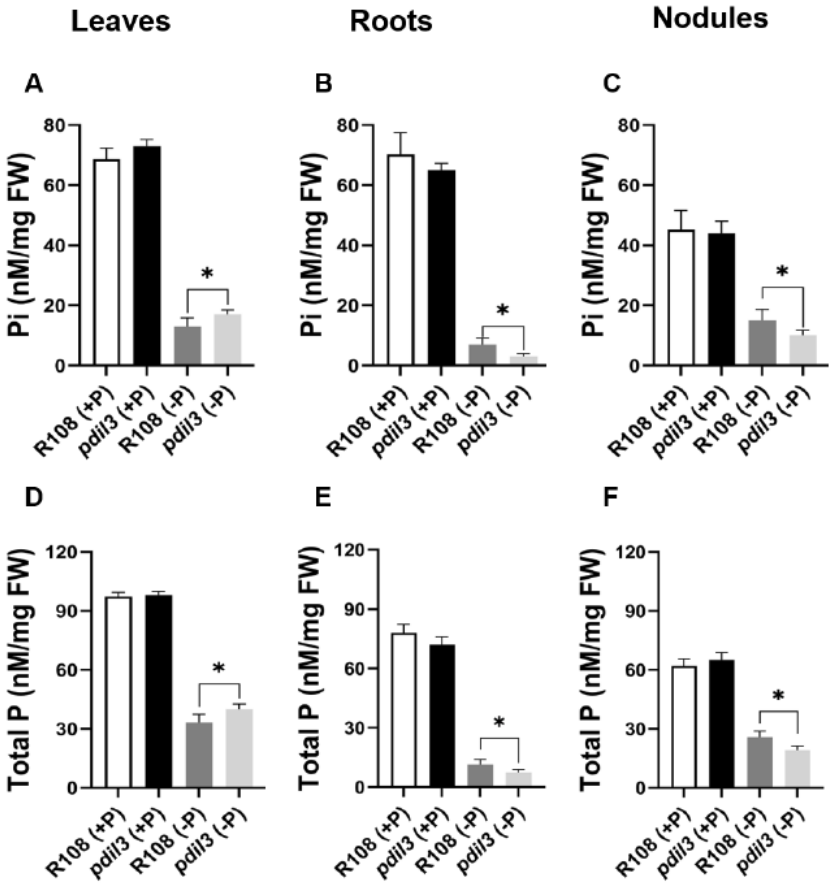

Figure 3.4: **Total phosphorus and inorganic phosphate content in leaves, roots, and nodules of *pdil3 and* R108 plants in phosphorus (P) depleted conditions.**

A, B, and C. Inorganic Phosphate (Pi) content in leaves, roots, and nodules of *pdil3* and R108 plants grown under sufficient phosphorus (+P) and absence of phosphorus (–P). D, E, and F. Total phosphorus content in leaves, roots, and nodules of *pdil3* and R108 plants grown under +P and –P conditions. N=6. The values are mean ± SD. Asterisks indicate a significant difference between WT and *pdil3*, as determined using one-way ANOVA analysis; *, P ≤ 0.05.

3.4.2 MALDI-MS Imaging Reveals Heterogenous Distribution of PC Species in *pdil3* Nodules

Among the membrane glycerolipids, PC species are the most abundant phospholipid class present in nodules (Gaude et al., 2004; Dokwal et al., 2021). PCs contain a quaternary ammonia group with a permanent positive charge, enabling their detection in tissue sections. Matrix-assisted laser/desorption ionization-mass spectrometry (MALDI-MS) imaging, a semi-quantitative technique has been used to spatially map distribution of PC in nodules of *M. truncatula* (Dokwal et al., 2021), animal tissues (Jackson et al., 2007; Chen et al., 2009; Fuchs et al., 2010), barley germinating seeds and *Brassica napus* developing seeds (Gorzolka et al., 2016; Woodfield et al., 2017; Lu et al., 2018; Colin and Jaillais, 2020). Additionally, we recently showed that differences in spatial distributions of PC observed in virtually dissected WT nodules (proximal, central, and distal; see chapter 2) during P stress by MALDI-MS imaging is semi-quantitative. It was compared and validated using ESI-MS analysis of extracted lipids from separated nodule sections (Dokwal et al., 2021). Thus, we used MALDI-MS imaging to examine and compare changes in each PC species distribution in nodules of *pdil3* with the WT in +P and -P treatments. Image maps for all the PC species created at the same scale showed that most PCs declined in abundance in -P *pdil3* nodules (Supp. Fig. S3.1). To compare whether there were changes in distribution of particular PC species in -P WT and *pdil3* nodules, we created image maps with similarly adjusted mol%

values of +P and -P nodules for each species. These data revealed that many PC species changed distribution in *pdil3* +P and -P nodules compared to WT.

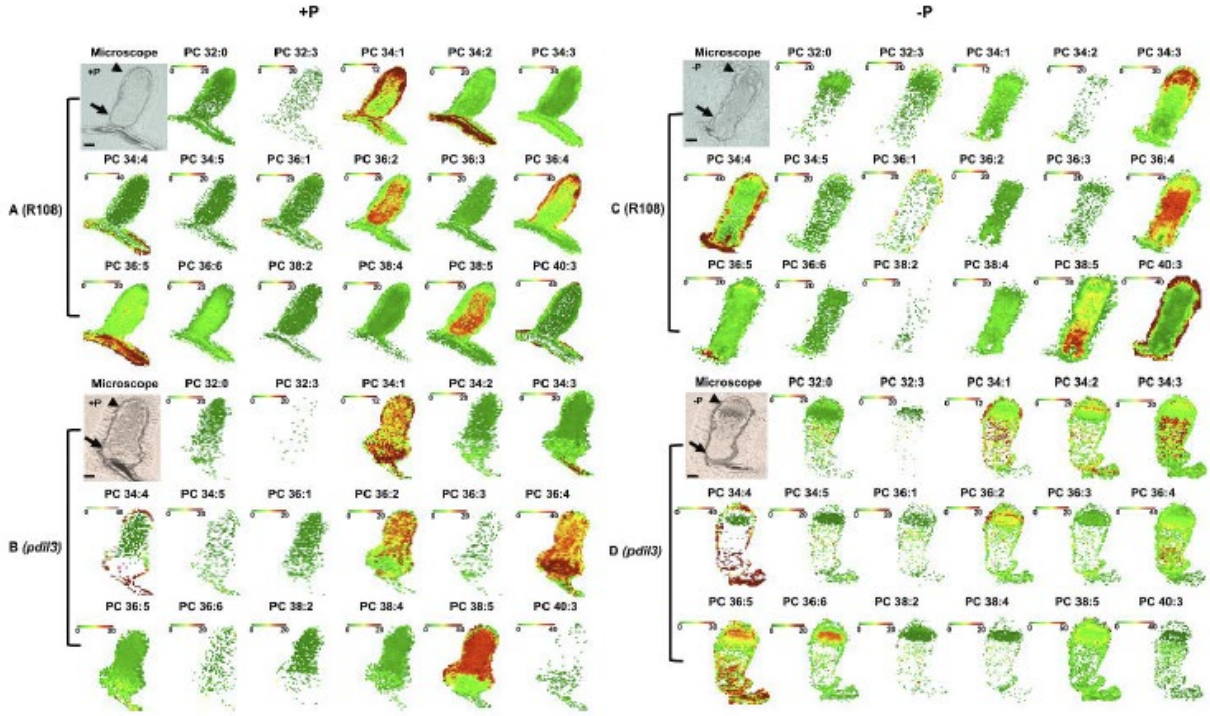

Figure 3.5: **MALDI-MS Imaging of phosphatidylcholine (PC) metabolites in *pdil3* nodules.**

A, B. Bright field images of R108 and *pdil3* nodule cross-section (25 µm) before coating with dihydroxybenzoic acid (DHB) matrix grown under +P. C, D. Bright field images of R108 and *pdil3* nodules cross-section (25 µm) before coating with DHB matrix grown under -P are shown on the left. A, B, C, and D represent Adjusted mol % distribution profiles. Bars = 500 µm. Proximal zone is indicated by arrowhead and distal zone by arrow. MALDI scale shows mol% with green and red representing low and high levels, respectively. Representative images of N = 5 each for +P and –P.

PC 34:1 and 36:4 were most abundant in peripheral tissues of WT +P nodules and were highly abundant throughout the cross-section of *pdil3* +P nodule. In contrast, distribution of PC 36:4 was very low in central part of *pdil3* nodule compared to WT under P stress (Fig. 3.5 A-D). In a similar vein, PC 36:2 and 38:5 species, which were both abundant in the central parts of WT +P nodule, were observed to have lower distribution in proximal part of *pdil3* +P nodule (Fig. 3.5 A and B). In -P conditions, PC 36:2 species had lowered distribution throughout the WT nodule but were fairly abundant in zone I of

pdil3, PC 38:5 was present in low abundance in *pdil3* nodule but had high abundance in the proximal parts of WT nodule (Fig. 3.5 C and D). In P starvation spatial changes observed in WT and *pdil3* nodules for important PCs like 38:5 and 36:2 do not seem to colocalize with the presence of rhizobia as noted on the X-gal staining (Fig. 3.3 F, H and Fig. 3.5 C, D). Another key PC species, PC 36:5 had lower abundance in *pdil3* +P nodules than WT; surprisingly its abundance increased in the apical and distal regions of *pdil3* nodules under P starvation compared to WT (Fig. 3.5 A-D). Spatial localization of PC 36:5 in -P *pdil3* and WT nodule was also distinct than the presence of rhizobia (Figs. 3.3 F, H and 3.5 C, D). Curiously, PC 34:3 in -P conditions had relatively higher abundance in central and proximal part of *pdil3* nodule as compared to distal part of Zone II in WT (Fig. 3.5 C and D). Some species did not show major changes in spatial distributions between WT and *pdil3* nodules regardless of the growth conditions (Fig. 3.6).

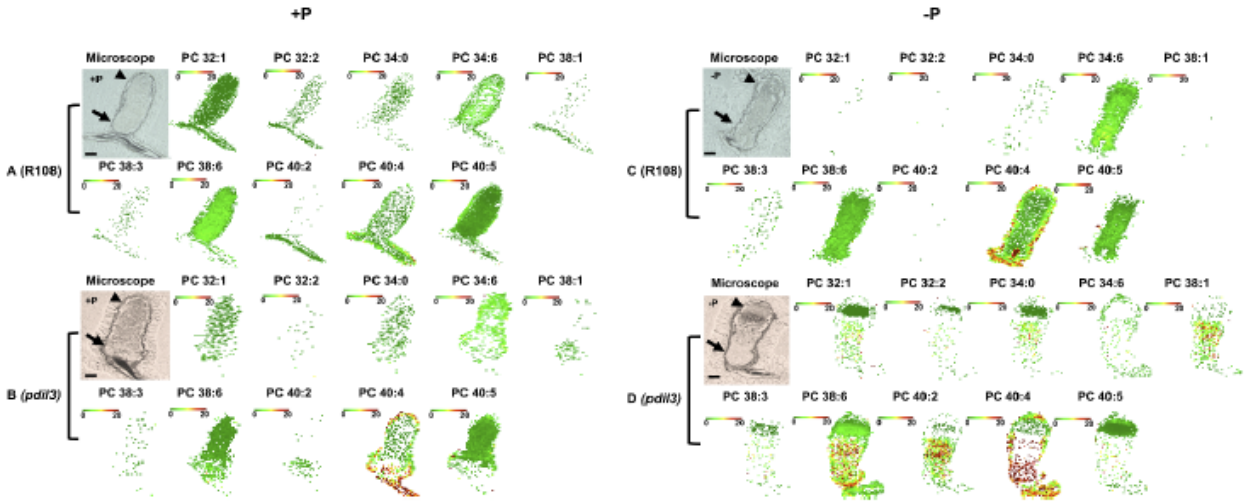

Figure 3.6: **MALDI-MS imaging of phosphatidylcholine (PC) metabolites in *pdil3* nodules.**

A, B. Bright field images of R108 and *pdil3* nodule cross-section (25 µm) before coating with dihydroxybenzoic acid (DHB) matrix grown under +P. C, D. Bright field images of R108 and *pdil3* nodules cross-section (25 µm) before coating with DHB matrix grown under -P are shown on the left. A, B, C, and D represent Adjusted mol % distribution profiles. Bars = 500 µm. Proximal zone is indicated by arrowhead and distal zone by arrow. MALDI scale shows mol% with green and red representing low and high levels, respectively. Representative images of N = 5 each for +P and –P.

3.5 Discussion

P is a key component of many macromolecules and ATP, and plays a key role in regulating enzymatic reactions and signal transduction (Chiou and Lin, 2011; Dai et al., 2016). Despite high amounts of total P in soils, the inorganic phosphate (Pi) that can be directly acquired by plants is low, and globally approximately 70% of cultivated land suffers from Pi deficiency (Plaxton and Tran, 2011). To cope with P deficiency, plants have evolved numerous strategies to acquire Pi from soils. The involvement of miR399 and *PHO2* in the regulation of Pi acquisition has been well established in plants (Bari et al., 2006). Additionally, *PDIL3* (lncRNA) is predicted to negatively regulate the expression of Pi transporter in *M. truncatula* by sequence complementarity (Wang et al., 2017) (Fig. 3.1). P deficiency down-regulates *PDIL3* resulting in up-regulation of Pi transporter (Wang et al., 2017) involved in P acquisition. Higher P contents in the leaves of Pi-deficient *pdil3* than those in WT under non-symbiotic conditions was reported in Wang *et al*., 2017, thus demonstrating a regulatory role in Pi acquisition (Wang et al., 2017). It is important to note that Wang et al. (2017) studied *pdil3* mutants in non-symbiotic, N replete growth conditions.

This study focused on studying the impact of severe P deficiency on growth, symbiotic nitrogen fixing efficiency, and changes in spatial distribution of PC species in nodules of *pdil3* compared to WT. We have confirmed in our previous study that, in symbiotic conditions, growth of *M. truncatula* is impaired in P deprivation compared to +P plants in our aeroponic growth system, showing that -P plants were stressed similarly to those in previous studies of P starvation in *M. truncatula* (Sulieman et al., 2013; Sulieman et al., 2013), *M. sativa* (Sulieman et al., 2013; Sulieman et al., 2013), rice (Li et al., 2001),

A. thaliana (Williamson et al., 2001; Morcuende et al., 2007), and switchgrass (Ding et al., 2021). We used the previously established aeroponics growth system for this study (Dokwal et al., 2021). In severe P starvation, *pdil3* plants had better shoot growth, increased shoot fresh and dry weight, but reduced nitrogen fixation activity and rhizobial occupancy (Figs. 3.2 and 3.3). Differences in nodule phenotype were observed by X-gal staining of rhizobia, where, in P sufficient conditions, rhizobia were primarily observed throughout the central part including zone II, interzone II/III, and zone III of WT and *pdil3* nodules (Fig. 3.3 E and G). In -P conditions, WT nodules had rhizobia restricted to distal part of zone II with some faint localization in interzone II/III, probably followed by zone IV extending to the distal end of the nodule (Fig. 3.3 F). *pdil3* nodules had fewer rhizobia in distal part of zone II and interzone II/III than -P WT nodules revealing distinctive patterns of rhizobial localization and manifesting developmental perturbations in different zones that appeared to be occurring more in *pdil3* nodule development under P starvation (Fig. 3.3 F and H). Nitrogenase activity associated with differentiated bacteroids in zone III was also reduced in *pdil3* nodules compared to WT under low P environments (Fig. 3.3 I). A higher accumulation of P was observed in leaves of *pdil3* than WT (Fig. 3.3 A and D), while -P roots and nodules of *pdil3* had lower P content than WT (Fig. 3.3 B, C, E and F). Thus, growth of nodulated root systems were more impacted than shoots in *pdil3* under P stress and symbiotic conditions.

PC species are the major type of membrane glycerolipid in the nodules of *M. truncatula* and other legumes (Gaude et al., 2004; Dokwal et al., 2021). Under P deprivation, the nodules of *M. truncatula* and other lipids showed increases in galactolipids like monogalactosyldiacylglycerol (MGDG) and digalactosyldiacylglycerol

(DGDG) with simultaneous decrease in major phospholipids like PC and phosphatidylethanolamine (PE) (Gaude et al., 2004; Si et al., 2019; Dokwal et al., 2021). In this study, we wanted to compare the response of the *pdil3* mutant to WT for differences of PC distribution. If *PDIL3*'s effects are uniform throughout the plant, one would expect to see similar nodule phenotypes with respect to PC species' distributions in *pdil3* mutant nodules as WT, with the only changes reflecting differences in the positions of the developmental zones in *pdil3* nodules as compared to WT. If *PDIL3*'s are not uniform in the plant, one would anticipate seeing spatial distribution differences.

PC 36:4 which was highly abundant in the periphery of the WT +P nodule had completely re-localized in the central part i.e., zone III under starved conditions, exhibiting distributions different than that of the rhizobia as observed by X-gal staining. In case of *pdil3*, PC 36:4 was highly abundant throughout the central part of the +P nodule with distribution that was somewhat similar to starved WT nodule. But, in -P conditions, PC 36:4 had drastically reduced abundance throughout the *pdil3* nodule, again, manifesting distinct localization patterns than rhizobia (Figs. 3.3 E-H and 3.5). PC 36:5 and 36:6 throughout had similar abundance in +P and -P nodules of WT and +P nodule of *pdil3*. In -P conditions, their abundance increased fairly in zone II of *pdil3* nodule colocalizing with the rhizobia (Figs. 3.3 E-H and 3.5). In a similar vein, PC 34:3 had similar distribution in +P nodules of WT and *pdil3*. In contrast it changed its localization in the apex (zone I and II) of the -P WT nodule and zone III and IV of -P *pdil3* nodule, colocalizing to some extent with the presence of rhizobia (Figs. 3.3 E-H and 3.5). Our results showed spatial differences and heterogeneity of many PC species between WT and *pdil3* in both +P and -P conditions (Fig. 3.5 A-D). These differences in spatial distribution of PC species

observed here may be due to differences in cell- and tissue-specific regulation of membrane lipid metabolism during nodule development in *pdil3*. One potential explanation for these differences is that *PDIL3*, and potentially other genes regulating the plant's responses to P stress, are themselves regulated differentially in nodules undergoing P stress.

In -P symbiotic growth conditions, our acetylene reduction assay data, differential P accumulation observed in leaves and nodulated roots, along with changes observed in PC spatial distribution strongly suggest that *PDIL3*'s role is not just suppression of the Pi transporter, but it may also influence P partitioning between shoots and nodulated roots, which needs to be investigated. A global metabolic profiling study would certainly help in this aspect; plant metabolomics has become a powerful tool to explore various aspects of plant physiology and response to nutrient stress (Hong et al., 2016). Additionally, metabolomics has the ability to detect a vast array of metabolites with a simple extraction, thereby allowing quick and precise analysis of metabolites (Kumar et al., 2017).

Recent reports have provided evidence highlighting regulatory roles of lncRNAs in numerous biological processes in plants (Chekanova, 2015). For instance, in *A. thaliana* two lncRNAs *COOLAIR* transcribed from the antisense strand of *FLOWERING LOCUS (FLC)* are involved in regulation of flowering by altering the expression of *FLC* (Swiezewski et al., 2009). *APOLO* and *ASCO* have been shown to control root development in *A. thaliana* (Ariel et al., 2014). *H1D1* facilitates photomorphogenesis in *A. thaliana* induced by red light (Wang et al., 2014). Lowered expression of *LDMAR* leads to male sterility under long-day conditions (Ding et al., 2012), while *GmEnod40* is participates in the control of sucrose use in nitrogen-fixing nodules of soybean (Yang et

al., 1993; Rohrig et al., 2002; Campalans et al., 2004). In this study, we have investigated further the metabolic role of *PDIL3* in response to low P environments. The shoot phenotype observed in this study shows that the P taken up by the roots is translocated preferentially into shoots for important biological functions, such as photophosphorylation, at the expense of roots nodules being stressed with low P amounts.

3.6 Supplemental Data for Chapter 3

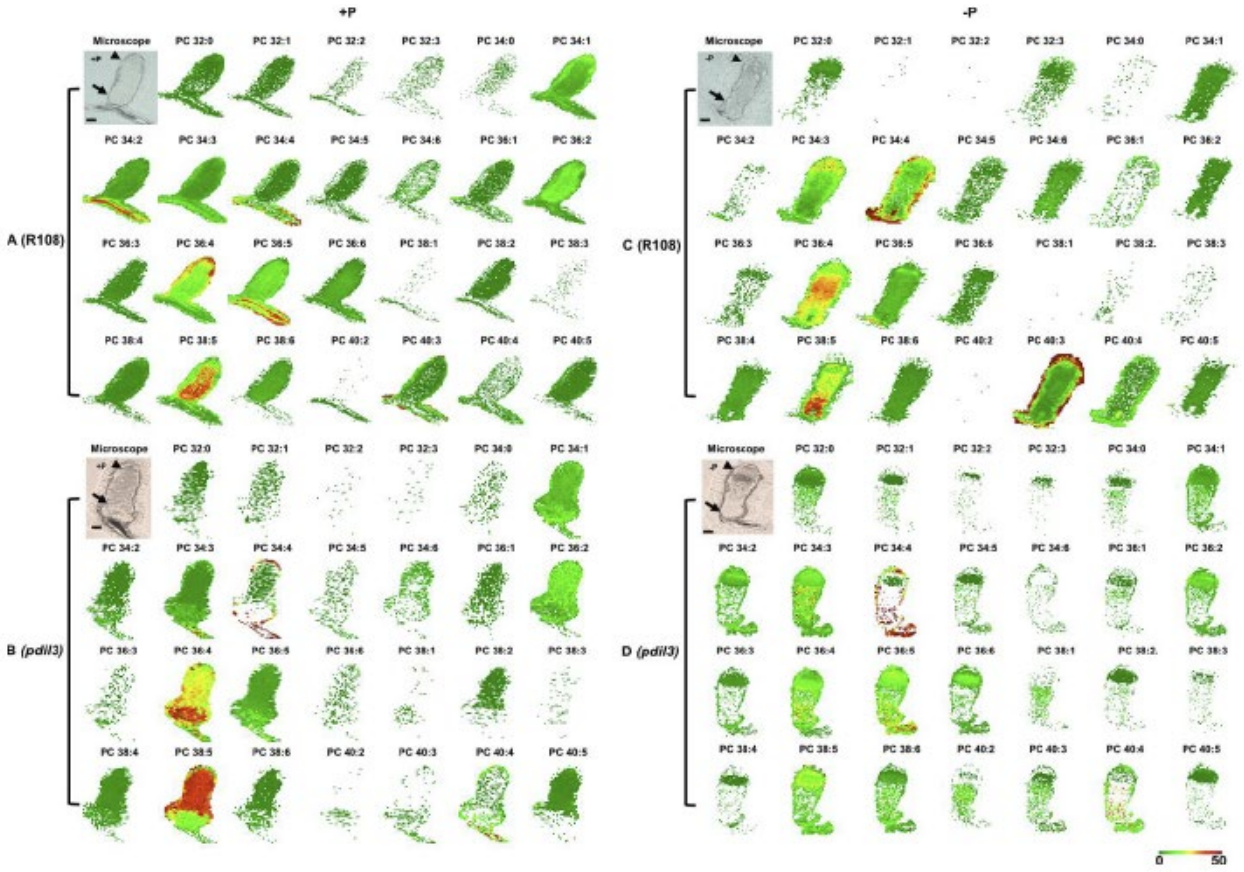

Supplemental Figure S3.1 MALDI-MS imaging of phosphatidylcholine (PC) metabolites in *pdil3* nodules.

A, B. Bright field images of R108 and *pdil3* nodule cross-section (25 µm) before coating with dihydroxybenzoic acid (DHB) matrix grown under +P. C, D. Bright field images of R108 and *pdil3* nodules cross-section (25µm) before coating with DHB matrix grown under -P are shown on the left. A, B, C, and D represent Normalized mol % distribution profiles. Bars = 500 µm. Proximal zone is indicated by arrowhead and distal zone by arrow. MALDI scale shows mol% with green and red representing low and high levels, respectively. Representative images of N = 5 each for +P and –P.

CHAPTER 4

METABOLITE SHIFT IN *Medicago truncatula* OCCURS IN PHOSPHORUS DEPRIVATION*

4.1 Abstract

Symbiotic nitrogen fixation entails successful interaction between legume hosts and rhizobia that occur in specialized organs called nodules. N_2-fixing legumes have higher demand of phosphorus (P) than legumes grown on mineral N. *Medicago truncatula* is an important model plant for characterization of effects of P deficiency at the molecular level. Hence, a study was carried out to address the alteration in metabolite levels besides those of membrane lipids of *M. truncatula* grown aeroponically and subjected to four weeks of P stress. First, GC-MS based untargeted metabolomics employed initially revealed changes in metabolic profile of nodules with increased levels of amino acids and sugars, and decline in amounts of organic acids. Subsequently, LC-MS/MS was used to quantify these compounds including phosphorylated metabolites in the overall plant. Our results showed drastic reduction in levels of organic acids and phosphorylated compounds in -P leaves with moderate reduction in -P roots and nodules. Additionally, sugars and amino acids were elevated in whole plant under P deprivation. These findings provide evidence that N_2-fixation in *M. truncatula* is mediated through N feedback mechanism that in parallel is related to C and P metabolism.

4.2 Introduction

Phosphorus (P) is an essential nutrient required for plant growth and has a vital

* This chapter has been submitted as a manuscript to the Journal of Experimental Botany.

role both in metabolic processes and as a structural component of cellular macromolecules (Goldstein et al., 1988; Raghothama, 1999). A majority of arable land is P deficient and global P reserves for use as agricultural supplements are anticipated to deplete rapidly in the next few decades (Vance et al., 2003; Lambers et al., 2006; Cordell et al., 2009; Ha and Tran, 2014). Consequently, crop growth and yield are expected to fall due to low P availability; this is especially important for legumes grown symbiotically because their N_2 fixing nodules have high P requirements (Sulieman and Tran, 2013). Legumes are vital components of crop and forage agroecosystems, particularly in developing countries (Jain et al., 2007; Tran and Nguyen, 2009; Thao and Tran, 2012). Temperate legumes like the model legume *Medicago truncatula* that is nodulated by soil bacterium *Sinorhizobium meliloti* spp, forms indeterminate nodules which have a persistent apical meristem leading to formation of different developmental zones (Vasse et al., 1990; Roux et al., 2014).

M. truncatula is being studied as a model for legume responses to many biotic and abiotic stresses, especially N and P nutrient stresses, because of its strong genetic and genomic resources. These include its diploid nature, modest genome size of ~ 550Mbp, short seed generation time, ease of genetic transformation, availability of mutant populations, diverse ecotypes, two of which have reference quality genomes, and well-studied symbiotic interactions for both rhizobial and mycorrhizal symbionts (Barker et al., 1990; Oldroyd et al., 2005; Valdes-Lopez and Hernandez, 2008; Young and Udvardi, 2009; Young and Bharti, 2012; Stanton-Geddes et al., 2013; de Bang et al., 2017; Moll et al., 2017; Zhou et al., 2017; Pecrix et al., 2018; Proust et al., 2018; Mergaert et al., 2020; Roy et al., 2020). *M. truncatula* nodulates specifically with the rhizobial species

Sinorhizobium meliloti, after a reciprocal signal exchange and rhizobial invasion into plant roots through plant-derived structures called infection threads (Oldroyd, 2013). The rhizobia are internalized in a process that resembles endocytosis, and become enveloped membranes of plant origin, the symbiosome membrane through which nutrient exchange occurs. After a maturation process, the internalized rhizobia, now called bacteroids, become competent to fix N_2 into ammonia and exchange it for plant photosynthate (Roy et al., 2020). *M. truncatula* develops indeterminate nodules containing a persistent meristem and gradients of development along their longitudinal axes, similar to other temperate legumes. In contrast, tropical legumes, like the model *Lotus japonicus* and the crop *Glycine max*, develop determinate nodules (HIRSCH, 1992).

Plants elicit a complex array of morphological, physiological, and metabolic strategies to acclimatize under P starvation (Vance et al., 2003; Plaxton and Tran, 2011). P is taken up and assimilated in the form of inorganic phosphate (Pi) by plants, playing a central role in all metabolic pathways and processes like photosynthesis and respiration (Plaxton and Tran, 2011). Several studies have demonstrated the ability of plants to reprioritize internal Pi use and maximize external Pi acquisition in P stress (Morcuende et al., 2007; Zheng et al., 2009; Nilsson et al., 2010). In absence of P, plants alter their metabolism to scavenge and conserve internal Pi. For instance, phospholipids in the membranes are replaced by sulfo- and galactolipids, and plants use metabolic bypass reactions depending on inorganic pyrophosphate (PPi) rather than Pi (Gaude et al., 2004; Plaxton and Tran, 2011; Okazaki et al., 2013; Dokwal et al., 2021). One of those bypasses is a PPi-dependent glycolysis enabling plants to maintain carbon flow into the citric acid cycle. Additionally, a non-energy conserving pathway involves an alternate oxidase where

respiration can be maintained even when ADP and Pi levels are low (Uhde-Stone et al., 2003; Florez-Sarasa et al., 2014; Wang et al., 2014). In parallel, plants secrete large amounts of organic acids to achieve an increased solubility of Pi in soils (Vance et al., 2003; Muller et al., 2015).

Metabolite profiling is a powerful tool for studying plant stress responses, notably, abiotic stresses involving shortage of nutrients such as P (Guy et al., 2008; Shulaev et al., 2008; Kráľová et al., 2012; Obata and Fernie, 2012; Jorge et al., 2016). Previous studies in leaves and roots of *Arabidopsis* (Morcuende et al., 2007), white lupin (Muller et al., 2015) and barley (Huang et al., 2008); nodules of common bean (Hernandez et al., 2009) and *M. truncatula* (Sulieman et al., 2013) have investigated the impact of P stress on limited number of metabolites. In these studies, plants were subjected to P deficiency for one to three weeks. Recently, we evaluated the growth of *M. truncatula* under prolonged periods of P starvation for four weeks after nodulation and studied P deficit's impact on membrane lipids and their distribution in nodules (Dokwal et al. 2021). The present study also examines *M. truncatula* after a more prolonged period of P deprivation. It exploits modern metabolite profiling and provides detailed information on the repertoire of metabolites that exhibit changes in *M. truncatula* plants during P deprivation. In this report we used a combination of untargeted (GC-MS) and liquid chromatography mass spectrometry-based targeted metabolic profiling to investigate the effects of prolonged P-starvation on leaves, roots, and nodules of *M. truncatula*. This study covers a wide range of metabolites (115); sugars/sugar alcohols, amino acids, phosphorylated compounds, and organic acids and fills gaps integrating shoot, root, and nodule response of P deficient plants. This data enables a better understanding of how *M. truncatula* plants undergo

metabolic changes in various organs to sustain survival and N_2 fixing nodule functioning under P stress.

4.3 Materials and Methods

4.3.1 Chemicals

Metabolite standards, methoxyamine hydrochloride, and pyridine were purchased from Sigma. [U-^{13}C]glucose, [U-^{13}C]glycine, and [U-^{13}C]fumarate were obtained from Isotec. Potassium hydroxide (45%, v/v), methylene chloride, chloroform, N-methyl-N-trimethylsilytrifluoroacetamide plus 1% trimethylchlorosilane (MSTFA + 1% TMCS) and LC-MS grade solvents such as acetonitrile, methanol, water, and LC-MS grade formic acid were purchased from Fisher Scientific.

4.3.2 Seed Collection, Surface Sterilization and Germination

M. truncatula R108 (WT) pods were crushed for seed collection. Concentrated H_2SO_4 for 5 minutes was used for seeds scarification, rinsed in sterile water, surface sterilized with 6 % sodium hypochlorite for 1.5 minutes, and rinsed with sterile water. The seeds were imbibed in sterile water for 3 days at 4 °C in the dark, and then transferred to 1% water agar petri dishes. The plates were inverted and kept in the dark for 2 days until germination occurred.

4.3.3 Plant Growth in Aeroponics System

Germinated seedlings were grown on aeroponic chambers as previously described (Veereshlingam et al., 2004; Barker et al., November 2006). For planting germinated seedlings, a 20 gal. trash can (aeroponic chamber) with a modified black plexiglass lid containing 4 mm holes was used. A misting humidifier sealed with silicon

sealant was powering the aeroponic chamber. Plants were grown simultaneously in two aeroponic chambers with Lullien's medium (Lullien et al., 1987) as described previously in +P and -P conditions (Dokwal et al., 2021). Plants from both growth conditions were inoculated with *S. meliloti* Rm41 and grown for four weeks.

4.3.4 Harvesting, Drying, Weighing, and Grinding of the Different Tissues

Leaves, roots, and nodules from each plant were harvested using sharp razor blades and collected in separate tubes after 28 days. Harvested tissues were immediately flash-frozen in liquid nitrogen and lyophilized for five days. Then, tissues were transferred to a 10 mL stainless steel jar containing one 10 mm stainless steel ball and were crushed for 3 minutes at 30 Hz using a MM400 ball meal. Pulverized extracts were transferred to 2 mL screw cap tubes from which a corresponding amount of powder was weighed for total proteins, untargeted and targeted metabolomics analyses.

4.3.5 Total Protein Content in Leaves, Roots, and Nodules

5 mg of pulverized dried leaf, root, and nodule was used for the extraction and quantification of total proteins as previously described (Cocuron et al., 2014). Briefly, the samples were defatted by adding 1 mL of hexanes/isopropanol (2:1; v/v), ground, spun and their organic phase was removed. These steps were repeated two more times. The pellet was then dried under nitrogen, and the proteins were extracted as described (Cocuron et al., 2014) and quantified using the Biorad DC Protein Kit II. Five biological replicates were used for each tissue from different growth conditions.

4.3.6 Untargeted GC-MS Analysis of Intracellular Metabolites

Ten mg of +/-P nodule powder was utilized for the extraction and profiling of soluble

metabolites by GC-MS. Two hundred nmol of [U-^{13}C]glycine was added as an internal standard to pre-chilled tubes containing nodule powder. Samples were centrifuged at 17,000 g at 4 ºC for 30 seconds, and 1 mL of cold chloroform:methanol:water (1:2.5:1; v/v/v) solution was added as the extraction solvent. Tubes were then vortexed at 4 ºC for 5 minutes and spun at 17,000 g for 5 minutes at 4 ºC. Supernatant was transferred to a new 2 mL microcentrifuge tube placed on ice, and 400 µL of cold ultrapure water was added. Extracts were vortexed, centrifuged at 17,000 g at 4 ºC for 5 minutes, and the upper phase (water-methanol mixture, 'polar phase') was transferred to a new 1.5 mL microcentrifuge tube. The methanol was evaporated at 30 ºC using a speed-vacuum, then extracts were flash-frozen, and lyophilized at -80 ºC for 24 hours.

After lyophilization, extracts were resuspended in 250 µL of methanol:water (50:50; v/v), vortexed, and centrifuged at 17,000 g at room temperature for 30 seconds. Samples were transferred to 3 kDa Amicon Ultra 0.5 mL centrifugal devices previously washed with ultrapure water to remove glycerol. Pre-conditioning of the filtering devices with ultrapure water consisted in adding 0.5 mL of ultrapure water, then, spinning at 14,000 g for 25 minutes at room temperature, and finally centrifuging the filters upside down at 1,000 g for 2 minutes to remove any residual solution. These steps were repeated twice. The extracts, after loading on the filtering devices, were spun at 14,000 g at room temperature for 30 minutes. 200 µL of eluates were pipetted into 250 µL GC-MS inserts placed in pre-labeled 1.5 mL tubes, and methanol was evaporated at 30 ºC using a speed-vacuum. Samples were flash-frozen in liquid nitrogen and lyophilized at -80 ºC for 24 hours before derivatization. Inserts containing the dried extracts were placed in GC-MS vials, and 200 µL of methylene chloride was added. The samples were flushed with a

gentle stream of nitrogen at room temperature. Then, 50 µL of a 20 mg/mL methoxyamine hydrochloride solution in pyridine was pipetted into the vials. Extracts were flushed with a stream of nitrogen, vortexed, and incubated at 40 °C for 90 minutes under constant agitation. Finally, 50 µL of MSTFA + 1% TMCS derivative reagent was added to the methoxylated extracts. The samples were flushed with nitrogen for 5-10 seconds and incubated at 40°C for 50 minutes under constant vortexing. The derivatized extracts were ready for GC-MS analysis.

Alkylsilyl derivatives were analyzed using a Thermo Trace 1310 gas chromatograph coupled to an ISQ single quadrupole mass spectrometer. Derivatized metabolites were first separated using a TG-5MS capillary (30 m x 0.25 mm x 0.50 µm) column from Thermo Fisher, and helium as carrier gas set up at a constant flow rate of 1.4 mL/min. The GC conditions were as follows: initial temperature was set to 70 °C and hold for 5 minutes. The oven temperature was then raised to 235 °C at 3 °C/minute. A second ramp was applied at a rate of 6 °C/minute to reach a final temperature of 320 °C which was held for 15 minutes. The injection temperature was fixed at 300 °C and a split ratio of 10 was selected for the injection mode. One µL of alkylsilyl derivatives was injected onto the column. For the MS analysis, the mass spectra were acquired using electron impact ionization in positive ion mode over a mass range from 50 to 1100 amu. The ion source and the interface temperatures were respectively set to 300 °C and 325 °C.

GC-MS data were analyzed following four consecutive steps. First, they were acquired and processed using Xcalibur 2.2 software. Second, GC-MS chromatograms were aligned using XCMS Online (Tautenhahn et al., 2012). Third, statistical analysis was

conducted through MetaboAnalyst 4.0 (Chong et al., 2018) to identify “peak/mass” pair(s) or features that are significantly different between experimental conditions. Finally, alkylsilyl derivatives were identified using the National Institute of Standards and Technology (NIST) 17 library and an in-house library.

4.3.7 Targeted LC-MS/MS Analysis of Soluble Compounds

Five mg of ground leaf, root, and nodule tissues were used for the targeted metabolomics analyses. Water-soluble metabolites such as sugars, sugar alcohols, amino acids, organic acids, and phosphorylated compounds were extracted using boiling water following a previous protocol published (Cocuron et al., 2014). One hundred, 40 and 10 nmol of [U-^{13}C]glucose, [U-^{13}C]glycine, and [U-^{13}C]fumarate were respectively added to each tube as internal standards.

After extraction and lyophilization of the soluble metabolites, the samples were resuspended in 500 µL of ultrapure water, vortexed, and briefly centrifuged. One hundred fifty µL of extract was added to a 0.2 µm nanosep MF centrifugal device, spun at 17,000 g at 4 ºC for 10 minutes to analyze sugars and sugar alcohols. The remainder (350 µL) was transferred to 3 kDa Amicon filters, centrifuged at 14,200 g at 4 ºC for 60 minutes to quantify amino acids, organic acids, and phosphorylated compounds.

The intracellular metabolites were resolved and quantified using Agilent 1290 Infinity II high performance liquid chromatography coupled to an AB Sciex QTRAP6500 + mass spectrometer system as previously described (Cocuron et al., 2014). For sugars and sugar alcohols, 40 µL of extract was diluted in a 2 mL LC-MS vial containing 960 µL of acetonitrile/water (60:40; v/v) solution. Two µL, 2 µL, 5 µL of the diluted nodule, root, and leaf samples, respectively were injected onto the column. For the amino acids, 20 µL

aliquot of extract was added to a LC-MS vial containing 980 µL of aqueous 1 mM hydrochloric acid, and 2 µL of the diluted samples for all tissues was injected onto the column. For the phosphorylated compounds and organic acids, 100 µL of leaf extract and 50 µL of root/nodule extracts was diluted in 900 µL and 950 µL of nanopure water, respectively. Five µL was injected onto the column. Four biological replicates were used for each tissue from each growth condition.

4.3.8 Statistical Analysis

To determine statistical differences for each experiment, a Student t-test ($p < 0.05$) was performed using GraphPad Prism 8 Software. Principal component analysis (PCA), supervised partial least-squares discriminate analysis (PLS-DA), and heat mapping analyses were performed using MetaboAnalyst 4.0 (Chong et al., 2018). Briefly, the metabolomics data were first normalized by log-transformation, mean-centered, and divided by the standard deviation of each variable.

4.4 Results

4.4.1 Phosphorous Deprivation Affects the Metabolite Profile of *M. truncatula* Nodules

N_2-fixing legumes have a higher demand for P than legumes growing on mineral N. Indeed, growing nodules are strong P sinks in legumes such as *Glycine max* (Sa and Israel, 1991) and *Lupinus albus* (Schulze et al., 2006). Therefore, P deficiency would affect the metabolism of the nodule, and consequently of the overall plant. A GC-MS based untargeted metabolomics approach was used to investigate metabolic differences in nodules subjected or not to four weeks of P deficiency. A total of 86 features were detected, and their normalized intensity is reported in Table 4.1 and Supplementary Table S4.1. Principal component analysis (PCA) revealed different metabolic profiles between

+/-P nodules (Fig. 4.1) with the principal component 1 (PC1) explaining 71.2% of the variance.

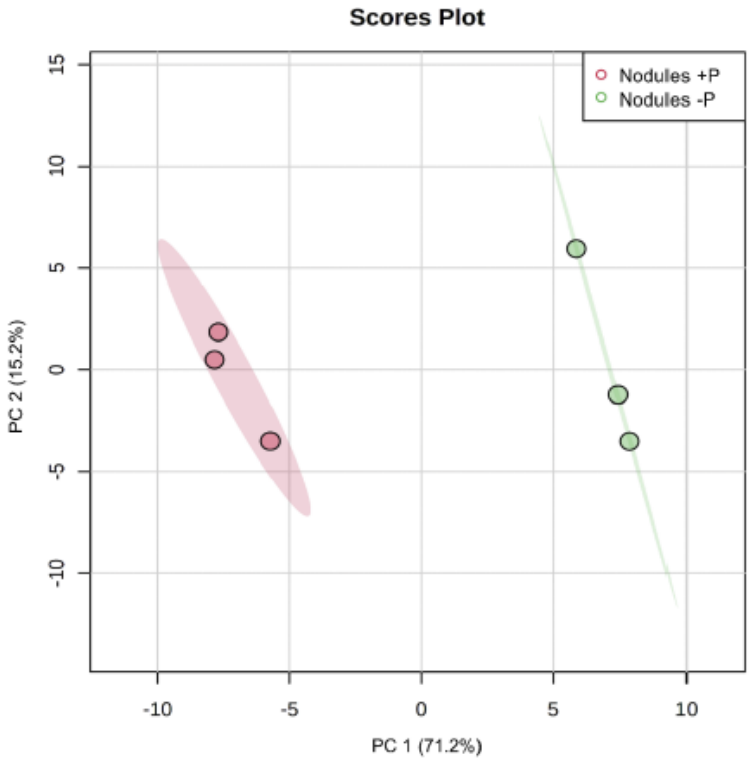

Figure 4.1: **Principal component analysis (PCA) of the features detected by GC-MS in nodule extracts of *Medicago truncatula* from +P and -P conditions.**

M. truncatula R108 nodules were harvested 28 days post inoculation (DPI) with *S. meliloti* Rm41. N=3 biological replicates for each growth condition. Shaded red and green regions in this plot represent 95% confidence intervals for the two treatments.

From the 86 features detected by GC-MS, 53 were differentially accumulated in nodules between +P and -P (Table 4.1). Of these 53 features, 17 metabolites were identified with a probability score ≥ 60% using NIST 17 and an in-house library (Table 4.1). The remaining 33 features did not show any significant differences in nodules between the two treatments (Supplementary Table S4.1). The identified peaks belonged to three main classes of metabolites: sugars, amino acids, and organic acids (Table 4.1, Supplementary Table S4.1).

Table 4.1: List of metabolites/features differentially accumulated in nodules from +P and -P which were detected by untargeted metabolomics.

17 metabolites in the table below were identified by peak search with NIST 17 and in-house library with a probability score of at least 60%. Data shown represents the average normalized peak intensity ± standard deviation of N=3 biological replicates; $p<0.05$.

[a] Compound name or [b] Mass-to-charge (m/z)	Retention time (minutes)	Average normalized intensity ± SD		[c] Ln (FC)
		Nodules +P	Nodules -P	
174.10[b]	46.80	1.27E-03 ± 2.18E-04	9.60E-02 ± 7.39E-03	-4.32
Fructose[a]	52.17	2.84E-03 ± 5.73E-04	3.17E-02 ± 4.35E-03	-2.41
217.10[b]	52.52	1.96E-03 ± 3.83E-04	2.13E-02 ± 3.25E-03	-2.39
Glucose[a]	53.05	3.02E-03 ± 1.24E-04	2.09E-02 ± 3.48E-03	-1.93
Tryptophan[a]	62.85	1.52E-03 ± 1.49E-04	9.37E-03 ± 1.38E-03	-1.82
205.20[b]	53.67	5.98E-04 ± 5.69E-05	3.20E-03 ± 4.29E-04	-1.68
333.20[b]	56.92	6.14E-04 ± 4.62E-05	2.63E-03 ± 5.27E-04	-1.45
174.10[b]	50.25	1.29E-03 ± 2.50E-04	4.90E-03 ± 2.67E-04	-1.33
188.10[b]	51.53	4.95E-04 ± 2.00E-04	1.88E-03 ± 3.23E-04	-1.33
259.17[b]	56.35	5.21E-04 ± 3.60E-04	1.93E-03 ± 2.50E-04	-1.31
264.10[b]	51.25	1.26E-03 ± 4.20E-04	4.46E-03 ± 1.27E-03	-1.27
174.20[b]	35.17	3.81E-04 ± 5.99E-05	1.30E-03 ± 4.26E-04	-1.23
236.10[b]	74.15	4.05E-04 ± 5.03E-05	1.29E-03 ± 2.58E-04	-1.16
217.10[b]	79.02	1.98E-03 ± 7.37E-04	6.32E-03 ± 9.37E-04	-1.16
292.20[b]	48.37	4.82E-04 ± 2.85E-05	1.52E-03 ± 1.98E-04	-1.15
241.10[b]	30.55	3.31E-04 ± 8.40E-05	9.71E-04 ± 3.25E-04	-1.08
204.10[b]	76.33	3.37E-04 ± 4.42E-05	9.92E-04 ± 1.47E-04	-1.08
259.20[b]	81.72	7.59E-04 ± 2.98E-04	2.24E-03 ± 2.99E-04	-1.08

(table continues)

[a] Compound name or [b] Mass-to-charge (m/z)	Retention time (minutes)	Average normalized intensity ± SD		[c] Ln (FC)
		Nodules +P	Nodules -P	
218.20[b]	35.53	6.59E-04 ± 9.30E-05	1.86E-03 ± 6.55E-04	-1.04
Inositol[a]	59.18	7.45E-03 ± 5.56E-04	1.79E-02 ± 2.63E-03	-0.88
275.20[b]	54.30	1.19E-03 ± 1.11E-04	2.87E-03 ± 4.35E-04	-0.88
204.10[b]	81.53	7.12E-03 ± 2.70E-03	1.70E-02 ± 1.94E-03	-0.87
Tyrosine[a]	53.80	1.70E-03 ± 3.35E-04	3.88E-03 ± 4.82E-04	-0.82
Asparagine[a]	37.33	2.31E-03 ± 6.86E-04	5.18E-03 ± 1.04E-03	-0.81
Pyruvate[a]	16.58	5.09E-04 ± 5.02E-05	1.03E-03 ± 2.57E-04	-0.71
159.10[b]	41.28	2.91E-03 ± 6.58E-04	5.85E-03 ± 8.33E-04	-0.70
218.10[b]	42.62	1.48E-03 ± 1.12E-04	2.86E-03 ± 4.88E-04	-0.66
Lysine[a]	38.63	2.24E-03 ± 3.60E-04	3.55E-03 ± 3.32E-04	-0.46
α-ketoglutarate[a]	40.63	6.23E-04 ± 7.43E-05	9.63E-04 ± 1.65E-04	-0.44
174.20[b]	53.22	2.37E-03 ± 2.72E-04	3.68E-03 ± 3.43E-04	-0.44
Mannose[a]	52.82	8.08E-04 ± 1.77E-05	1.15E-03 ± 2.62E-05	-0.35
204.10[b]	62.17	3.12E-03 ± 2.12E-04	4.05E-03 ± 4.92E-04	-0.26
156.10[b]	38.43	2.44E-02 ± 5.25E-04	1.83E-02 ± 1.89E-03	0.28
204.06[b]	19.88	3.04E-02 ± 2.64E-03	2.24E-02 ± 2.46E-03	0.30
245.00[b]	45.12	3.04E-02 ± 2.64E-03	2.24E-02 ± 2.46E-03	0.30
Glutamate[a]	42.38	3.95E-02 ± 1.23E-03	2.80E-02 ± 5.70E-03	0.34
239.20[b]	34.00	1.95E-03 ± 2.58E-04	1.33E-03 ± 1.82E-04	0.38
204.10[b]	52.90	2.92E-03 ± 4.35E-05	1.96E-03 ± 1.81E-04	0.40
Aspartate[a]	38.48	2.07E-02 ± 5.26E-04	9.57E-03 ± 1.69E-03	0.77
156.06[b]	22.73	6.66E-03 ± 1.48E-03	2.99E-03 ± 2.97E-04	0.80

(table continues)

[a] Compound name or [b] Mass-to-charge (m/z)	Retention time (minutes)	Average normalized intensity ± SD		[c] Ln (FC)
		Nodules +P	Nodules -P	
Citrate[a]	50.00	4.16E-02 ± 1.40E-03	1.83E-02 ± 2.55E-03	0.82
184.00[b]	13.00	8.40E-04 ± 2.98E-05	3.40E-04 ±1.01E-04	0.91
152.10[b]	15.80	2.32E-03 ± 1.86E-04	9.35E-04 ± 1.18E-04	0.91
281.10[b]	22.98	7.63E-04 ± 4.63E-05	3.02E-04 ± 3.87E-05	0.93
174.20[b]	25.65	4.36E-03 ± 7.18E-04	1.42E-03 ± 1.62E-04	1.12
239.23[b]	44.42	1.40E-03 ± 2.04E-04	3.91E-04 ± 9.78E-05	1.28
299.10[b]	27.70	7.00E-01 ± 2.87E-02	1.78E-01 ± 1.35E-02	1.37
Valine[a]	18.30	1.25E-04 ± 3.73E-05	2.07E-05 ± 7.62E-06	1.80
Malate[a]	37.20	1.94E-01 ± 5.83E-03	2.61E-02 ± 2.17E-03	2.01
147.10[b]	20.70	8.55E-03 ± 1.79E-03	5.73E-04 ± 3.35E-04	2.70
Malonic acid[a]	24.22	1.96E-01 ± 2.13E-02	9.06E-03 ± 1.12E-03	3.07
Succinate[a]	29.27	1.94E-02 ± 3.01E-03	7.98E-04 ± 4.09E-04	3.19
141.10[b]	32.07	1.13E-03 ± 5.81E-04	3.57E-05 ± 1.01E-05	3.45

[a] Identified metabolites. [b] Unidentified metabolites.[c] Natural logarithm of the fold change (FC) i.e., Ln (Nodules +P/Nodules -P)

Most of the free sugars were more abundant in -P nodules: fructose, glucose, and mannose were found to be 11.1, 6.9, and 1.4-fold higher, respectively. Additionally, inositol, the only sugar alcohol identified, was elevated by 2.4 fold under P deprivation (Table 4.1). In +P nodules, valine, aspartate, and glutamate were increased by 6.0, 2.1 and 1.4 fold, respectively, whereas in -P nodules, tryptophan, tyrosine, asparagine, and lysine were raised by 6.2, 2.2, 2.2 and 1.6 fold, respectively (Table 4.1). The content in the organic acids pyruvate and α-ketoglutarate was greater by 2.0 and 1.6 fold in -P nodules, respectively, while succinate, malonic acid, malate, and citrate drastically declined by 24.2, 21.5, 7.5 and 2.3 fold, respectively (Table 4.1). Amongst the 36 unidentified peaks, 22 of them were significantly higher in -P nodules while 14 in +P (Table 4.1).

4.4.2 Changes in Whole-Plant Metabolism in *M. truncatula* and Its Nodules Subjected to P Deprivation

Based on our GC-MS data, the metabolism of the nodules is affected under P deprivation (Fig. 4.1, Table 4.1). Consequently, other plant organs, such as leaves and roots of *M. truncatula* may undergo a metabolic shift in absence of P. To investigate this possibility, a LC-MS/MS based targeted metabolomics approach was used to quantify three main classes of intracellular compounds that showed a significant metabolic shift in our initial GC-MS study on nodules: (1) amino acids and associated derivatives; (2) sugars and sugar alcohols; and (3) organic acids. Additionally, P deprivation is expected to perturb the levels of intracellular phosphorylated metabolites. Therefore, this class of compounds, which are intermediaries of the glycolysis, oxidative pentose phosphate pathway (OPPP), and energy metabolism, were included in the analyses.

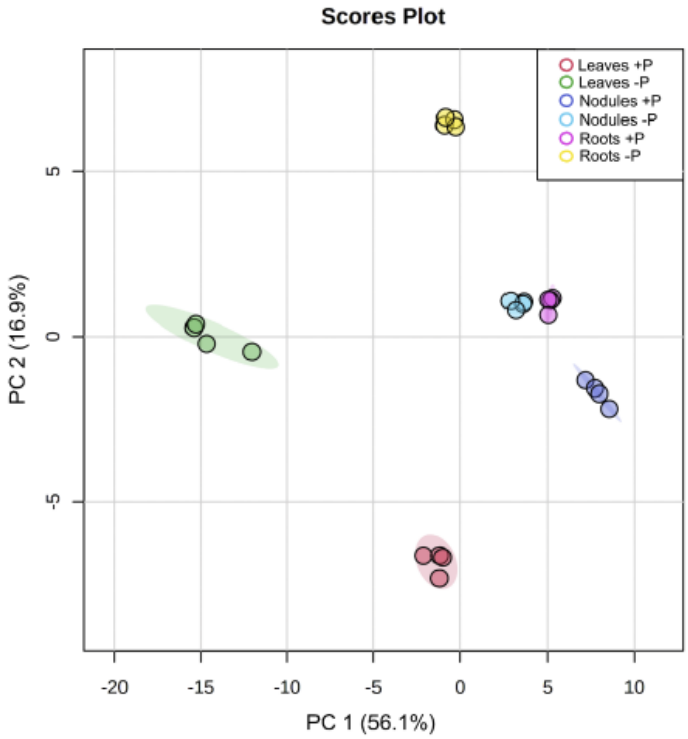

Figure 4.2: PCA of the metabolites quantified by LC-MS/MS in leaves, roots, and nodules from *M. truncatula* grown in +P and -P conditions.

Shaded regions in the PCA plot represent 95% confidence intervals. N=4 biological replicates.

Overall, 115 metabolites were monitored, of which 97 were detected and quantified: 27 amino acids, nine sugars and sugar alcohols, 44 phosphorylated metabolites, and 17 organic acids (Supplementary Table S4.2). A PCA of the entire dataset revealed a clear separation between the roots, leaves, and nodules under the two growth conditions (Fig. 4.2), indicating a metabolic shift in all the organs due to P starvation. The principal components 1 and 2 explained 56.1% and 16.9% of the variance, respectively. Interestingly, in absence of P, the metabolism of the nodules was similar to that of roots under control conditions (Fig. 4.2).

Figure 4.3 is a heat map comparing the levels of primary metabolites among organs in *M. truncatula* subjected or not to P deprivation. Compounds with the same pattern of distribution clustered together.

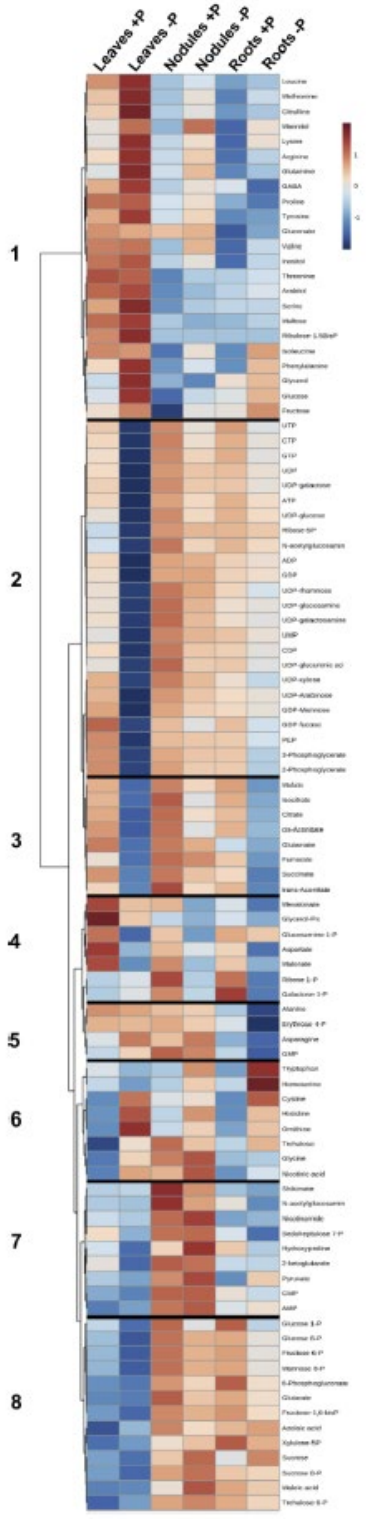

Figure 4.3: **Heatmap analysis of the intracellular metabolites in leaves, roots, and nodules from *M. truncatula* grown in +P and -P.**

Colors represent metabolite relative intensity with red and blue symbolizing higher and lower values, respectively.

In cluster 1, most of the metabolites are amino acids and their derivatives, ribulose 1,5-bisphosphate (substrate for RuBisCO), and free sugars. All the metabolites in cluster 3 show highest abundance in -P leaves compared to any other organ irrespective of the growth conditions. Ribulose 1,5-bisphosphate, component of Calvin cycle, was exclusively present in the leaves (Fig. 4.3). Some amino acids (methionine to valine) and mannitol were moderately abundant in -P nodules compared to +P. Sugars and amino acids like isoleucine, phenylalanine, glucose, and fructose were also higher in -P roots than +P (Fig. 4.3). The cluster 2 solely contains phosphorylated metabolites related to energy metabolism and nucleotide-sugars. Although all the metabolites in cluster 2 decreased in each organ under P deprivation, the most drastic decline was measured in -P leaves (Fig. 4.3). The cluster 3 groups organic acids from tricarboxylic acid (TCA) cycle whose levels decreased in –P leaves and roots. +P nodules had the highest abundance of all these organic acids, and only showed a mild reduction under P stress (Fig. 4.3). In cluster 4, most of the metabolite levels were higher in organs under normal growth conditions than in absence of P (Fig. 4.3).

The cluster 5 groups compounds whose amounts were maintained in +/-P nodules. Alanine and erythrose 4-phosphate levels were equivalent in +/-P leaves while asparagine and GMP accumulated in -P leaves. All metabolites of cluster 5 were reduced in +/-P roots compared to all other organs of *M. truncatula* (Fig. 4.3). The cluster 6 includes amino acids, trehalose, and nicotinic acid. These metabolites were found to be generally higher under –P in each organ. Tryptophan, homoserine, and cysteine were the most abundant in –P roots, histidine, and ornithine in –P leaves, and glycine and nicotinic acid in –P nodules (Fig. 4.3). The levels of the compounds from cluster 7 were the highest

in nodules independently of the treatment (Fig. 4.3). Finally, cluster 8 includes phosphorylated sugars, sucrose, and intermediaries of the OPPP. Levels of all these metabolites were the lowest in +/-P leaves in comparison to the other organs (Fig. 4.3).

4.4.3 Different Shifts in Intracellular Metabolites in Leaves, Roots, and Nodules of *M. truncatula* in Absence of P

To further investigate the effects of P deprivation on each class of metabolite, partial least squares discriminant analysis (PLS-DA) was performed to identify the most important features contributing to the variation in different organs of *M. truncatula* in absence of P (Chong et al., 2018).

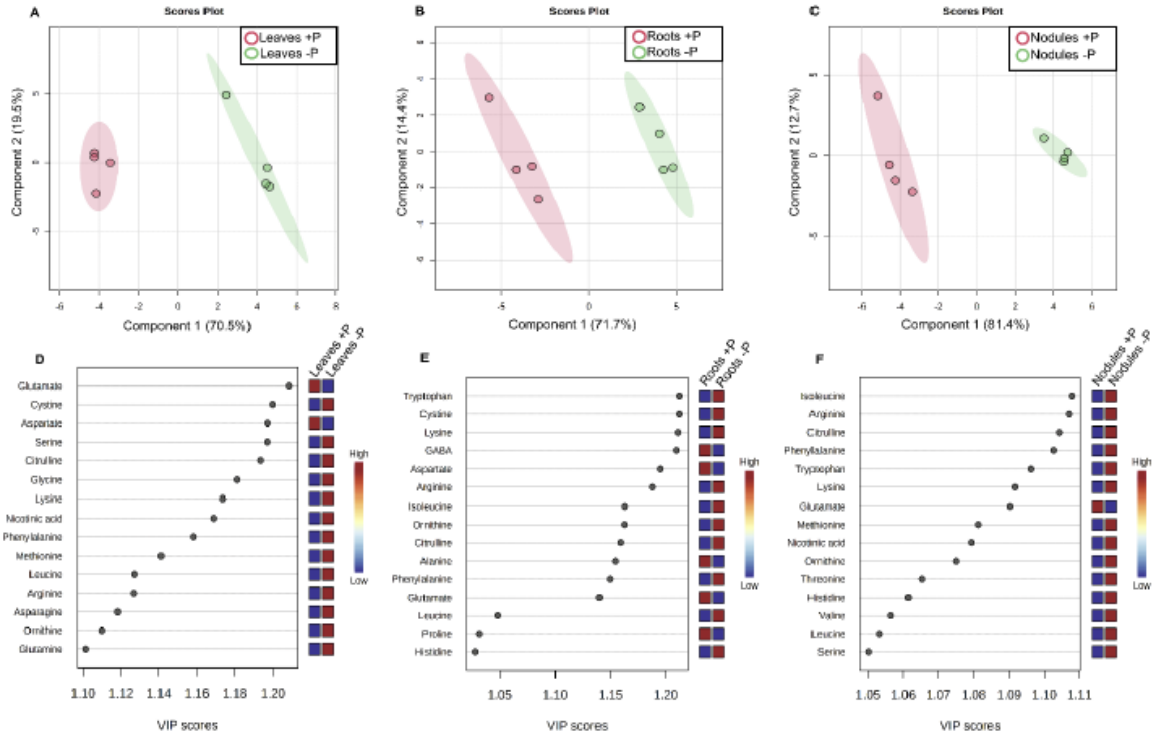

Figure 4.4: **Partial least-squares discriminant analysis (PLS-DA) of amino acids showing separation between tissues of *M. truncatula* from +P and –P conditions.**

Leaves (A), Roots (B) and Nodules (C) from +P and -P conditions. Shaded regions in the PLS-DA plot represent 95% confidence intervals. Variable importance in projection (VIP) scores showing top 15 important amino acids that contribute the most to the PLS-DA plot of leaves (D), roots (E) and nodules (F). Colors in the variable importance in projection plot represents relative intensity, where red and blue symbolize higher and lower values, respectively. N=4 biological replicates for each organ and growth condition.

4.4.3.1 The Pool of Free Amino Acids Increased Under P-Stress

Over half of the amino acids were significantly increased in P-deficient organs (Supp.Table S4.2). PLS-DA and variable importance in projection (VIPs) revealed metabolic differences for amino acids for each organ of *M. truncatula* between +P and -P growth conditions (Fig. 4.4). Ccomponent 1 clearly separated the two treatments, accounting for 70.5%, 71.7%, and 81.4% of the variance for leaves, roots, and nodules, respectively (Fig. 4.4A, B, C). The VIPs, which are weighed sum of squares of the PLS loadings for a given component (Xia et al., 2012; Chong et al., 2018), are represented by the most important features (metabolites) responsible for the separation between respective tissues under +P and -P conditions. Fifteen most important amino acids responsible for the variation in leaves, roots, and nodules are highlighted in VIP plots (Fig. 4.4D, E, F). Most of the amino acids were higher under P stress with citrulline, lysine, phenylalanine, leucine, arginine, and ornithine common to the three organs under investigation (Fig. 4.4D, E, F). Glutamate was lower under P deprivation in all the organs of *M. truncatula*. Aspartate, generally present amongst the top 15 features in leaves and roots, was also reduced in P-starvation. GABA, alanine, and proline were some other amino acids which declined only in -P roots (Fig. 4.4D, E, F).

The most drastic impacts were observed in –P leaves where glutamate and citrulline had a 13.5-fold decrease and a 11.8-fold increase, respectively. As a comparison, the most extreme change observed in nodules was for tryptophan which increased by 2.4-fold under P deprivation. Asparagine, the most abundant amino acids in leaves and nodules. increased by at least 38% in the absence of P, while it declined by 39% in –P roots (Fig. 4.5, Supp. Table S4.2).

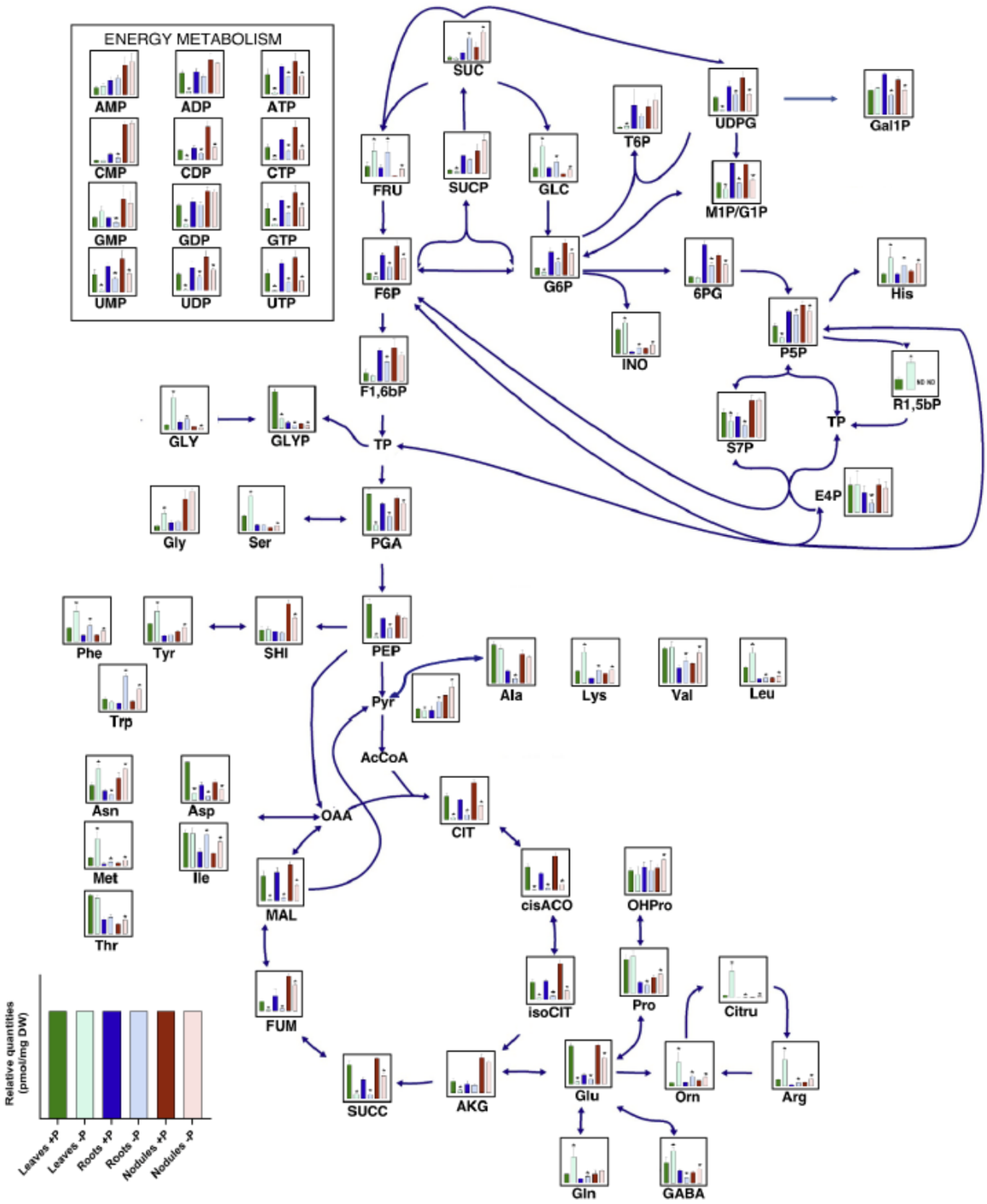

Figure 4.5: **Metabolic map of leaves, roots, and nodules of *M. truncatula* grown in +P and -P conditions with *S. meliloti* Rm41 after 28 days post inoculation (DPI).**

This is a representation of the data from Supplementary Table S2. Values are expressed as relative quantity in pmol per mg dry weight (DW) of tissue and are the average ± SD of four biological replicates. SUC, sucrose; FRU, fructose; GLC, glucose; INO, inositol; GLY, glycerol; Ala, alanine; Arg, arginine; Asn, asparagine; Asp, aspartate; Lys, lysine; Gln, glutamine; Glu, glutamate; Gly, glycine; His, histidine; OHPro, hydroxyproline; Leu, leucine; Ile, isoleucine; Met, methionine; Phe, phenylalanine; Pro, proline; Ser, serine; Thr, threonine; Trp, tryptophan; Tyr, tyrosine; Val, valine; GABA, 4-aminobutyric acid; Orn, ornithine; Citru, citrulline; T6P, trehalose 6-phosphate; UDPG, UDP-glucose; SUCP, sucrose 6-phosphate; Gal1P, galactose 1-phosphate; M1P/G1P, mannose 1-phosphate/glucose 1-phosphate; F6P, fructose 6-phosphate; G6P, glucose 6-phosphate; 6PG, 6-phosphogluconic acid; P5P, pentose 5-phosphates; R1,5-bP, ribulose 1,5-bisphosphate; S7P, sedoheptulose 7-phosphate; E4P, erythrose 4-phosphate; F1,6bP, fructose 1,6-bisphosphate; GLYP, glycerol-phosphates; TP, triose phosphates; PGA, 2–3 phosphoglycerates; PEP, phosphoenolpyruvate; SHI, shikimate; Pyr, pyruvate; AcCoA, acetyl-CoA; CIT, citrate; cisACO, cis-aconitate; isoCIT, isocitrate; AKG, a-ketoglutarate; SUCC, succinate; FUM, fumarate; MAL, malate; OAA, oxaloacetate. Not detected (ND). * indicate values are significant at $p<0.05$.

Interestingly, tryptophan, precursor of secondary metabolites and hormone indole-3-acetic acid (Ljung et al., 2002; Kriechbaumer and Glawischnig, 2005), had a 5.2-fold increase in –P roots, becoming the most abundant amino acid in roots under P deprivation. Basic amino acids, arginine, histidine, and lysine increased from 33% to 277% in P-starved organs. Several other amino acids that exhibited significantly higher levels in all the tissues under P deprivation were methionine, leucine, phenylalanine, citrulline, ornithine, and nicotinic acid (Fig. 4.5, Supp. Table S4.2). Conversely, glutamate and aspartate were reduced by at least 33% and up to 93% in P-deficient organs. Moreover, all the amino acids, except valine, found to be significantly different between the two conditions with our metabolite profiling in nodules, were confirmed by quantitative targeted metabolomics (Table 4.1, Supplementary Table S4.2).

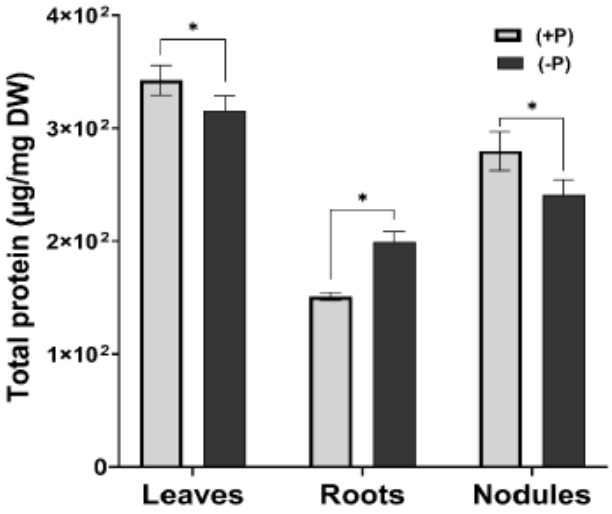

Figure 4.6: **Total Protein abundance in leaves, roots, and nodules of *M. truncatula*.**
Bar graphs represent the average ± SD of N=5 biological replicates. Values are expressed as micrograms of total protein per milligram DW of tissue. * indicate values are significant at $p<0.05$

Finally, we estimated that the pool of free amino acids increased under P deprivation by 5.2, 4.3, and 2.5 µg/mg DW in leaves, nodules, and roots, respectively. In parallel, total protein levels were significantly reduced in leaves and nodules in absence

of P by 26.4 and 38.6 µg/mg DW, respectively, whereas they were increased in –P roots by 48.5 µg/mg DW (Fig. 4.6). Thus, the decline in total protein content under P starvation might account for the higher abundance of free amino acids in leaves and nodules. However, the enhanced levels of total proteins and free amino acids in –P roots can only be due to a larger flow of carbon (C) through amino acid biosynthetic pathways.

4.4.3.2 Increase of Sugars and Decrease of Organic Acids Under P Deprivation

A distinct segregation in the metabolic profile for organic acids and sugars was noted in the PLS-DA plots between different growth conditions with reference to component 1, revealing 70.4%, 65.4%, and 80.6% of the variation in leaves, roots, and nodules of *M. truncatula*, respectively (Fig. 4.7A, B, C). The VIP plots underlines 15 key organic acids and sugars responsible for the distinction in leaves, roots, and nodules (Fig. 4.7D, E, F). Inositol, glucose, and fructose were accumulating in all P-deficient organs (Fig. 4.7D, E, F). In parallel, malonate and intermediates of the TCA cycle (cis- and trans-aconitate, succinate, citrate, isocitrate, and malate) were commonly lower in all the organs under P deprivation (Fig. 4.7D, E, F).

Most of the sugars and sugar alcohols accumulated in different organs of *M. truncatula* under P deficiency. Conversely, a large majority of the organic acids decreased under P deprivation (Fig. 4.5, Supp. Table S4.2). The most extreme impact of P stress was measured in leaves where cis-aconitate, malonate, and malate had a 41.5-, 13.4-, and 12.5-fold drop, respectively. Sucrose, the most abundant sugar in roots and nodules, was elevated by at least 2.2 fold under P deficiency, whereas its levels remain unaltered in leaves. Fructose and glucose increased up to 3.3 and 8.6-fold in all -P organs,

respectively (Fig. 4.5, Supp. Table S4.2); fructose became the most abundant sugar in –P leaves.

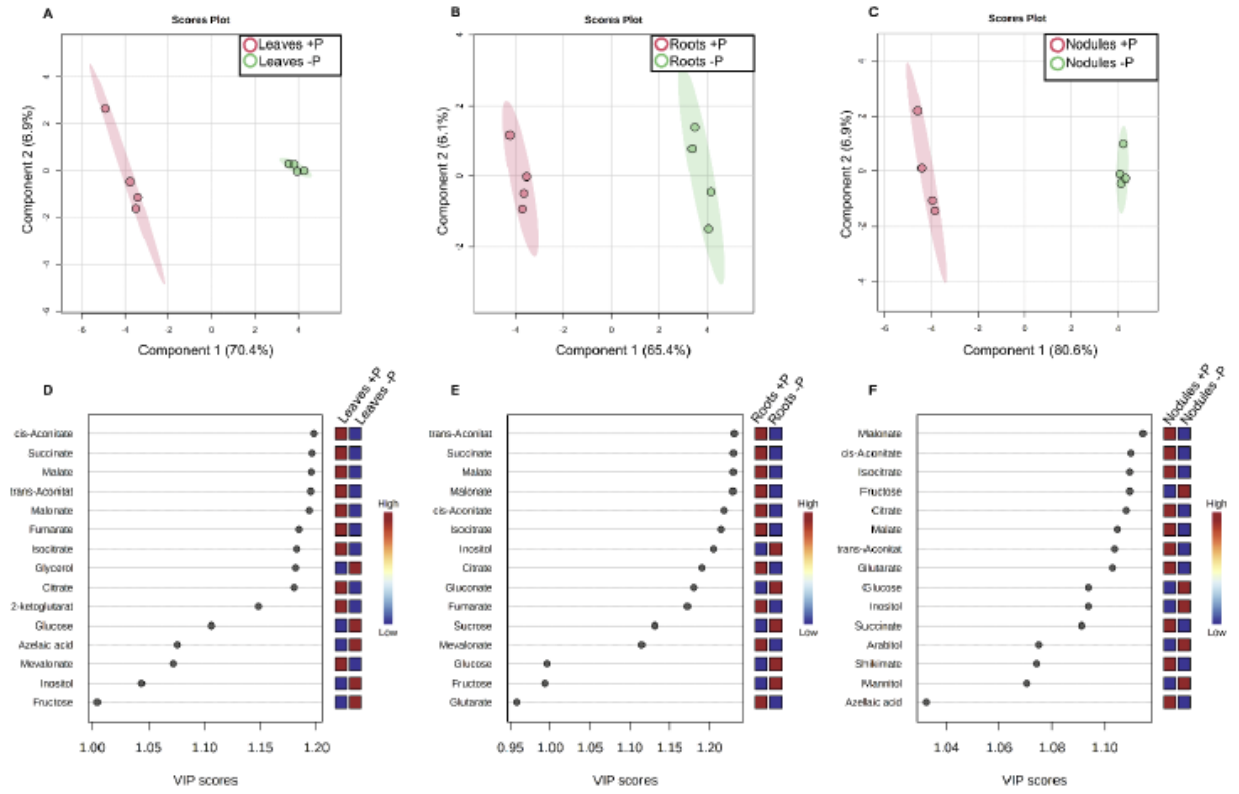

Figure 4.7: **PLS-DA of sugars and organic acids showing separation between tissues of *M. truncatula* from +P and –P conditions.**

Leaves (A), Roots (B) and Nodules (C) from +P and -P conditions. Shaded regions in the PLS-DA plot represent 95% confidence intervals. VIP scores showing top 15 important amino acids that contribute the most to the PLS-DA plot of leaves (D), roots (E) and nodules (F). Colors in the variable importance in projection plot represents relative intensity, where red and blue symbolize higher and lower values, respectively. N=4 biological replicates for each organ and growth condition.

In parallel, the contents in sugar alcohols, inositol, and glycerol, were significantly increased by at least 25% and up to 504% in all P-starved tissues (Fig. 4.5, Supp. Table S4.2). It is important to note that fructose, glucose, and inositol were also found to be more abundant in -P nodules in our GC-MS analysis (Table 4.1). Malonate and malate were found to be the most abundant organic acids in all organs under control conditions, with levels reaching 58,862 pmol/mg DW of malonate in leaves, and 36,004 pmol/mg DW

of malate in nodules. The levels of malonate and malate dropped under P deprivation by at least 72% and 55%, respectively. Besides these two metabolites, the quantities of several other organic acids also significantly diminished in all organs under P-stress: mevalonate and intermediaries of the TCA cycle (citrate, succinate, isocitrate, fumarate, and cis- and trans-aconitate) decreased by 26%-97% (Fig. 4.5, Supp. Table S4.2). These results corroborate our GC-MS profiling where citrate, malate, and succinate demonstrated similar downward trends in -P nodules (Table 4.1, Supplementary Table S4.2). Conversely, the levels of azelaic acid, involved in defense response, rose by 47% in -P leaves (Zoeller et al., 2012) (Supplementary Table S4.2).

4.4.3.3 Phosphorylated Metabolites Dropped Under P Deficiency

In the absence of P, the PLS-DA plot of the phosphorylated metabolites showed a direct separation along component 1, describing 76.7%, 73.8%, and 71.8% of the variance for leaves, roots, and nodules, respectively (Fig. 4.8A, B, C). The levels of all the top 15 phosphorylated compounds declined in all the organs in absence of P, as illustrated in the VIP plots (Fig. 4.8D, E, F). The VIP plot mainly includes intermediaries of glycolysis and cell wall precursors for leaves, metabolites from glycolysis, OPPP, and energy metabolism for roots, and amino-sugars, cell wall precursors, and OPPP intermediaries for nodules (Fig. 4.8D, E, F).

The majority of phosphorylated compounds were significantly lower in all organs of *M. truncatula* due to P deficiency. The most abundant phosphorylated metabolites were glycerol-phosphate in the leaves, and UDP-glucuronic acid in the roots and nodules, independently of the treatment. Once again, leaves were the organ undergoing the most drastic changes due to P deprivation: over a 10-fold decrease was observed for UDP-

glucosamine, UDP-arabinose, UDP, ATP, ADP, CTP, UTP, UDP-galactose, GDP-Mannose, and UDP-xylose, and over a 20-fold drop for CTP, GDP-fucose, and phosphoenolpyruvate (PEP).

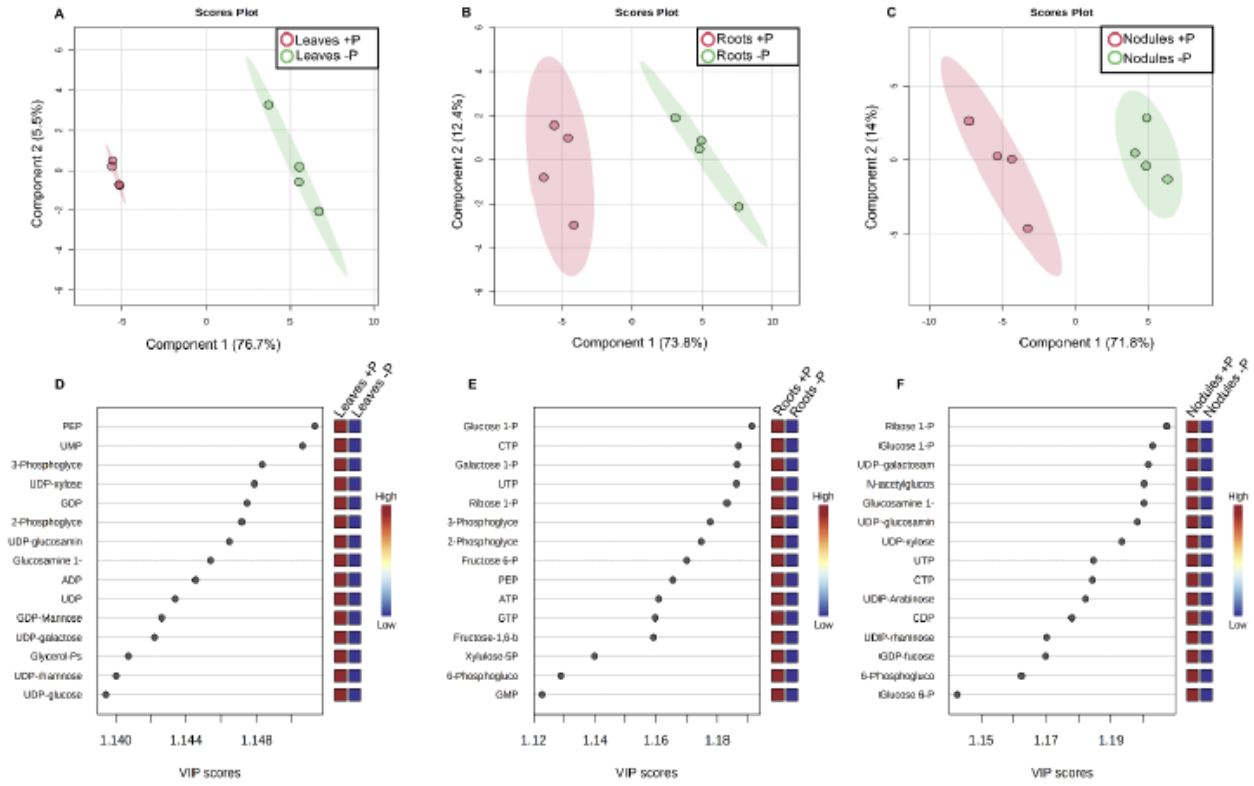

Figure 4.8: **PLS-DA of phosphorylated metabolites showing separation between tissues of *M. truncatula* from +P and –P conditions.**

Leaves (A), Roots (B) and Nodules (C) from +P and -P conditions. Shaded regions in the PLS-DA plot represent 95% confidence intervals. VIP scores showing top 15 important amino acids that contribute the most to the PLS-DA plot of leaves (D), roots (E) and nodules (F). Colors in the variable importance in projection plot represents relative intensity, where red and blue symbolize higher and lower values, respectively. N=4 biological replicates for each organ and growth condition.

Interestingly, most of these compounds are cell wall precursors or involved in energy metabolism. Under P deficiency, the largest changes in roots were UTP (3.1-fold decrease), and CTP and UTP in nodules (3.1- and 3.2-fold reduction, respectively). Phosphorylated sugars, glucose 6-phosphate, glucose 1-phosphate and fructose 6-phosphate, declined by at least 30% in P deficiency. Glycerol-phosphate, an important

precursor required for the synthesis of phospholipids, showed a reduction in all organs under P deprivation, from 30% reduction in nodules to 72% in leaves (Fig. 4.5, Supp. Table S4.2). P-deficient tissues also exhibited a 35% to 95% drop in the levels of energy carriers (ATP, CTP, GTP, and UTP); the strongest decline was CTP with a 19.6-fold reduction in -P leaves (Fig 4.5, Supplementary table S4.2). Interestingly, ribulose 1,5-bisphosphate, component of Calvin cycle only detected in leaves, followed a 2.7-fold increase in -P condition (Fig. 4.5, Supp. Table S4.2). Finally, under P starvation, levels of most phosphorylated metabolites were the highest in nodules (Fig. 4.5, Supp. Table S4.2).

4.5 Discussion

P deficiency is a key abiotic stress that affects nodulation, N_2 fixation, legume growth and productivity (Tesfaye et al., 2007). N_2-fixing legumes are notorious for having a high P demand compared to those grown in mineral N (Graham, 1981; Vance et al., 2003; Sulieman and Tran, 2015). Various biological processes that require high amounts of energy to sustain contribute to the plant's high P requirement. These processes include nitrogenase activity, signal transduction/enzyme regulation involving phosphorylation, biosynthesis of nucleic acids and membrane lipids, and maintenance of homeostasis (Graham and Vance, 2000). There are not many studies in legumes concerning the impact of prolonged P deficiency on overall plant metabolism, especially legumes grown in symbiotic conditions. However, some studies have been reported in non-legume plants like barley (Huang et al., 2008) and *Arabidopsis* (Morcuende et al., 2007) where plants were grown in P stress for shorter duration. The present long duration study used four weeks of P deprivation after plants were grown in P replete media for 10 days. The

research started with comparative metabolic profiling of +P to -P *M. truncatula* nodules where most sugars/sugar alcohols and amino acids were found to be elevated, and organic acids were found to be reduced in P-starvation compared to +P replete conditions (Table 1, Supplementary Table S1). Similar findings were reported in a GC-MS study carried out in leaves and roots of white lupin (Muller et al., 2015) and barley (Huang et al., 2008). Based on the experimental evidence showing that P deprivation affects the metabolism of *M. truncatula* nodules, a targeted metabolomics approach was employed to quantify the impact of P deprivation at the whole plant level, comparing leaves, roots and nodules.

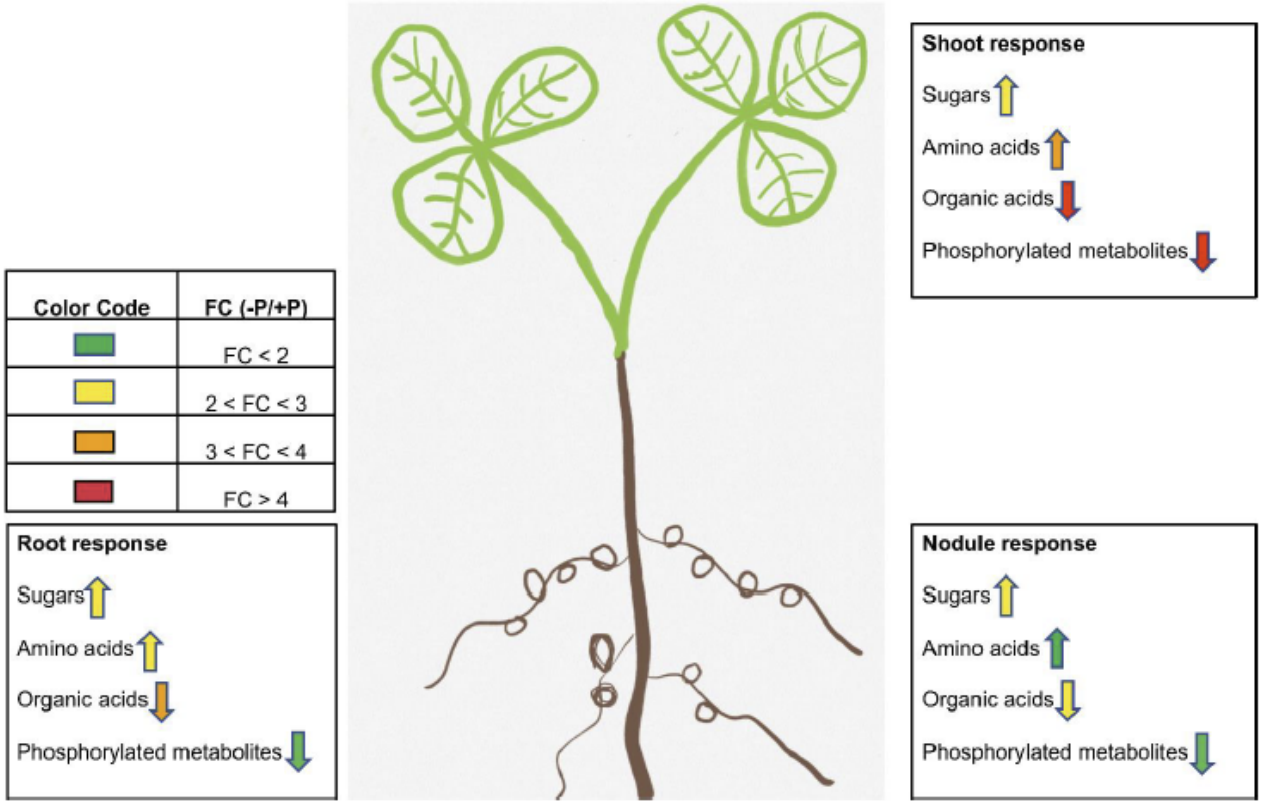

Figure 4.9: **Schematic summary of metabolic and physiological responses observed in -P deficient tissues of *M. truncatula*.**

Fold change (FC); upward and downward arrow indicates increase and decrease in the overall metabolite profile for a class of compounds.

Metabolic profiling revealed that P starvation impacts major classes of metabolites differently: leaves, roots, and nodules display distinct global metabolic phenotypes, summarized in Fig. 4.8. In absence of P, the most drastic shift was seen in leaves where the levels of organic acids and phosphorylated metabolites decreased severely, at least four-fold, while substantial to moderate increases, two- to four-fold, in the amounts of sugars and amino acids was observed (Fig. 4.8). Small boosts in the concentrations of sugars and amino acids was also seen in roots, however, amounts of organic acids declined moderately, especially when compared to the change in phosphorylated metabolites, which declined less than two-fold (Fig. 4.8). In –P nodules compared to +P, the levels of sugars increased more than amino acids. In contrast, the quantity of organic acids was more decreased than phosphorylated metabolites, similar to, but of lesser magnitude than the situation in roots (Fig. 4.8).

P deficiency enhanced the accumulation of sugars like glucose and fructose in the shoots of P-deficient *M. truncatula* (Fig. 4.3 and 4.8; Supp. Table S2). This significant increase in monosaccharides and extremely lowered levels of phosphorylated metabolites like glucose-6-phosphate, fructose-6-phopshate, and ATP in –P leaves compared to roots and nodules, indicates a lower flow of carbon through glycolysis. Glycerol phosphates, a structural element of phospholipids, also declined radically in leaves (Supp. Table S2). These data are consistent with the previous reports in leaves of barley (Huang et al., 2008), white lupin (Muller et al., 2015), and *Arabidopsis* (Morcuende et al., 2007). Severe P stress depletes inorganic P (Pi) pools in all the P starved organs of *M. truncatula* (Dokwal et al., 2021). Under these conditions organic P from phospholipids and small phosphorylated metabolites serves as an alternative source

of P for plant cells (Plaxton, 2004). Plants tend to replace phospholipids with sulfo- and galactolipids as a mechanism to conserve P for other biological processes. Decreases in the amounts of major phospholipids like phosphatidylcholine and phosphatidylethanolamine with simultaneous increase in galactolipids like monogalactosyldiacylglycerol (MGDG) and digalactosyldiacylglycerol (DGDG) in overall plant under P stress is well investigated in *M. truncatula* (Dokwal et al., 2021) and soybean (Gaude et al., 2004). Moreover, -P leaves also exhibited the strongest reduction, compared to roots and nodules, in energy carriers like UTP, CTP, GTP and ADP (Fig. 3 and 8; Supp. Table S2). Depleted intracellular levels of Pi and the consequent reduction in ATP/ADP ratio are proposed to negatively affect the photosynthetic electron transport chain in leaves, reported in barley and *Arabidopsis* (Carstensen et al., 2018). In *M. truncatula* reported here, we found that several TCA cycle intermediates including fumarate, succinate, citrate, and malate were substantially lowered in -P leaves compared to +P leaves (Fig. 3 and 5; Supp. Table S2). TCA cycle intermediates were more lowered in leaves than roots or nodules in P deprivation, suggesting that the TCA cycle is hampered (Fig. 5 and 8). This is consistent with the previous observation of decreased levels of many organic acids in P deficient leaves of *Arabidopsis* (Misson et al., 2005). Reduced levels of organic acids generate two possible explanations: first, because organic acids serve as precursors for increased synthesis of amino acids like asparagine, methionine, glutamine, and GABA in P stress, elevations in the amino acids could lead to depletion of the organic acids (Fig. 5; Supp. Table S2). Second, the TCA cycle could slow down generally in leaves leading to less production of NADH/$FADH_2$ and therefore generating less ATP, and accounting for significantly reduced quantities of energy carriers

in -P leaves. Future experiments are necessary to test these hypotheses. Azelaic acid, a derivative of oleic acid, has been proposed to play a role in plant defense in response to stress by inducing systemic acquired resistance and priming salicylic acid (Zoeller et al., 2012; Djami-Tchatchou et al., 2017). Our results showed increased levels of azelaic acid in -P leaves, indicating the potential for a survival mechanism being induced in *M. truncatula* to cope with P-stress. Azelaic acid levels have been previously shown to change in P-stressed leaves of *Zea mays* plants, with the direction of change dependent on whether the cultivar is P-deprivation tolerant or sensitive (Ganie et al., 2015). This phenomenon also bears further investigation.

Many amino acids demonstrated sharp increases in -P leaves compared to that observed in roots and nodules (Fig. 8). This result could indicate an N feedback mechanism which is inversely related to P supply in the growth medium, a hypothesis previously proposed after similar observations (Almeida et al., 2000; Schulze and Drevon, 2005). P starvation led to a decline in the rhizobial nitrogenase activity in *M. truncatula* nodules (Dokwal et al., 2021). A possible explanation for this phenomenon is that P deficiency impacts plant growth, resulting in a lower demand for newly fixed N_2, an energy expensive mechanism as previously proposed (Fischinger et al., 2006). Thus, a shoot derived signal is probably sent to the nodule through the phloem to induce the down-regulation of the nitrogenase activity (Sulieman, 2011). This hypothesis was supported by the higher abundance of free amino acids in the phloem sap of *M. truncatula* at low concentrations of P (Sulieman et al., 2013). Asparagine, highly abundant in -P leaves and nodules (Fig. 5; Supplementary Table S2), has been hypothesized as the shoot signal,

or as a precursor to the signal, that interacts with the nodule machinery to down-regulate nitrogenase activity (Sulieman and Tran, 2013).

The results from our targeted metabolomics revealed increases in sugars for -P roots and nodules (Fig. 8). Our results corroborate earlier studies showing sucrose, the main carbohydrate source for nodules, was the most abundant sugar in P starved roots and nodules (Schulze et al., 2002). Substantially elevated levels of fructose were also observed in -P roots and nodules (Supp. Table S2). Similar findings have been noted in roots of barley (Huang et al., 2008) and nodules of common bean (Hernandez et al., 2007). We observed severe decreases in the levels of UTP and CTP in roots and nodules under P deficiency, which has not yet been reported. Indeed, the metabolic pools of the pyrimidine nucleotides were found to be markedly lower than their purine nucleotide counterparts in all –P tissues; strikingly, the UMP pool is significantly lower in –P nodules while the other NMP pools remain unaffected in nodules (Fig. 5; Supp. Table 2). UTP provides the energy for carbohydrate anabolic processes by forming UDP-monosaccharide intermediates. UDP sugar intermediates (Supp. Table S2) were found to decrease substantially in –P leaves (levels are 83% to 94% of the amounts found in +P leaves) while in roots and nodules, the decrease was found to be about half that much (14% to 51% lower in –P roots/nodules compared to +P roots/nodules) (Supp. Table S2). The GDP-monosaccharide precursors GDP-mannose and GDP-fucose showed similar profiles in the respective tissues. Much of this metabolism provides precursors for cell wall biosynthesis and growth, these UDP-monosaccharide levels likely reflect lower levels of cell growth in roots and nodules with major decreases in leaf tissue. TCA cycle intermediates citrate, malate, succinate, and fumarate that serve as a precursor for

synthesis of amino acids were diminished in -P roots. These findings were consistent with the previous findings described in roots of barley (Huang et al., 2008), *M. truncatula* (Sulieman et al., 2013) and *Arabidopsis (Morcuende et al., 2007)*. Tryptophan, the most abundant amino acid in roots, increased under P stress (Fig. 3 and 5; Supp. Table S2). Previous studies in P deficient roots of *A. thaliana* (Pant et al., 2015) and white lupin (Muller et al., 2015) have noted similar results. Plants use tryptophan for the synthesis of auxins, thereby promoting lateral root growth during limited supply of P (Ljung et al., 2002; Kriechbaumer and Glawischnig, 2005; Mano and Nemoto, 2012; Dokwal et al., 2021). Other aromatic amino acids: phenylalanine, and tyrosine, were also elevated in -P tissues (Fig. 5; Supplementary Table S2). These amino acids are precursors of phenylpropanoid pathway that synthesizes flavonoids which are required by legumes for establishment of successful symbiotic relationship, and generally in plants for cell wall precursors (Tohge et al., 2013).

Globally, the metabolic profile of -P nodules was similar to that of +P roots (Fig. 2). Interestingly, nodules had lower percentage changes in -P conditions compared to +P conditions in all classes of the metabolites compared to other tissues in -P conditions (Fig. 8). These data suggest that legumes strategically allocate resources to nodules during P stress to sustain N_2 fixation. It is important to recognize that the metabolomics approach taken in our study and previous metabolomics studies undertaken to probe N_2 fixing nodules cannot distinguish between those metabolites that are in the plant cell portion of the nodule from those that are in the internalized bacteroids within the plant cells (Hernandez et al., 2007; Hernandez et al., 2009; Sulieman et al., 2013; Sulieman and Tran, 2013; Sulieman et al., 2013; Sulieman and Tran, 2015; Akram et al., 2017). The

plant transports dicarboxylic acids to bacteroids for the TCA cycle to fuel the high ATP levels required to sustain N_2 fixation, along with the N-source arginine, with alanine and ammonium released by the rhizobia to the plant (Watson et al., 1988; Flores-Tinoco et al., 2020). It is interesting to note that arginine levels rise in all –P tissues measured, with a smaller increase found in nodules compared to roots and leaves, consistent with a role for arginine as an N source for the rhizobia, and thus consumed by the rhizobia. The high levels of TCA cycle intermediates in –P nodules are expected to originate from both bacteroids and plant metabolism. In contrast, the higher levels of glycolytic intermediates that are maintained in –P nodules compared to –P leaves and roots are expected to mostly reflect the plant host's metabolic portion because bacteroids do not rely on glycolysis as a source of TCA cycle intermediates (Salminen and Streeter, 1987).

Enhanced enzyme activities, such as that of phosphoenolpyruvate carboxylase (PEPC), are necessary to sustain N_2 fixation (Sulieman and Tran, 2015). Previous studies have shown enhanced activities of nodule PEPC, malate dehydrogenase and malic enzyme with a concomitant decline in pyruvate kinase activity in nodules in P deprivation. This has been hypothesized to bypass the need for pyruvate kinase necessary to supply carbon to the TCA pool, when ATP levels required for pyruvate kinase activity are lower because of P starvation (Sulieman and Tran 2015). The bypass allows the continued ability of cells to synthesize more organic acids, like malate and succinate or provide pyruvate via a non-adenylate and non-Pi requiring metabolic route (Sulieman and Tran, 2015). During P deficiency, dicarboxylates not only serve as C fuel for bacteroids to sustain nitrogenase activity but also are transformed to oxaloacetate to generate asparagine, the principle N export in legumes (Schulze et al., 2006; Stevens et al., 2019).

For legumes like *M. truncatula* growing in low P conditions, the need for continued reliance on nitrogen fixation is accommodated by several key adaptations that occur in the whole pant. In the absence of P, leaves suffered the most drastic global metabolic shift compared to roots and especially nodules. Overall, the results of this study provide a basic groundwork for in-depth molecular dissection concerning the relationship of P availability and N_2 fixing capacity in legumes.

4.6 Supplemental Data for Chapter 4

Supplemental Table 4.1 List of compound/features non- significantly accumulated in nodules from +P and -P which were detected by untargeted metabolomics.

Data shown represents the average normalized peak intensity ± standard deviation of N=3 biological replicates.

(a) Compound name or (b) Mass-to-charge (m/z)	Retention time (minutes)	Average normalized intensity ± SD	
		Nodules +P	Nodules -P
Alanine[a]	19.27	1.21E-03 ± 1.03E-04	2.23E-03 ± 2.58E-03
Serine[a]	26.73	1.27E-04 ± 6.37E-05	1.36E-04 ± 6.90E-05
Fumarate[a]	30.73	6.54E-03 ± 9.45E-04	6.43E-03 ± 6.64E-04
GABA[a]	38.75	1.76E-02 ± 3.72E-03	2.13E-02 ± 2.85E-03
Glutamine[a]	48.07	1.72E-03 ± 9.98E-04	3.25E-03 ± 3.97E-04
Shikimate[a]	49.48	1.59E-03 ± 1.02E-04	1.31E-03 ± 2.30E-04
Raffinose[a]	74.73	2.65E-01 ± 9.65E-02	7.41E-01 ± 3.43E-01
171.10[b]	12.25	3.16E-03 ± 1.45E-04	4.74E-03 ± 1.07E-03
221.10[b]	13.65	8.54E-04 ± 2.47E-04	1.06E-03 ± 4.10E-04
374.20[b]	15.27	8.94E-03 ± 6.74E-04	1.23E-02 ± 2.02E-03
174.10[b]	27.27	2.61E-02 ± 1.73E-03	1.91E-02 ± 4.39E-03
158.20[b]	27.53	7.84E-04 ± 6.66E-05	9.66E-04 ± 3.14E-04
158.20[b]	28.57	1.04E-03 ± 8.72E-05	1.33E-03 ± 4.06E-04
217.08[b]	31.20	3.91E-03 ± 1.32E-03	5.10E-03 ± 4.90E-04
204.20[b]	31.68	1.62E-03 ± 6.93E-04	2.78E-03 ± 2.98E-04

(table continues)

(a) Compound name or (b) Mass-to-charge (m/z)	Retention time (minutes)	Average normalized intensity ± SD	
		Nodules +P	Nodules -P
218.20[b]	32.92	6.42E-04 ± 1.26E-04	1.15E-03 ± 3.57E-04
160.10[b]	34.18	1.48E-03 ± 2.03E-04	1.06E-03 ± 3.39E-04
174.20[b]	34.45	1.42E-03 ± 2.04E-04	1.50E-03 ± 1.75E-04
244.10[b]	39.58	1.73E-04 ± 3.35E-05	1.41E-03 ± 7.97E-04
188.20[b]	42.98	3.95E-03 ± 3.20E-03	8.24E-04 ± 1.89E-04
260.20[b]	45.98	7.75E-04 ± 1.44E-04	1.01E-03 ± 1.69E-04
217.10[b]	48.20	1.28E-02 ± 8.37E-04	1.13E-02 ± 1.49E-03
295.20[b]	48.50	7.07E-04 ± 4.70E-04	3.58E-04 ± 2.10E-05
260.30[b]	54.68	4.77E-04 ± 4.28E-04	2.05E-03 ± 1.73E-03
333.20[b]	57.85	6.32E-04 ± 7.61E-05	9.02E-04 ± 1.97E-04
333.20[b]	58.42	1.26E-03 ± 1.05E-04	1.04E-03 ± 2.26E-04
352.20[b]	59.70	4.63E-05 ± 2.30E-05	1.14E-03 ± 8.39E-04
245.10[b]	59.87	1.66E-03 ± 2.75E-04	2.34E-03 ± 4.01E-04
204.10[b]	62.52	3.22E-02 ± 1.79E-03	2.97E-02 ± 3.02E-03
217.10[b]	68.90	4.11E-03 ± 9.73E-04	5.51E-03 ± 4.34E-04
204.10[b]	73.12	9.95E-04 ± 1.85E-04	8.91E-04 ± 1.16E-04
204.10[b]	76.77	6.65E-04 ± 8.81E-05	8.79E-04 ± 1.55E-04
207.10[b]	90.27	2.35E-03 ± 1.49E-03	1.60E-03 ± 2.61E-04

[a] Identified metabolites; [b] Unidentified metabolites

Supplemental Table 4.2 Targeted metabolomic analyses of *M. truncatula* leaves, roots, and nodules grown in +P and -P conditions with *S. meliloti* Rm41 after 28 DPI.

Metabolite concentrations are expressed as picomoles per milligram DW. Data are the average ± SD of 4 independent experiments. ND represents not detected. Values in bold are significantly different ($p<0.05$) between respective tissues from +P and -P conditions. PD represent phosphorus deficient tissues.

	Average ± SD					
	Leaves +P	**Leaves -P**	**Roots +P**	**Roots -P**	**Nodules +P**	**Nodules -P**
Amino Acids						
Glutamate	2.10E+04 ± 1.61E+03	1.56E+03 ± 2.05E+02	5.21E+03 ± 8.21E+02	2.82E+03 ± 2.46E+02	2.14E+04 ± 1.28E+03	1.43E+04 ± 6.24E+02
Aspartate	1.61E+04 ± 1.57E+03	2.87E+03 ± 5.65E+02	6.45E+03 ± 1.06E+03	1.74E+03 ± 1.77E+02	7.69E+03 ± 1.14E+03	4.61E+03 ± 2.07E+02
Tryptophan	7.82E+03 ± 1.47E+03	5.42E+03 ± 1.0E+03	4.66E+03 ± 4.27E+02	2.44E+04 ± 1.88E+03	6.02E+03 ± 8.04E+02	1.46E+04 ± 7.94E+02
GABA	6.80E+03 ± 1.96E+03	1.09E+04 ± 9.35E+02	4.09E+03 ± 2.23E+02	1.90E+03 ± 7.68E+01	3.45E+03 ± 3.29E+02	4.70E+03 ± 4.46E+02
Serine	9.70E+03 ± 7.95E+02	2.20E+04 ± 1.57E+03	3.90E+03 ± 4.72E+02	3.87E+03 ± 3.49E+02	2.27E+03 ± 2.69E+02	3.46E+03 ± 1.26E+02
Histidine	1.07E+03 ± 1.86E+02	2.94E+03 ± 1.09E+03	1.05E+03 ± 1.93E+02	2.05E+03 ± 5.26E+02	1.39E+03 ± 1.81E+02	2.27E+03 ± 8.53E+01
Lysine	1.59E+03 ± 9.53E+01	3.93E+03 ± 6.50E+02	7.00E+02 ± 2.57E+01	1.69E+03 ± 1.01E+02	1.29E+03 ± 5.63E+01	1.73E+03 ± 5.18E+01
Threonine	4.29E+03 ± 2.15E+02	4.01E+03 ± 2.12E+02	1.63E+03 ± 2.24E+02	1.85E+03 ± 2.67E+02	1.10E+03 ± 9.29E+01	1.59E+03 ± 6.67E+01
Valine	1.80E+03 ± 9.32E+01	1.86E+03 ± 3.15E+02	8.12E+02 ± 1.42E+02	1.18E+03 ± 1.68E+02	1.05E+03 ± 7.71E+01	1.58E+03 ± 1.45E+02
Leucine	2.62E+03 ± 1.63E+02	5.06E+03 ± 9.33E+02	6.20E+02 ± 7.23E+01	8.03E+02 ± 3.66E+01	7.99E+02 ± 6.98E+01	1.11E+03 ± 5.39E+01
Arginine	1.23E+03 ± 1.24E+02	4.65E+03 ± 1.51E+03	2.76E+02 ± 3.88E+01	6.68E+02 ± 5.25E+01	7.40E+02 ± 3.29E+01	1.38E+03 ± 7.98E+01
Homoserine	7.61E+02 ± 5.16E+01	6.06E+02 ± 6.10E+01	7.98E+02 ± 2.94E+02	1.74E+03 ± 2.83E+02	7.25E+02 ± 2.14E+01	9.93E+02 ± 9.12E+01
Isoleucine	1.72E+03 ± 1.48E+02	1.68E+03 ± 2.72E+02	7.97E+02 ± 1.32E+02	1.62E+03 ± 6.68E+01	7.19E+02 ± 2.86E+01	1.26E+03 ± 6.23E+01
Phenylalanine	1.38E+03 ± 5.38E+01	3.00E+03 ± 5.83E+02	6.55E+02 ± 9.34E+01	1.61E+03 ± 3.07E+02	6.72E+02 ± 3.49E+01	1.07E+03 ± 4.21E+01
Nicotinamide	2.25E+02 ± 2.35E+01	1.92E+02 ± 2.65E+01	1.49E+02 ± 2.79E+01	1.66E+02 ± 1.92E+01	5.87E+02 ± 3.66E+01	7.36E+02 ± 4.78E+01
Tyrosine	9.12E+02 ± 6.59E+01	1.51E+03 ± 3.10E+02	3.10E+02 ± 2.61E+01	3.50E+02 ± 3.54E+01	5.26E+02 ± 4.66E+01	7.27E+02 ± 4.49E+01
Ornithine	6.26E+01 ± 1.36E+01	4.05E+02 ± 1.79E+02	6.95E+01 ± 5.87E+00	1.70E+02 ± 3.38E+01	1.02E+02 ± 4.14E+00	1.57E+02 ± 1.44E+01
Methionine	2.60E+02 ± 1.73E+01	8.30E+02 ± 2.28E+02	6.60E+01 ± 3.37E+01	1.34E+02 ± 2.19E+01	1.01E+02 ± 1.21E+01	1.84E+02 ± 1.09E+01
Nicotinic acid	1.57E+01 ± 6.08E+00	1.01E+02 ± 2.11E+01	1.90E+01 ± 8.97E+00	4.04E+01 ± 7.32E+00	8.86E+01 ± 4.03E+00	1.74E+02 ± 2.42E+01
Hydroxyproline	6.14E+01 ± 9.75E+00	4.97E+01 ± 2.47E+01	7.21E+01 ± 1.54E+01	6.20E+01 ± 2.76E+01	6.97E+01 ± 1.04E+01	9.38E+01 ± 3.94E+00
Citrulline	1.73E+02 ± 4.77E+01	2.04E+03 ± 4.93E+02	1.70E+01 ± 1.91E+00	3.58E+01 ± 5.51E+00	4.00E+01 ± 4.02E+00	9.01E+01 ± 2.91E+00
Asparagine	3.65E+04 ± 7.24E+03	7.55E+04 ± 9.85E+03	2.32E+04 ± 5.16E+03	1.41E+04 ± 2.58E+03	5.41E+04 ± 1.24E+04	7.51E+04 ± 3.86E+03
Alanine	6.93E+03 ± 6.61E+02	6.19E+03 ± 7.84E+02	2.26E+03 ± 1.96E+02	8.64E+02 ± 1.94E+02	5.23E+03 ± 7.77E+02	4.66E+03 ± 2.55E+02
Glutamine	3.51E+03 ± 8.24E+01	1.08E+04 ± 3.67E+03	1.86E+03 ± 2.96E+02	2.57E+03 ± 2.14E+02	3.49E+03 ± 1.61E+03	4.99E+03 ± 1.79E+02
Glycine	3.12E+02 ± 6.53E+01	1.16E+03 ± 1.69E+02	5.24E+02 ± 1.45E+02	5.88E+02 ± 7.14E+01	2.06E+03 ± 5.69E+02	2.56E+03 ± 1.82E+02
Proline	2.07E+03 ± 2.99E+02	2.26E+03 ± 2.85E+02	6.53E+02 ± 8.16E+01	4.77E+02 ± 4.79E+01	9.48E+02 ± 1.46E+02	1.16E+03 ± 3.94E+01
Cysteine	ND	ND	ND	ND	ND	ND

(table continues)

	Average ± SD					
	Leaves +P	Leaves -P	Roots +P	Roots -P	Nodules +P	Nodules -P
Cystine	ND	5.78E+01 ± 2.31E+01	ND	7.63E+01 ± 2.03E+01	8.25E+00 ± 3.13E-01	1.25E+01 ± 2.11E+00
Sugars						
Sucrose	1.39E+04 ± 4.52E+03	8.17E+03 ± 3.72E+03	3.84E+04 ± 1.39E+04	1.15E+05 ± 1.02E+04	6.84E+04 ± 2.67E+04	1.47E+05 ± 7.19E+03
Glucose	8.81E+03 ± 3.77E+03	2.93E+04 ± 5.01E+03	8.69E+03 ± 1.15E+03	1.43E+04 ± 3.58E+03	3.19E+03 ± 3.36E+02	7.21E+03 ± 5.61E+02
Glycerol	3.43E+03 ± 7.93E+02	2.07E+04 ± 2.69E+03	5.13E+03 ± 1.43E+03	7.21E+03 ± 2.02E+02	2.15E+03 ± 2.47E+02	1.48E+03 ± 1.55E+02
Inositol	8.89E+03 ± 6.35E+02	1.11E+04 ± 8.25E+02	7.41E+02 ± 1.34E+02	2.17E+03 ± 2.80E+02	2.03E+03 ± 1.30E+02	3.21E+03 ± 1.16E+02
Fructose	1.46E+04 ± 5.91E+03	3.59E+04 ± 1.08E+04	1.24E+04 ± 4.51E+03	3.42E+04 ± 1.37E+04	1.29E+03 ± 1.71E+02	1.12E+04 ± 1.39E+03
Mannitol	1.12E+03 ± 1.82E+02	1.51E+03 ± 1.80E+02	7.17E+02 ± 1.28E+02	1.19E+03 ± 3.70E+02	8.84E+02 ± 9.61E+01	1.50E+03 ± 9.59E+01
Maltose	5.86E+02 ± 2.38E+02	8.48E+02 ± 1.23E+02	7.83E+01 ± 3.38E+01	1.22E+02 ± 1.02E+02	9.21E+01 ± 3.01E+01	6.66E+01 ± 6.90E+00
Arabitol	2.01E+02 ± 2.19E+01	2.52E+02 ±1.83E+01	3.78E+01 ± 5.99E+00	4.95E+01 ± 8.25E+00	1.80E+01 ± 1.09E+00	2.78E+01 ± 2.16E+00
Erythritol/Threitol	ND	ND	ND	ND	ND	ND
Sorbitol	ND	ND	ND	ND	ND	ND
Galactitol	ND	ND	ND	ND	ND	ND
Trehalose	9.03E+01 ± 9.55E+01	1.90E+02 ± 6.18E+01	1.29E+02 ± 5.83E+01	2.57E+02 ± 5.96E+01	4.07E+02 ± 1.64E+02	2.71E+02 ± 1.38E+02
Phosphorylated metabolites						
UDP-glucuronic acid	1.59E+03 ± 4.13E+02	2.76E+02 ± 1.77E+02	2.50E+03 ± 1.21E+03	1.42E+03 ± 4.57E+01	4.63E+03 ± 3.71E+02	2.27E+03 ± 6.96E+02
Glucose-6-phosphate	5.44E+02 ± 7.38E+01	2.41E+02 ± 3.79E+01	1.71E+03 ± 3.27E+02	9.87E+02 ± 5.46E+01	2.37E+03 ± 2.54E+02	1.63E+03 ± 6.11E+01
Glycerol-Phosphates	7.99E+03 ± 6.10E+02	2.23E+03 ± 3.15E+02	1.36E+03 ± 3.59E+02	7.66E+02 ± 8.56E+01	1.13E+03 ± 1.34E+02	7.89E+02 ± 2.48E+01
UDP-rhamnose	4.04E+02 ± 3.50E+01	5.20E+01 ± 1.27E+01	4.87E+02 ± 8.62E+01	2.97E+02 ± 2.48E+01	1.06E+03 ± 5.89E+01	7.30E+02 ± 4.87E+01
CDP	3.07E+02 ± 3.27E+01	1.19E+01 ± 6.26E+00	3.73E+02 ± 6.65E+01	2.09E+02 ± 2.58E+01	1.03E+03 ± 1.83E+02	4.01E+02 ± 1.63E+01
Fructose-6-phosphate	2.03E+02 ± 2.44E+01	9.56E+01 ± 2.12E+01	7.28E+02 ± 6.35E+01	3.85E+02 ± 3.35E+01	9.70E+02 ± 1.36E+02	6.33E+02 ± 2.45E+01
3-Phosphoglycerate	7.86E+02 ± 1.13E+02	1.23E+02 ± 7.21E+00	5.74E+02 ± 3.26E+01	3.11E+02 ± 2.66E+01	6.92E+02 ± 5.75E+01	5.82E+02 ± 1.85E+01
Ribose-5-phosphate	2.85E+02 ± 3.97E+01	9.07E+01 ± 1.74E+01	5.42E+02 ± 3.25E+01	4.83E+02 ± 3.27E+01	6.55E+02 ± 7.40E+01	5.47E+02 ± 4.25E+01
2-Phosphoglycerate	7.03E+02 ± 1.09E+02	1.13E+02 ± 6.66E+00	5.00E+02 ± 3.09E+01	2.75E+02 ± 2.43E+01	6.39E+02 ± 5.31E+01	5.00E+02 ± 2.28E+01
Mannose-6-phosphate	1.49E+02 ± 2.46E+01	7.72E+01 ± 1.36E+01	4.74E+02 ± 8.54E+01	2.74E+02 ± 1.68E+01	6.32E+02 ± 6.99E+01	4.38E+02± 8.21E+00
UDP-glucose	2.39E+02 ± 2.92E+01	2.88E+01 ± 7.52E+00	4.32E+02 ± 9.37E+01	2.90E+02 ± 1.35E+01	5.93E+02 ± 1.17E+02	2.97E+02 ± 2.31E+01
ATP	3.59E+02 ± 1.08E+02	2.91E+01 ± 1.52E+01	4.92E+02 ± 2.73E+01	3.16E+02 ± 2.51E+01	5.84E+02 ± 1.48E+02	3.31E+02 ± 9.93E+00
UDP-galactosamine	1.66E+02 ± 1.30E+01	1.90E+01 ± 5.78E+00	1.67E+02 ± 1.59E+01	1.36E+02 ± 1.94E+01	4.74E+02 ± 3.24E+01	2.46E+02 ± 1.30E+01
Erythrose4-phosphate	3.89E+02 ± 1.14E+02	3.97E+02 ± 1.81E+02	2.80E+02 ± 9.78E+01	1.29E+02 ± 5.37E+01	3.92E+02 ± 7.90E+01	3.46E+02 ± 8.35E+01
UTP	2.01E+02 ± 4.71E+01	1.06E+01 ± 7.80E+00	3.18E+02 ± 3.66E+01	1.01E+02 ± 1.06E+01	3.83E+02 ± 7.35E+01	1.20E+02 ± 1.01E+01

(table continues)

	Average ± SD					
	Leaves +P	Leaves -P	Roots +P	Roots -P	Nodules +P	Nodules -P
ADP	2.33E+02 ± 3.41E+01	2.00E+01 ± 4.48E+00	2.47E+02 ± 3.76E+01	1.96E+02 ± 2.61E+01	3.79E+02 ± 7.72E+01	3.37E+02 ± 2.90E+01
UDP-Arabinose	2.82E+02 ± 1.34E+01	1.63E+01 ± 1.03E+01	1.91E+02 ± 2.72E+01	1.53E+02 ± 1.22E+01	3.63E+02 ± 2.76E+01	2.38E+02 ± 8.58E+00
UDP	1.33E+02 ± 1.69E+01	6.80E+00 ± 2.43E+00	1.89E+02 ± 5.13E+01	1.09E+02 ± 1.81E+01	2.81E+02 ± 4.67E+01	1.71E+02 ± 1.62E+01
CMP	1.34E+01 ± 1.27E+00	1.21E+01 ± 1.28E+01	4.75E+01 ± 9.06E+00	2.76E+01 ± 3.97E+00	2.12E+02 ± 1.94E+01	2.20E+02 ± 1.29E+01
CTP	8.23E+01 ± 2.25E+01	4.19E+00 ± 3.10E+00	1.30E+02 ± 5.49E+00	5.78E+01 ± 5.76E+00	2.11E+02 ± 4.15E+01	6.74E+01 ± 5.98E+00
PEP	2.98E+02 ± 4.64E+01	1.34E+01 ± 1.40E+00	1.70E+02 ± 1.73E+01	8.83E+01 ± 8.08E+00	1.95E+02 ± 2.29E+01	1.75E+02 ± 8.18E+00
UDP-glucosamine	2.98E+02 ± 4.64E+01	4.17E+00 ± 1.04E+00	5.38E+01 ± 5.76E+00	4.62E+01 ± 5.80E+00	1.86E+02 ± 1.32E+01	9.27E+01 ± 6.76E+00
6-Phosphogluconate	4.16E+01 ± 6.04E+00	3.50E+01 ± 7.89E+00	2.50E+02 ± 2.42E+01	1.14E+02 ± 2.29E+01	1.84E+02 ± 1.85E+01	1.22E+02 ± 4.01E+00
UDP-galactose	9.77E+01 ± 8.95E+00	8.58E+00 ± 2.46E+00	1.09E+02 ± 2.20E+01	7.08E+01 ± 4.07E+00	1.74E+02 ± 2.96E+01	1.05E+02 ± 8.21E+00
GTP	8.79E+01 ± 2.45E+01	1.03E+01 ± 3.94E+00	1.30E+02 ± 1.41E+01	6.67E+01 ± 7.01E+00	1.68E+02 ± 3.66E+01	9.31E+01 ± 2.31E+00
N-acetylglucosamine6--phosphate	4.62E+01 ± 7.33E+00	1.00E+01 ± 1.98E+00	9.86E+01 ± 6.95E+00	7.41E+01 ± 1.24E+01	1.52E+02 ± 1.19E+01	7.67E+01 ± 3.93E+00
GDP-Mannose	1.32E+02 ± 1.05E+01	8.42E+00 ± 2.78E+00	8.33E+01 ± 9.55E+00	6.69E+01 ± 8.10E+00	1.33E+02 ± 2.43E+01	8.99E+01 ± 4.78E+00
GMP	4.28E+01 ± 6.22E+00	6.76E+01 ± 2.28E+01	4.17E+01 ± 6.49E+00	1.99E+01 ± 3.44E+00	1.20E+02 ± 6.06E+01	1.03E+02 ± 5.12E+01
Galactose-1-phosphate	8.07E+01 ± 2.19E+01	8.79E+01 ± 1.49E+00	1.35E+02 ± 4.86E+00	6.39E+01 ± 5.82E+00	1.16E+02 ± 9.05E+00	8.15E+01± 6.41E+00
Fructose-1,6-bisphosphate	2.79E+01 ± 1.28E+01	1.86E+01 ± 7.07E+00	1.04E+02 ± 6.55E+00	6.57E+01 ± 5.32E+00	1.13E+02 ± 2.96E+01	8.75E+01 ± 1.09E+01
UMP	4.22E+01 ± 3.89E+00	6.94E+00 ± 5.22E-01	6.65E+01 ± 6.96E+00	4.70E+01 ± 4.88E+00	1.06E+02 ± 1.66E+01	7.42E+01 ± 5.16E+00
GDP	4.65E+01 ± 4.87E+00	6.24E+00 ± 9.67E-01	5.43E+01 ± 7.67E+00	4.75E+01 ± 5.34E+00	7.75E+01 ± 9.86E+00	7.66E+01 ± 5.01E+00
N-acetylglucosamine-1-phosphate	3.76E+01 ± 8.72E+00	3.61E+01 ± 5.64E+00	4.40E+01 ± 5.94E+00	3.14E+01 ± 6.43E+00	7.12E+01 ± 5.28E+00	5.41E+01 ± 2.75E+00
Sedoheptulose-7-phosphate	4.72E+01 ± 6.30E+00	3.03E+01 ± 9.51E+00	3.95E+01 ± 6.96E+00	2.19E+01 ± 2.54E+00	7.02E+01 ± 8.12E+00	7.13E+01 ± 2.67E+00
UDP-xylose	3.76E+01 ± 2.84E+00	2.72E+00 ± 6.22E-01	2.28E+01 ± 3.13E+00	1.37E+01 ± 3.95E+00	5.64E+01 ± 3.03E+00	3.44E+01 ± 2.04E+00
AMP	1.24E+01 ± 2.22E+00	1.53E+01 ± 4.06E+00	2.48E+01 ± 5.92E+00	2.84E+01 ± 5.69E+00	4.95E+01 ± 1.39E+01	5.55E+01 ± 1.40E+01
Ribose-1-phosphate	2.40E+01 ± 1.26E+01	2.33E+01 ± 4.07E+00	3.89E+01 ± 5.79E+00	1.41E+01 ± 7.66E-01	4.41E+01 ± 3.01E+00	1.98E+01 ± 9.19E-01
Xylulose-5-phosphate	5.07E+00 ± 1.75E+00	9.58E+00 ±5.79E+00	1.47E+02 ± 1.86E+01	6.77E+01 ± 1.22E+01	3.77E+01 ± 8.04E+00	5.42E+01 ± 7.04E+00
Sucrose-6-phosphate	4.60E+00 ± 7.01E-01	2.64E+00 ± 5.32E-01	2.29E+01 ± 1.41E+01	1.75E+01 ± 1.89E+00	2.88E+01 ± 8.68E+00	4.10E+01 ± 6.80E+00
GDP-fucose	3.93E+01 ± 1.63E+00	1.70E+00 ± 8.69E-01	1.86E+01 ± 2.90E+00	8.73E+00 ± 3.34E+00	1.90E+01 ± 2.29E+00	1.02E+01 ± 8.33E-01
Trehalose-6-phosphate	9.37E-01 ± 3.71E-01	1.82E+00 ± 1.16E-01	1.53E+01 ± 1.03E+01	8.26E+00 ± 1.29E+00	1.43E+01 ± 4.19E+00	1.81E+01 ± 3.96E+00
Glucosamine-1-phosphate	1.71E+01 ± 7.44E-01	4.77E+00 ± 5.70E-01	1.41E+01 ± 1.13E+00	1.23E+01 ± 1.31E+00	1.25E+01 ± 9.79E-01	6.17E+00 ± 3.48E-01

(table continues)

	Average ± SD					
	Leaves +P	Leaves -P	Roots +P	Roots -P	Nodules +P	Nodules -P
Ribulose-1,5-bisphosphate	4.05E+01 ± 9.51E+00	1.08E+02 ± 1.44E+01	ND	ND	ND	ND
GDP-glucose	ND	ND	ND	ND	ND	ND
UDP-galacturonic acid	ND	ND	ND	ND	ND	ND
ADP-glucose	ND	ND	ND	ND	ND	ND
Deoxyxylulose-5-phosphate	ND	ND	ND	ND	ND	ND
IMP	ND	ND	ND	ND	ND	ND
IDP	ND	ND	ND	ND	ND	ND
ITP	ND	ND	ND	ND	ND	ND
Glucosamine-6-phosphate	ND	ND	ND	ND	ND	ND
Organic acids						
Malonate	5.89E+04 ± 5.81E+03	4.38E+03 ± 9.28E+02	2.15E+04 ± 1.40E+03	6.00E+03 ± 8.14E+02	3.61E+04 ± 1.17E+03	6.75E+03 ± 2.92E+02
Malate	2.45E+04 ± 4.96E+03	1.96E+03 ± 1.07E+02	2.83E+04 ± 4.64E+03	3.44E+03 ± 5.48E+02	3.60E+04 ± 3.16E+03	1.61E+04 ± 3.09E+02
Citrate	1.44E+04 ± 1.89E+03	1.45E+03 ± 4.33E+02	1.22E+04 ± 6.99E+02	3.25E+03 ± 1.01E+03	2.28E+04 ± 1.93E+03	8.61E+03 ± 2.55E+02
Pyruvate	7.48E+03 ± 9.33E+02	5.96E+03 ± 7.23E+02	6.11E+03 ± 3.53E+03	1.30E+04 ± 1.51E+03	1.75E+04 ± 2.04E+03	2.39E+04 ± 4.10E+03
Succinate	3.37E+03 ± 4.24E+02	4.51E+02 ± 3.98E+01	1.94E+03 ± 1.88E+02	4.36E+02 ± 5.59E+01	4.03E+03 ± 9.97E+01	2.36E+03 ± 2.03E+02
2-ketoglutarate	1.20E+03 ± 2.74E+02	3.14E+02 ± 7.47E+01	9.28E+02 ± 3.49E+02	8.32E+02 ± 5.18E+01	3.57E+03 ± 3.71E+02	3.13E+03 ± 1.71E+02
Isocitrate	7.35E+02 ± 9.75E+01	7.77E+01 ± 2.07E+01	7.84E+02 ± 6.91E+01	1.49E+02 ± 3.98E+01	1.55E+03 ± 1.72E+02	3.61E+02 ± 1.31E+01
Fumarate	4.26E+02 ± 1.01E+02	6.12E+01 ± 6.77E+00	6.62E+02 ± 3.00E+02	9.93E+01 ± 1.77E+01	1.52E+03 ± 1.12E+02	1.12E+03 ± 9.22E+01
cis-Aconitate	9.46E+02 ± 1.32E+02	2.28E+01 ± 3.94E+00	6.78E+02 ± 3.84E+01	9.04E+01 ± 2.75E+01	1.41E+03 ± 1.70E+02	2.44E+02 ± 1.91E+01
Ascorbate	ND	ND	ND	ND	ND	ND
Glutarate	4.36E+01 ± 4.80E+00	3.92E+01 ± 5.13E+00	2.47E+02 ± 5.26E+01	1.54E+02 ± 3.73E+01	3.99E+02 ± 1.46E+01	1.91E+02 ± 1.54E+01
Shikimate	9.01E+01 ± 2.78E+01	9.30E+01 ± 2.41E+01	7.92E+01 ± 7.87E+00	6.82E+01 ± 8.90E+00	2.93E+02 ± 3.11E+01	1.82E+02 ± 2.76E+00
Gluconate	1.83E+02 ± 9.36E+00	1.67E+02 ± 2.03E+01	4.83E+01 ± 4.13E+00	7.16E+01 ± 4.51E+00	1.50E+02 ± 1.30E+01	1.59E+02 ± 2.52E+00
Maleic acid	1.48E+01 ± 1.82E+00	1.62E+01 ± 1.45E+00	1.48E+02 ± 1.12E+02	8.37E+01 ± 2.01E+01	6.54E+01 ± 3.06E+01	2.17E+02 ± 5.02E+01
trans-Aconitate	1.65E+01 ± 2.46E+00	0.00E+00 ± 0.00E+00	2.28E+01 ± 4.76E+00	0.00E+00 ± 0.00E+00	6.24E+01 ± 8.89E+00	1.60E+01 ± 1.16E+00
Azelaic acid	1.67E+01 ± 7.64E-01	2.44E+01 ± 3.77E+00	4.14E+01 ± 8.97E+00	4.38E+01 ± 1.32E+00	4.75E+01 ± 3.52E+00	3.58E+01 ± 2.07E+00
Mevalonate	1.85E+01 ± 1.24E+00	1.38E+01 ± 1.36E+00	1.14E+01 ± 1.65E+00	7.71E+00 ± 8.62E-02	1.44E+01 ± 2.67E+00	8.94E+00 ± 3.88E-01
Quinic acid	ND	ND	ND	ND	ND	ND
Sebacic acid	ND	ND	ND	ND	ND	ND

(table continues)

	Average ± SD					
	Leaves +P	Leaves -P	Roots +P	Roots -P	Nodules +P	Nodules -P
Tartaric acid	ND	ND	ND	ND	ND	ND
Pimelic acid	ND	ND	ND	ND	ND	ND
Adipic acid	ND	ND	ND	ND	ND	ND
Suberic acid	ND	ND	ND	ND	ND	ND

CHAPTER 5

DISCUSSION

There are several major findings reported in this thesis. First, we studied the impact of acute P deficiency on growth and development, membrane lipid composition, and spatial changes in distribution of PC in nodules of *M. truncatula* R108 (WT) plants inoculated with *S. meliloti* and growing in SNF conditions for four weeks. In P-stressed environments, *M. truncatula* R108 (WT) plants showed impaired SNF activity, reduced growth and biomass, increased lateral root number, and accumulated less phosphate in all P-starved organs. ESI-MS analysis of membrane lipids showed that GL increased in absence of P, with decline in the levels of all phospholipids, the majority of which are PC and PE, in P-deficient tissues. Subsequently, MALDI-MS imaging of PC revealed heterogenous distributions of several species in nodules, with homogenous localizations of other PC species. In the absence of P, we observed changes in some PC distributions. Taken together, the data show that specific PC species are differentially distributed in nodules and their synthesis and degradation are also likely to be specifically regulated in diverse nodule zones and cell types. The data suggested that these processes may also be regulated differentially in P stress. Thus, membrane lipid remodeling is not uniform across the nodule during P stress (Dokwal et al., 2021). We reported ion suppression caused by PC in nodules that interfered with the detection of GLs using MALDI-MSI (Dokwal et al. 2021). This study emphasizes the importance of technological advances that are needed to localize GLs and other key PLs besides PC species found in cell membranes (Petkovic et al., 2001; Fuchs et al., 2009; Emerson et al., 2010; Fuchs et al.,

2010; Horn et al., 2012; Woodfield et al., 2017; Stopka et al., 2018; Colin and Jaillais, 2020).

PDIL3 was first identified and characterized in *M. truncatula* by Wang et al., 2017 (Wang et al., 2017). It is known to regulate Pi-deficiency signaling and transport in *M. truncatula* (Wang et al., 2017). *PDIL3* encodes a lncRNA, not a protein, and is believed to act by interfering with signaling in P stress. It is hypothesized to act by binding to the transcript of Pi transporter in WT through sequence complementarity, thereby downregulating it and preventing further uptake of P (Wang et al., 2017). In the second part of this thesis, a comparative study was conducted to investigate response of *pdil3*, a mutant containing a *Tnt1* insert in its gene, in response to P deficiency. In this study, *pdil3* plants were grown in P replete and deplete conditions for four weeks post nodulation in parallel with R108 (WT). In absence of P, *pdil3* plants showed better shoot growth and biomass, and accumulated more phosphate in shoots than WT in our lab, as reported (Wang et al. 2017). Nodulated roots of -P *pdil3* plants had lowered phosphate content, reduced nodule dry weight, impaired SNF, and less rhizobial occupancy in nodules than WT. No significant differences were noted in the phenotype between *pdil3* and WT +P plants. Consequently, MALDI-MS imaging was employed to spatially compare the distribution of PC in nodules of *pdil3* with WT. Differences in spatial distribution of many PC species were observed between WT and *pdil3* nodules in +P conditions. The majority of the PCs had lower abundance in -P *pdil3* nodules compared to WT; these were also differentially distributed from those found in WT and +P nodules. Thus, our findings conducted from -P symbiotic growth conditions show that *PDIL3* likely does not regulate the P deficiency response uniformly across nodules. They also strongly suggest that

PDIL3's role is not limited to suppression of its cognate *Medtr1g074930* gene encoding the Pi transporter, but it might also sway P partitioning between shoots and nodulated roots. The mechanism that causes these changes is not yet clear.

Metabolite profiling is an important tool used for examining plants response to different kinds of stress, including, deficiency of nutrients such as P (Guy et al., 2008; Shulaev et al., 2008; Kráľová et al., 2012; Obata and Fernie, 2012; Jorge et al., 2016). Plants undergo many metabolic and physiological changes to cope with P stress (Vance et al., 2003; Plaxton and Tran, 2011). In the final part of my dissertation, I exploited modern metabolite profiling to get deeper understanding on the repertoire of metabolites that show alterations in WT *M. truncatula* during severe P deficiency. Initially, a GC-MS based untargeted metabolomics study showed variation in the metabolic profile of the nodules, with increased sugars and amino acids, and decline in organic acids. Consequently, LC-MS/MS based targeted metabolomics was used to quantify these compounds including phosphorylated metabolites in leaves, roots, and nodules of *M. truncatula*. In the absence of P, leaves showed the strongest metabolic shift with most reduction in the levels of organic acids and phosphorylated metabolites compared to roots and nodules. Additionally, sugars and amino acids were elevated in all -P organs. The metabolic profile of -P nodules was similar to that of +P roots. Overall, nodules showed the fewest changes, suggesting that *M. truncatula* partitions biochemical precursors and energy sources toward nodules in P stress, presumably to maintain N supply. Thus, this study gives a clearer picture of how, with respect to metabolite shifts, *M. truncatula* plants undergo biochemical and pathway changes in all P deficient organs for better survival and maintenance of SNF under P stress. These studies set a baseline for understanding

mechanisms by which P stress is tolerated during SNF growth in the model legume *M. truncatula*. Future studies in model organisms, including *M. truncatula*, to examine genetic and genomic responses to P stress are likely to uncover more genes that can mitigate the effects of such stress. The results in this thesis provide a baseline for measuring the potential mitigation.

CHAPTER 6

FUTURE DIRECTIONS

The work presented in this thesis shows the importance of P as a macronutrient for legumes, especially when grown in symbiotic conditions. The results showed in this dissertation describe entail different physiological and metabolic changes that are elicited in *M. truncatula* by severe P stress. New technological advances in mass spectrometry and gene expression profiling studies are required to more fully comprehend the mechanisms by which legumes adapt to cope with P stress. Some of the immediate experiments that could be carried out to build on the results in this thesis are listed below.

- Need for spatial mapping of galactolipids in Medicago nodules
- Comparative transcriptomics study between R108 and *pdil3*
- Transcriptomic analyses to identify causative genes for P-efficient genotypes

6.1 Need for Spatial Mapping of Galactolipids in Medicago Nodules*

To fully understand the spectrum of membrane lipid patterning in P deprived nodules compared to those from legumes grown in P replete conditions will require new methods to quantitate and image PL and GL accumulation and turnover with tissue and cellular resolution (Stopka et al., 2018; Agtuca et al., 2020; Colin and Jaillais, 2020). GLs will be of interest to localize in nodules because they are found in nodules and increase during P deprivation (Gaude et al., 2004; Si et al., 2019; Dokwal et al., 2021) this study.

However, the ion suppression caused by PC in nodules interferes with GL

* Section 6.1 of this chapter is mostly reproduced from Dhiraj Dokwal, Trevor B Romsdahl, Daniel A Kunz, Ana Paula Alonso, Rebecca Dickstein, Phosphorus deprivation affects composition and spatial distribution of membrane lipids in legume nodules, *Plant Physiology*, 2021;, kiaa115, https://doi.org/10.1093/plphys/kiaa115, with permission from Oxford University Press.

detection in the same tissue using MALDI–MSI (Supp. Fig. S2.7; Supplemental Dataset S2.1). Ion suppression by PC of other lipids has been previously observed (Petkovic et al., 2001; Fuchs et al., 2009; Emerson et al., 2010; Fuchs et al., 2010; Horn et al., 2012; Woodfield et al., 2017; Stopka et al., 2018; Colin and Jaillais, 2020). Thus, technological advances are needed to localize GLs and less ionizable PLs found in cell membranes (Agtuca et al., 2020; Colin and Jaillais, 2020).

Below are some modification or advances that might help in alleviating ion suppression usually observed in MALDI-MSI –

- Tissues are usually embedded using an optimal cutting temperature (OCT) polymer for easy and precise cryosectioning. However, OCT is known to cause suppression in MS ion signal and an alternative procedure may possibly permit better spatial imaging (Todd et al., 2001).
- Inclusion of an internal standard in the matrix helps in improved analysis as it allows for tissue-specific correction and making spatial imaging more quantitative technique (Atkinson et al., 2007; Kallback et al., 2012).
- Improved MALDI imaging of other membrane lipids in positive mode along with PC can also be attained using graphene oxide (new matrix) (Wang et al., 2017).

6.2 Comparative Transcriptomics Study between R108 and *pdil3*

Recent advances in sequencing techniques have a variety of biological functions of lncRNAs in response to stress such salinity, drought, N/P deficiency, excess light, extreme temperature, hypoxia, and bacterial pathogens (Song and Zhang, 2017). It is important to conduct a comparative transcriptomics studies between *pdil3* and R108 (WT) to get a deeper understanding of the mechanisms by which genes regulated by the *pdil3* lncRNA respond to different stresses, including P stress combined with N stress. Two more *pdil* mutants; *pdil1* and *pdil2* were identified in (Wang et al., 2017). *pdil2* (lncRNA) is thought to regulate P uptake in WT in a similar mechanism like *pdil3* by downregulating

transcripts of *Medtr1g074930* encoding Pi transporter in *M. truncatula* through sequence complementarity. *pdil1* (lncRNA) competitively binds to miR399 which is responsible for degradation of *PHO2*, encoding a ubiquitin-conjugating E2 enzyme responsible for the degradation of Pi transporters for Pi uptake in WT (Wang et al., 2017). Similar studies to the one conducted in chapter 4 on other *pdil* mutants, *pdil1* and *pdil2* (Wang et al. 2017), similar to the one carried out in this thesis on *pdil3*, will help in understanding whether they play a localized or systemic role in plants adaptation to low P environments.

6.3 Transcriptomic Analysis to Identify Causative Genes for P-Efficient Genotypes

Thousands of plant genes differentially expressed in response to P deficiency, have been identified in various plant species including Arabidopsis, potato, rice, wheat, common bean, and white lupin (Misson et al., 2005; Hernandez et al., 2007; Hernandez et al., 2009; Hammond et al., 2011; Oono et al., 2011; O'Rourke et al., 2013). The gene regulatory networks that are vital in sensing and responding to P stress are complex among different plant species. Despite the technological advances in next-generation sequencing, there are no reports on comparative gene expression profiling in leaves, roots, and nodules of *M. truncatula* grown under severe P starvation. Such a study in future will pave the way in supporting findings of our current study on the metabolite levels and will also help in identifying many candidate genes that are key in adaptation of legumes to low P environments.

REFERENCES

Agtuca BJ, Stopka SA, Evans S, Samarah L, Liu Y, Xu D, Stacey MG, Koppenaal DW, Pasa-Tolic L, Anderton CR, Vertes A, Stacey G (2020) Metabolomic profiling of wild-type and mutant soybean root nodules using laser-ablation electrospray ionization mass spectrometry reveals altered metabolism. Plant J 103: 1937-1958

Akram NA, Shafiq F, Ashraf M (2017) Ascorbic Acid-A Potential Oxidant Scavenger and Its Role in Plant Development and Abiotic Stress Tolerance. Front Plant Sci 8: 613

Al-Niemi TS, Kahn ML, McDermott TR (1997) P Metabolism in the Bean-Rhizobium tropici Symbiosis. Plant Physiol 113: 1233-1242

Almeida JP, Hartwig UA, Frehner M, Nosberger J, Luscher A (2000) Evidence that P deficiency induces N feedback regulation of symbiotic N2 fixation in white clover (Trifolium repens L.). J Exp Bot 51: 1289-1297

Ariel F, Jegu T, Latrasse D, Romero-Barrios N, Christ A, Benhamed M, Crespi M (2014) Noncoding transcription by alternative RNA polymerases dynamically regulates an auxin-driven chromatin loop. Mol Cell 55: 383-396

Arondel V, Lemieux B, Hwang I, Gibson S, Goodman HM, Somerville CR (1992) Map-based cloning of a gene controlling omega-3 fatty acid desaturation in Arabidopsis. Science 258: 1353-1355

Atkinson SJ, Loadman PM, Sutton C, Patterson LH, Clench MR (2007) Examination of the distribution of the bioreductive drug AQ4N and its active metabolite AQ4 in solid tumours by imaging matrix-assisted laser desorption/ionisation mass spectrometry. Rapid Commun Mass Spectrom 21: 1271-1276

Bari R, Datt Pant B, Stitt M, Scheible WR (2006) PHO2, microRNA399, and PHR1 define a phosphate-signaling pathway in plants. Plant Physiol 141: 988-999

Barker D, Pfaff T, Moreau D, Groves E, Ruffel S, Lepetit M, Whitehand S, Maillet F, Nair RM, Journet E (November 2006) Growing *M. truncatula*: choice of substrates and growth conditions *In Medicago truncatula* handbook p26

Barker DG, Bianchi S, Blondon F, Dattée Y, Duc G, Essad S, Flament P, Gallusci P, Génier G, Guy P, Muel X, Tourneur J, Dénarié J, Huguet T (1990) Medicago truncatula, a model plant for studying the molecular genetics of theRhizobium-legume symbiosis. Plant Molecular Biology Reporter 8: 40-49

Barker DG, Pfaff T, Moreau D, Groves E, Ruffel S, Lepetit M, Whitehand S, Maillet F, Nair RM, Journet E-P (2006) Growing M. truncatula: choice of substrates and growth conditions. Medicago truncatula: 1-26

Ben Amor B, Wirth S, Merchan F, Laporte P, d'Aubenton-Carafa Y, Hirsch J, Maizel A, Mallory A, Lucas A, Deragon JM, Vaucheret H, Thermes C, Crespi M (2009) Novel long non-protein coding RNAs involved in Arabidopsis differentiation and stress responses. Genome Res 19: 57-69

Benedito VA, Torres-Jerez I, Murray JD, Andriankaja A, Allen S, Kakar K, Wandrey M, Verdier J, Zuber H, Ott T, Moreau S, Niebel A, Frickey T, Weiller G, He J, Dai X, Zhao PX, Tang Y, Udvardi MK (2008) A gene expression atlas of the model legume Medicago truncatula. Plant J 55: 504-513

Boisson-Dernier A, Chabaud M, Garcia F, Becard G, Rosenberg C, Barker DG (2001) Agrobacterium rhizogenes-transformed roots of Medicago truncatula for the study of nitrogen-fixing and endomycorrhizal symbiotic associations. Mol Plant Microbe Interact 14: 695-700

Bolling C, Fiehn O (2005) Metabolite profiling of Chlamydomonas reinhardtii under nutrient deprivation. Plant Physiol 139: 1995-2005

Boss WF, Im YJ (2012) Phosphoinositide signaling. Annu Rev Plant Biol 63: 409-429

Brewin N (2012) The Role of the Plant Plasma Membrane. The Plant Plasma Membrane: Structure, Function and Molecular Biology: 351

Brosnan CA, Voinnet O (2009) The long and the short of noncoding RNAs. Curr Opin Cell Biol 21: 416-425

Brugger B, Erben G, Sandhoff R, Wieland FT, Lehmann WD (1997) Quantitative analysis of biological membrane lipids at the low picomole level by nano-electrospray ionization tandem mass spectrometry. Proc Natl Acad Sci U S A 94: 2339-2344

Burleigh SH, Harrison MJ (1997) A novel gene whose expression in Medicago truncatula roots is suppressed in response to colonization by vesicular-arbuscular mycorrhizal (VAM) fungi and to phosphate nutrition. Plant Mol Biol 34: 199-208

Campalans A, Kondorosi A, Crespi M (2004) Enod40, a short open reading frame-containing mRNA, induces cytoplasmic localization of a nuclear RNA binding protein in Medicago truncatula. Plant Cell 16: 1047-1059

Cannon SB (2013) The model legume genomes. Methods Mol Biol 1069: 1-14

Carstensen A, Herdean A, Schmidt SB, Sharma A, Spetea C, Pribil M, Husted S (2018) The Impacts of Phosphorus Deficiency on the Photosynthetic Electron Transport Chain. Plant Physiol 177: 271-284

Cebolla A, Vinardell JM, Kiss E, Olah B, Roudier F, Kondorosi A, Kondorosi E (1999) The mitotic inhibitor ccs52 is required for endoreduplication and ploidy-dependent cell enlargement in plants. EMBO J 18: 4476-4484

Chekanova JA (2015) Long non-coding RNAs and their functions in plants. Curr Opin Plant Biol 27: 207-216

Chekanova JA, Gregory BD, Reverdatto SV, Chen H, Kumar R, Hooker T, Yazaki J, Li P, Skiba N, Peng Q, Alonso J, Brukhin V, Grossniklaus U, Ecker JR, Belostotsky DA (2007) Genome-wide high-resolution mapping of exosome substrates reveals hidden features in the Arabidopsis transcriptome. Cell 131: 1340-1353

Chen R, Hui L, Sturm RM, Li L (2009) Three dimensional mapping of neuropeptides and lipids in crustacean brain by mass spectral imaging. J Am Soc Mass Spectrom 20: 1068-1077

Chiou TJ, Aung K, Lin SI, Wu CC, Chiang SF, Su CL (2006) Regulation of phosphate homeostasis by MicroRNA in Arabidopsis. Plant Cell 18: 412-421

Chiou TJ, Lin SI (2011) Signaling network in sensing phosphate availability in plants. Annu Rev Plant Biol 62: 185-206

Chong J, Soufan O, Li C, Caraus I, Li S, Bourque G, Wishart DS, Xia J (2018) MetaboAnalyst 4.0: towards more transparent and integrative metabolomics analysis. Nucleic Acids Res 46: W486-W494

Cocuron JC, Anderson B, Boyd A, Alonso AP (2014) Targeted metabolomics of Physaria fendleri, an industrial crop producing hydroxy fatty acids. Plant Cell Physiol 55: 620-633

Colin LA, Jaillais Y (2020) Phospholipids across scales: lipid patterns and plant development. Curr Opin Plant Biol 53: 1-9

Cook DR (1999) Medicago truncatula--a model in the making! Curr Opin Plant Biol 2: 301-304

Cordell D, Drangert J-O, White S (2009) The story of phosphorus: Global food security and food for thought. Global Environmental Change 19: 292-305

Cruz-Ramirez A, Oropeza-Aburto A, Razo-Hernandez F, Ramirez-Chavez E, Herrera-Estrella L (2006) Phospholipase DZ2 plays an important role in extraplastidic galactolipid biosynthesis and phosphate recycling in Arabidopsis roots. Proc Natl Acad Sci U S A 103: 6765-6770

Dai X, Wang Y, Zhang WH (2016) OsWRKY74, a WRKY transcription factor, modulates tolerance to phosphate starvation in rice. J Exp Bot 67: 947-960

de Bang TC, Lay KS, Scheible WR, Takahashi H (2017) Small peptide signaling pathways modulating macronutrient utilization in plants. Curr Opin Plant Biol 39: 31-39

de Lajudie P, Laurent-Fulele E, Willems A, Torck U, Coopman R, Collins MD, Kersters K, Dreyfus B, Gillis M (1998) Allorhizobium undicola gen. nov., sp. nov., nitrogen-fixing bacteria that efficiently nodulate Neptunia natans in Senegal. Int J Syst Bacteriol 48 Pt 4: 1277-1290

de Rudder KE, Sohlenkamp C, Geiger O (1999) Plant-exuded choline is used for rhizobial membrane lipid biosynthesis by phosphatidylcholine synthase. J Biol Chem 274: 20011-20016

de Rudder KE, Thomas-Oates JE, Geiger O (1997) Rhizobium meliloti mutants deficient in phospholipid N-methyltransferase still contain phosphatidylcholine. J Bacteriol 179: 6921-6928

Denarie J, Debelle F, Rosenberg C (1992) Signaling and host range variation in nodulation. Annu Rev Microbiol 46: 497-531

Devaiah SP, Roth MR, Baughman E, Li M, Tamura P, Jeannotte R, Welti R, Wang X (2006) Quantitative profiling of polar glycerolipid species from organs of wild-type Arabidopsis and a phospholipase Dalpha1 knockout mutant. Phytochemistry 67: 1907-1924

Dilworth MJ (1966) Acetylene reduction by nitrogen-fixing preparations from Clostridium pasteurianum. Biochimica et Biophysica Acta (BBA) - General Subjects 127: 285-294

Ding J, Lu Q, Ouyang Y, Mao H, Zhang P, Yao J, Xu C, Li X, Xiao J, Zhang Q (2012) A long noncoding RNA regulates photoperiod-sensitive male sterility, an essential component of hybrid rice. Proc Natl Acad Sci U S A 109: 2654-2659

Ding N, Huertas R, Torres-Jerez I, Liu W, Watson B, Scheible WR, Udvardi M (2021) Transcriptional, metabolic, physiological and developmental responses of switchgrass to phosphorus limitation. Plant Cell Environ 44: 186-202

Ding X, Zhang S, Wang R, Li S, Liao X (2016) AM fungi and rhizobium regulate nodule growth, phosphorous (P) uptake, and soluble sugar concentration of soybeans experiencing P deficiency. Journal of Plant Nutrition 39: 1915-1925

Djami-Tchatchou AT, Ncube EN, Steenkamp PA, Dubery IA (2017) Similar, but different: structurally related azelaic acid and hexanoic acid trigger differential metabolomic and transcriptomic responses in tobacco cells. BMC Plant Biol 17: 227

Dokwal D, Romsdahl TB, Kunz DA, Alonso AP, Dickstein R (2021) Phosphorus deprivation affects composition and spatial distribution of membrane lipids in legume nodules. Plant Physiology

Dormann P, Benning C (2002) Galactolipids rule in seed plants. Trends Plant Sci 7: 112-118

Duenas ME, Klein AT, Alexander LE, Yandeau-Nelson MD, Nikolau BJ, Lee YJ (2017) High spatial resolution mass spectrometry imaging reveals the genetically programmed, developmental modification of the distribution of thylakoid membrane lipids among individual cells of maize leaf. Plant J 89: 825-838

Emerson B, Gidden J, Lay JO, Jr., Durham B (2010) A rapid separation technique for overcoming suppression of triacylglycerols by phosphatidylcholine using MALDI-TOF MS. J Lipid Res 51: 2428-2434

Ferguson BJ, Indrasumunar A, Hayashi S, Lin MH, Lin YH, Reid DE, Gresshoff PM (2010) Molecular analysis of legume nodule development and autoregulation. J Integr Plant Biol 52: 61-76

Fischinger SA, Drevon JJ, Claassen N, Schulze J (2006) Nitrogen from senescing lower leaves of common bean is re-translocated to nodules and might be involved in a N-feedback regulation of nitrogen fixation. J Plant Physiol 163: 987-995

Flores-Tinoco CE, Tschan F, Fuhrer T, Margot C, Sauer U, Christen M, Christen B (2020) Co-catabolism of arginine and succinate drives symbiotic nitrogen fixation. Mol Syst Biol 16: e9419

Florez-Sarasa I, Lambers H, Wang X, Finnegan PM, Ribas-Carbo M (2014) The alternative respiratory pathway mediates carboxylate synthesis in white lupin cluster roots under phosphorus deprivation. Plant Cell Environ 37: 922-928

Franco-Zorrilla JM, Valli A, Todesco M, Mateos I, Puga MI, Rubio-Somoza I, Leyva A, Weigel D, Garcia JA, Paz-Ares J (2007) Target mimicry provides a new mechanism for regulation of microRNA activity. Nat Genet 39: 1033-1037

Fuchs B, Bischoff A, Suss R, Teuber K, Schurenberg M, Suckau D, Schiller J (2009) Phosphatidylcholines and -ethanolamines can be easily mistaken in phospholipid mixtures: a negative ion MALDI-TOF MS study with 9-aminoacridine as matrix and egg yolk as selected example. Anal Bioanal Chem 395: 2479-2487

Fuchs B, Suss R, Schiller J (2010) An update of MALDI-TOF mass spectrometry in lipid research. Prog Lipid Res 49: 450-475

Ganie AH, Ahmad A, Pandey R, Aref IM, Yousuf PY, Ahmad S, Iqbal M (2015) Metabolite Profiling of Low-P Tolerant and Low-P Sensitive Maize Genotypes under Phosphorus Starvation and Restoration Conditions. PLoS One 10: e0129520

Gaude N, Tippmann H, Flemetakis E, Katinakis P, Udvardi M, Dormann P (2004) The galactolipid digalactosyldiacylglycerol accumulates in the peribacteroid membrane of nitrogen-fixing nodules of soybean and Lotus. J Biol Chem 279: 34624-34630

Gemperline E, Jayaraman D, Maeda J, Ane JM, Li L (2015) Multifaceted investigation of metabolites during nitrogen fixation in Medicago via high resolution MALDI-MS imaging and ESI-MS. J Am Soc Mass Spectrom 26: 149-158

Goldstein AH, Baertlein DA, McDaniel RG (1988) Phosphate Starvation Inducible Metabolism in Lycopersicon esculentum: I. Excretion of Acid Phosphatase by Tomato Plants and Suspension-Cultured Cells. Plant Physiol 87: 711-715

Gorzolka K, Kolling J, Nattkemper TW, Niehaus K (2016) Spatio-Temporal Metabolite Profiling of the Barley Germination Process by MALDI MS Imaging. PLoS One 11: e0150208

Graham PH (1981) Some problems of nodulation and symbiotic nitrogen fixation in Phaseolus vulgaris L.: A review. Field Crops Research 4: 93-112

Graham PH, Vance CP (2000) Nitrogen fixation in perspective: an overview of research and extension needs. Field Crops Research 65: 93-106

Guy C, Kopka J, Moritz T (2008) Plant metabolomics coming of age. Physiol Plant 132: 113-116

Ha S, Tran LS (2014) Understanding plant responses to phosphorus starvation for improvement of plant tolerance to phosphorus deficiency by biotechnological approaches. Crit Rev Biotechnol 34: 16-30

Hammond JP, Broadley MR, Bowen HC, Spracklen WP, Hayden RM, White PJ (2011) Gene expression changes in phosphorus deficient potato (Solanum tuberosum L.) leaves and the potential for diagnostic gene expression markers. PLoS One 6: e24606

Hankin JA, Barkley RM, Murphy RC (2007) Sublimation as a method of matrix application for mass spectrometric imaging. J Am Soc Mass Spectrom 18: 1646-1652

Hernandez G, Ramirez M, Valdes-Lopez O, Tesfaye M, Graham MA, Czechowski T, Schlereth A, Wandrey M, Erban A, Cheung F, Wu HC, Lara M, Town CD, Kopka J, Udvardi MK, Vance CP (2007) Phosphorus stress in common bean: root transcript and metabolic responses. Plant Physiol 144: 752-767

Hernandez G, Valdes-Lopez O, Ramirez M, Goffard N, Weiller G, Aparicio-Fabre R, Fuentes SI, Erban A, Kopka J, Udvardi MK, Vance CP (2009) Global changes in the transcript and metabolic profiles during symbiotic nitrogen fixation in phosphorus-stressed common bean plants. Plant Physiol 151: 1221-1238

Hernández LE, Cooke DT (1996) Lipid composition of symbiosomes from pea root nodules. Phytochemistry 42: 341-346

Hirai MY, Yano M, Goodenowe DB, Kanaya S, Kimura T, Awazuhara M, Arita M, Fujiwara T, Saito K (2004) Integration of transcriptomics and metabolomics for understanding of global responses to nutritional stresses in Arabidopsis thaliana. Proc Natl Acad Sci U S A 101: 10205-10210

HIRSCH AM (1992) Developmental biology of legume nodulation. New Phytologist 122: 211-237

Holzl G, Dormann P (2019) Chloroplast Lipids and Their Biosynthesis. Annu Rev Plant Biol 70: 51-81

Hong J, Yang L, Zhang D, Shi J (2016) Plant Metabolomics: An Indispensable System Biology Tool for Plant Science. Int J Mol Sci 17

Horn PJ, Chapman KD (2014) Metabolite Imager: customized spatial analysis of metabolite distributions in mass spectrometry imaging. Metabolomics 10: 337-348

Horn PJ, Korte AR, Neogi PB, Love E, Fuchs J, Strupat K, Borisjuk L, Shulaev V, Lee YJ, Chapman KD (2012) Spatial mapping of lipids at cellular resolution in embryos of cotton. Plant Cell 24: 622-636

Hu Q, Noll RJ, Li H, Makarov A, Hardman M, Graham Cooks R (2005) The Orbitrap: a new mass spectrometer. J Mass Spectrom 40: 430-443

Huang CY, Roessner U, Eickmeier I, Genc Y, Callahan DL, Shirley N, Langridge P, Bacic A (2008) Metabolite profiling reveals distinct changes in carbon and nitrogen metabolism in phosphate-deficient barley plants (Hordeum vulgare L.). Plant Cell Physiol 49: 691-703

Israel DW (1987) Investigation of the role of phosphorus in symbiotic dinitrogen fixation. Plant Physiol 84: 835-840

Itoh S (1987) Characteristics of Phosphorus Uptake of Chickpea in Comparison with Pigeonpea, Soybean, and Maize. Soil Science and Plant Nutrition 33: 417-422

Jackson SN, Ugarov M, Egan T, Post JD, Langlais D, Albert Schultz J, Woods AS (2007) MALDI-ion mobility-TOFMS imaging of lipids in rat brain tissue. J Mass Spectrom 42: 1093-1098

Jain A, Vasconcelos MJ, Raghothama KG, Sahi SV (2007) Molecular Mechanisms of Plant Adaptation to Phosphate Deficiency. *In* Plant Breeding Reviews, pp 359-419

Jin KM, Nogita T, Toyoda H, Kawashima M, Hidano A (1990) Pedunculated pigmented eccrine poroma of the scalp with increased urinary excretion of 5-S-cysteinyldopa. J Dermatol 17: 555-558

Jones KM, Kobayashi H, Davies BW, Taga ME, Walker GC (2007) How rhizobial symbionts invade plants: the Sinorhizobium-Medicago model. Nat Rev Microbiol 5: 619-633

Jorge TF, Rodrigues JA, Caldana C, Schmidt R, van Dongen JT, Thomas-Oates J, Antonio C (2016) Mass spectrometry-based plant metabolomics: Metabolite responses to abiotic stress. Mass Spectrom Rev 35: 620-649

Kalapothakis JMD, Barran PE (2013) Ion Mobility Mass Spectrometry – Principles. *In* GCK Roberts, ed, Encyclopedia of Biophysics. Springer Berlin Heidelberg, Berlin, Heidelberg, pp 1142-1148

Kallback P, Shariatgorji M, Nilsson A, Andren PE (2012) Novel mass spectrometry imaging software assisting labeled normalization and quantitation of drugs and neuropeptides directly in tissue sections. J Proteomics 75: 4941-4951

Kim YJ, Zheng B, Yu Y, Won SY, Mo B, Chen X (2011) The role of Mediator in small and long noncoding RNA production in Arabidopsis thaliana. EMBO J 30: 814-822

Kopka J (2006) Current challenges and developments in GC-MS based metabolite profiling technology. J Biotechnol 124: 312-322

Kornienko AE, Guenzl PM, Barlow DP, Pauler FM (2013) Gene regulation by the act of long non-coding RNA transcription. BMC Biology 11: 59

Kráľová K, Jampílek J, Ostrovský I (2012) Metabolomics - Useful Tool for Study of Plant Responses to Abiotic Stresses. Ecological Chemistry and Engineering S 19: 133-161

Kriechbaumer V, Glawischnig E (2005) Auxin biosynthesis within the network of tryptophan metabolism. Journal of Nano and Bio Tech 2: 53-58

Kumar R, Bohra A, Pandey AK, Pandey MK, Kumar A (2017) Metabolomics for Plant Improvement: Status and Prospects. Front Plant Sci 8: 1302

Lambers H, Shane MW, Cramer MD, Pearse SJ, Veneklaas EJ (2006) Root structure and functioning for efficient acquisition of phosphorus: Matching morphological and physiological traits. Ann Bot 98: 693-713

Li H, Xia M, Wu P (2001) Effect of phosphorus deficiency stress on rice lateral root growth and nutrient absorption. Acta Botanica Sinica 43: 1154-1160

Liu A, Contador CA, Fan K, Lam HM (2018) Interaction and Regulation of Carbon, Nitrogen, and Phosphorus Metabolisms in Root Nodules of Legumes. Front Plant Sci 9: 1860

Liu J, Jung C, Xu J, Wang H, Deng S, Bernad L, Arenas-Huertero C, Chua NH (2012) Genome-wide analysis uncovers regulation of long intergenic noncoding RNAs in Arabidopsis. Plant Cell 24: 4333-4345

Liu TT, Zhu D, Chen W, Deng W, He H, He G, Bai B, Qi Y, Chen R, Deng XW (2013) A global identification and analysis of small nucleolar RNAs and possible intermediate-sized non-coding RNAs in Oryza sativa. Mol Plant 6: 830-846

Ljung K, Hull AK, Kowalczyk M, Marchant A, Celenza J, Cohen JD, Sandberg G (2002) Biosynthesis, conjugation, catabolism and homeostasis of indole-3-acetic acid in Arabidopsis thaliana. Plant Mol Biol 49: 249-272

Long SR (1996) Rhizobium symbiosis: nod factors in perspective. The Plant Cell 8: 1885

Lopez-Bucio J, de La Vega OM, Guevara-Garcia A, Herrera-Estrella L (2000) Enhanced phosphorus uptake in transgenic tobacco plants that overproduce citrate. Nat Biotechnol 18: 450-453

López-Lara IM, Gao J-L, Soto MJ, Solares-Pérez A, Weissenmayer B, Sohlenkamp C, Verroios GP, Thomas-Oates J, Geiger O (2005) Phosphorus-Free Membrane Lipids of Sinorhizobium meliloti Are Not Required for the Symbiosis with Alfalfa but Contribute to Increased Cell Yields Under Phosphorus-Limiting Conditions of Growth. Molecular Plant-Microbe Interactions® 18: 973-982

Lopez-Lara IM, Sohlenkamp C, Geiger O (2003) Membrane lipids in plant-associated bacteria: their biosyntheses and possible functions. Mol Plant Microbe Interact 16: 567-579

Lu S, Sturtevant D, Aziz M, Jin C, Li Q, Chapman KD, Guo L (2018) Spatial analysis of lipid metabolites and expressed genes reveals tissue-specific heterogeneity of lipid metabolism in high- and low-oil Brassica napus L. seeds. Plant J 94: 915-932

Lullien V, Barker DG, de Lajudie P, Huguet T (1987) Plant gene expression in effective and ineffective root nodules of alfalfa (Medicago sativa). Plant Mol Biol 9: 469-478

Mano Y, Nemoto K (2012) The pathway of auxin biosynthesis in plants. J Exp Bot 63: 2853-2872

Mergaert P, Kereszt A, Kondorosi E (2020) Gene Expression in Nitrogen-Fixing Symbiotic Nodule Cells in Medicago truncatula and Other Nodulating Plants. Plant Cell 32: 42-68

Miller KJ, Shon BC, Gore RS, Hunt WP (1990) The phospholipid composition ofBradyrhizobium spp. Current Microbiology 21: 205-210

Misson J, Raghothama KG, Jain A, Jouhet J, Block MA, Bligny R, Ortet P, Creff A, Somerville S, Rolland N, Doumas P, Nacry P, Herrerra-Estrella L, Nussaume L, Thibaud M-C (2005) A genome-wide transcriptional analysis using Arabidopsis thaliana Affymetrix gene chips determined plant responses to phosphate deprivation. Proceedings of the National Academy of Sciences of the United States of America 102: 11934

Misson J, Raghothama KG, Jain A, Jouhet J, Block MA, Bligny R, Ortet P, Creff A, Somerville S, Rolland N, Doumas P, Nacry P, Herrerra-Estrella L, Nussaume L, Thibaud MC (2005) A genome-wide transcriptional analysis using Arabidopsis thaliana Affymetrix gene chips determined plant responses to phosphate deprivation. Proc Natl Acad Sci U S A 102: 11934-11939

Moll KM, Zhou P, Ramaraj T, Fajardo D, Devitt NP, Sadowsky MJ, Stupar RM, Tiffin P, Miller JR, Young ND, Silverstein KAT, Mudge J (2017) Strategies for optimizing BioNano and Dovetail explored through a second reference quality assembly for the legume model, Medicago truncatula. BMC Genomics 18: 578

Morcuende R, Bari R, Gibon Y, Zheng W, Pant BD, Blasing O, Usadel B, Czechowski T, Udvardi MK, Stitt M, Scheible WR (2007) Genome-wide reprogramming of metabolism and regulatory networks of Arabidopsis in response to phosphorus. Plant Cell Environ 30: 85-112

Muchhal US, Raghothama KG (1999) Transcriptional regulation of plant phosphate transporters. Proc Natl Acad Sci U S A 96: 5868-5872

Muller J, Godde V, Niehaus K, Zorb C (2015) Metabolic Adaptations of White Lupin Roots and Shoots under Phosphorus Deficiency. Front Plant Sci 6: 1014

Nakamura Y, Andres F, Kanehara K, Liu YC, Dormann P, Coupland G (2014) Arabidopsis florigen FT binds to diurnally oscillating phospholipids that accelerate flowering. Nat Commun 5: 3553

Narasimhan R, Wang G, Li M, Roth M, Welti R, Wang X (2013) Differential changes in galactolipid and phospholipid species in soybean leaves and roots under nitrogen deficiency and after nodulation. Phytochemistry 96: 81-91

Nath M, Tuteja N (2016) NPKS uptake, sensing, and signaling and miRNAs in plant nutrient stress. Protoplasma 253: 767-786

Nikiforova VJ, Gakiere B, Kempa S, Adamik M, Willmitzer L, Hesse H, Hoefgen R (2004) Towards dissecting nutrient metabolism in plants: a systems biology case study on sulphur metabolism. J Exp Bot 55: 1861-1870

Nilsson L, Muller R, Nielsen TH (2010) Dissecting the plant transcriptome and the regulatory responses to phosphate deprivation. Physiol Plant 139: 129-143

Niu YF, Chai RS, Jin GL, Wang H, Tang CX, Zhang YS (2013) Responses of root architecture development to low phosphorus availability: a review. Ann Bot 112: 391-408

Noack LC, Jaillais Y (2020) Functions of Anionic Lipids in Plants. Annu Rev Plant Biol 71: 71-102

Nosengo N (2003) Fertilized to death. Nature 425: 894-895

O'Rourke JA, Yang SS, Miller SS, Bucciarelli B, Liu J, Rydeen A, Bozsoki Z, Uhde-Stone C, Tu ZJ, Allan D, Gronwald JW, Vance CP (2013) An RNA-Seq transcriptome analysis of orthophosphate-deficient white lupin reveals novel insights into phosphorus acclimation in plants. Plant Physiol 161: 705-724

Obata T, Fernie AR (2012) The use of metabolomics to dissect plant responses to abiotic stresses. Cell Mol Life Sci 69: 3225-3243

Ohlrogge JB, Jaworski JG (1997) REGULATION OF FATTY ACID SYNTHESIS. Annual Review of Plant Physiology and Plant Molecular Biology 48: 109-136

Okazaki Y, Otsuki H, Narisawa T, Kobayashi M, Sawai S, Kamide Y, Kusano M, Aoki T, Hirai MY, Saito K (2013) A new class of plant lipid is essential for protection against phosphorus depletion. Nat Commun 4: 1510

Oldroyd GE (2013) Speak, friend, and enter: signalling systems that promote beneficial symbiotic associations in plants. Nat Rev Microbiol 11: 252-263

Oldroyd GE, Harrison MJ, Udvardi M (2005) Peace talks and trade deals. Keys to long-term harmony in legume-microbe symbioses. Plant Physiol 137: 1205-1210

Oono Y, Kawahara Y, Kanamori H, Mizuno H, Yamagata H, Yamamoto M, Hosokawa S, Ikawa H, Akahane I, Zhu Z, Wu J, Itoh T, Matsumoto T (2011) mRNA-Seq Reveals a Comprehensive Transcriptome Profile of Rice under Phosphate Stress. Rice 4: 50-65

Pant BD, Pant P, Erban A, Huhman D, Kopka J, Scheible WR (2015) Identification of primary and secondary metabolites with phosphorus status-dependent abundance in Arabidopsis, and of the transcription factor PHR1 as a major regulator of metabolic changes during phosphorus limitation. Plant Cell Environ 38: 172-187

Pecrix Y, Staton SE, Sallet E, Lelandais-Brière C, Moreau S, Carrère S, Blein T, Jardinaud M-F, Latrasse D, Zouine M, Zahm M, Kreplak J, Mayjonade B, Satgé C, Perez M, Cauet S, Marande W, Chantry-Darmon C, Lopez-Roques C, Bouchez O, Bérard A, Debellé F, Muños S, Bendahmane A, Bergès H, Niebel A,

Buitink J, Frugier F, Benhamed M, Crespi M, Gouzy J, Gamas P (2018) Whole-genome landscape of Medicago truncatula symbiotic genes. Nature Plants 4: 1017-1025

Pecrix Y, Staton SE, Sallet E, Lelandais-Briere C, Moreau S, Carrere S, Blein T, Jardinaud MF, Latrasse D, Zouine M, Zahm M, Kreplak J, Mayjonade B, Satge C, Perez M, Cauet S, Marande W, Chantry-Darmon C, Lopez-Roques C, Bouchez O, Berard A, Debelle F, Munos S, Bendahmane A, Berges H, Niebel A, Buitink J, Frugier F, Benhamed M, Crespi M, Gouzy J, Gamas P (2018) Whole-genome landscape of Medicago truncatula symbiotic genes. Nat Plants 4: 1017-1025

Peoples MB, Brockwell J, Herridge DF, Rochester IJ, Alves BJR, Urquiaga S, Boddey RM, Dakora FD, Bhattarai S, Maskey SL, Sampet C, Rerkasem B, Khan DF, Hauggaard-Nielsen H, Jensen ES (2009) The contributions of nitrogen-fixing crop legumes to the productivity of agricultural systems. Symbiosis 48: 1-17

Pereira PAA, Bliss FA (1989) Selection of common bean (Phaseolus vulgaris L.) for N2 fixation at different levels of available phosphorus under field and environmentally-controlled conditions. Plant and Soil 115: 75-82

Perez Guerra JC, Coussens G, De Keyser A, De Rycke R, De Bodt S, Van De Velde W, Goormachtig S, Holsters M (2010) Comparison of developmental and stress-induced nodule senescence in Medicago truncatula. Plant Physiol 152: 1574-1584

Petkovic M, Schiller J, Muller M, Benard S, Reichl S, Arnold K, Arnhold J (2001) Detection of individual phospholipids in lipid mixtures by matrix-assisted laser desorption/ionization time-of-flight mass spectrometry: phosphatidylcholine prevents the detection of further species. Anal Biochem 289: 202-216

Plaxton W (2004) Encyclopedia of plant and crop science.

Plaxton WC, Tran HT (2011) Metabolic adaptations of phosphate-starved plants. Plant Physiol 156: 1006-1015

Poirier Y, Bucher M (2002) Phosphate transport and homeostasis in Arabidopsis. Arabidopsis Book 1: e0024

Ponting CP, Oliver PL, Reik W (2009) Evolution and functions of long noncoding RNAs. Cell 136: 629-641

Postgate JR (1982) The fundamentals of nitrogen fixation. CUP Archive

Proust H, Hartmann C, Crespi M, Lelandais-Briere C (2018) Root Development in Medicago truncatula: Lessons from Genetics to Functional Genomics. Methods Mol Biol 1822: 205-239

Raghothama KG (1999) Phosphate Acquisition. Annu Rev Plant Physiol Plant Mol Biol 50: 665-693

Rinn JL, Chang HY (2012) Genome regulation by long noncoding RNAs. Annu Rev Biochem 81: 145-166

Rohrig H, Schmidt J, Miklashevichs E, Schell J, John M (2002) Soybean ENOD40 encodes two peptides that bind to sucrose synthase. Proc Natl Acad Sci U S A 99: 1915-1920

Roux B, Rodde N, Jardinaud MF, Timmers T, Sauviac L, Cottret L, Carrere S, Sallet E, Courcelle E, Moreau S, Debelle F, Capela D, de Carvalho-Niebel F, Gouzy J, Bruand C, Gamas P (2014) An integrated analysis of plant and bacterial gene expression in symbiotic root nodules using laser-capture microdissection coupled to RNA sequencing. Plant J 77: 817-837

Roy S, Liu W, Nandety RS, Crook A, Mysore KS, Pislariu CI, Frugoli J, Dickstein R, Udvardi MK (2020) Celebrating 20 Years of Genetic Discoveries in Legume Nodulation and Symbiotic Nitrogen Fixation. Plant Cell 32: 15-41

Sa TM, Israel DW (1991) Energy status and functioning of phosphorus-deficient soybean nodules. Plant Physiol 97: 928-935

Salazar C, Jones MD, Sturtevant D, Horn PJ, Crossley J, Zaman K, Chapman KD, Wrona M, Isaac G, Smith NW, Shulaev V (2017) Development and application of sub-2-mum particle CO2 -based chromatography coupled to mass spectrometry for comprehensive analysis of lipids in cottonseed extracts. Rapid Commun Mass Spectrom 31: 591-605

Salminen SO, Streeter JG (1987) Uptake and Metabolism of Carbohydrates by Bradyrhizobium japonicum Bacteroids. Plant Physiol 83: 535-540

Schulze J, Drevon JJ (2005) P-deficiency increases the O2 uptake per N2 reduced in alfalfa. J Exp Bot 56: 1779-1784

Schulze J, Temple G, Temple SJ, Beschow H, Vance CP (2006) Nitrogen fixation by white lupin under phosphorus deficiency. Ann Bot 98: 731-740

Schulze J, Tesfaye M, Litjens RHMG, Bucciarelli B, Trepp G, Miller S, Samac D, Allan D, Vance CP (2002) Malate plays a central role in plant nutrition. Plant and Soil 247: 133-139

Shin H, Shin HS, Chen R, Harrison MJ (2006) Loss of At4 function impacts phosphate distribution between the roots and the shoots during phosphate starvation. Plant J 45: 712-726

Shiva S, Vu HS, Roth MR, Zhou Z, Marepally SR, Nune DS, Lushington GH, Visvanathan M, Welti R (2013) Lipidomic analysis of plant membrane lipids by direct infusion tandem mass spectrometry. Methods Mol Biol 1009: 79-91

Shuai P, Liang D, Tang S, Zhang Z, Ye CY, Su Y, Xia X, Yin W (2014) Genome-wide identification and functional prediction of novel and drought-responsive lincRNAs in Populus trichocarpa. J Exp Bot 65: 4975-4983

Shulaev V, Cortes D, Miller G, Mittler R (2008) Metabolomics for plant stress response. Physiol Plant 132: 199-208

Si Z, Yang Q, Liang R, Chen L, Chen D, Li Y (2019) Digalactosyldiacylglycerol Synthase Gene MtDGD1 Plays an Essential Role in Nodule Development and Nitrogen Fixation. Mol Plant Microbe Interact 32: 1196-1209

Song Y, Zhang D (2017) The Role of Long Noncoding RNAs in Plant Stress Tolerance. Methods Mol Biol 1631: 41-68

Stanton-Geddes J, Paape T, Epstein B, Briskine R, Yoder J, Mudge J, Bharti AK, Farmer AD, Zhou P, Denny R, May GD, Erlandson S, Yakub M, Sugawara M, Sadowsky MJ, Young ND, Tiffin P (2013) Candidate genes and genetic architecture of symbiotic and agronomic traits revealed by whole-genome, sequence-based association genetics in Medicago truncatula. PLoS One 8: e65688

Stevens GG, Pérez-Fernández MA, Morcillo RJL, Kleinert A, Hills P, Brand DJ, Steenkamp ET, Valentine AJ (2019) Roots and Nodules Response Differently to P Starvation in the Mediterranean-Type Legume Virgilia divaricata. Frontiers in Plant Science 10

Stopka SA, Khattar R, Agtuca BJ, Anderton CR, Pasa-Tolic L, Stacey G, Vertes A (2018) Metabolic Noise and Distinct Subpopulations Observed by Single Cell LAESI Mass Spectrometry of Plant Cells in situ. Front Plant Sci 9: 1646

Sturtevant D, Duenas ME, Lee YJ, Chapman KD (2017) Three-dimensional visualization of membrane phospholipid distributions in Arabidopsis thaliana seeds: A spatial perspective of molecular heterogeneity. Biochim Biophys Acta Mol Cell Biol Lipids 1862: 268-281

Sturtevant D, Lee YJ, Chapman KD (2016) Matrix assisted laser desorption/ionization-mass spectrometry imaging (MALDI-MSI) for direct visualization of plant metabolites in situ. Curr Opin Biotechnol 37: 53-60

Sulieman S (2011) Does GABA increase the efficiency of symbiotic N2 fixation in legumes? Plant Signal Behav 6: 32-36

Sulieman S, Ha CV, Schulze J, Tran LS (2013) Growth and nodulation of symbiotic Medicago truncatula at different levels of phosphorus availability. J Exp Bot 64: 2701-2712

Sulieman S, Schulze J, Tran LS (2013) Comparative Analysis of the Symbiotic Efficiency of Medicago truncatula and Medicago sativa under Phosphorus Deficiency. Int J Mol Sci 14: 5198-5213

Sulieman S, Tran LS (2013) Asparagine: an amide of particular distinction in the regulation of symbiotic nitrogen fixation of legumes. Crit Rev Biotechnol 33: 309-327

Sulieman S, Tran LS (2015) Phosphorus homeostasis in legume nodules as an adaptive strategy to phosphorus deficiency. Plant Sci 239: 36-43

Sulieman Y, Pengsakul T, Guo Y (2013) Development and Effects of Schistosoma japonicum (Trematoda) on its Intermediate Host, Oncomelania hupensis (Gastropoda). Iran J Parasitol 8: 212-218

Swiezewski S, Liu F, Magusin A, Dean C (2009) Cold-induced silencing by long antisense transcripts of an Arabidopsis Polycomb target. Nature 462: 799-802

Tang H, Krishnakumar V, Bidwell S, Rosen B, Chan A, Zhou S, Gentzbittel L, Childs KL, Yandell M, Gundlach H, Mayer KFX, Schwartz DC, Town CD (2014) An improved genome release (version Mt4.0) for the model legume Medicago truncatula. BMC Genomics 15: 312

Tautenhahn R, Patti GJ, Rinehart D, Siuzdak G (2012) XCMS Online: a web-based platform to process untargeted metabolomic data. Anal Chem 84: 5035-5039

Tesfaye M, Liu J, Allan DL, Vance CP (2007) Genomic and genetic control of phosphate stress in legumes. Plant Physiol 144: 594-603

Thao NP, Tran LS (2012) Potentials toward genetic engineering of drought-tolerant soybean. Crit Rev Biotechnol 32: 349-362

Tjellstrom H, Andersson MX, Larsson KE, Sandelius AS (2008) Membrane phospholipids as a phosphate reserve: the dynamic nature of phospholipid-to-digalactosyl diacylglycerol exchange in higher plants. Plant Cell Environ 31: 1388-1398

Todd PJ, Schaaff TG, Chaurand P, Caprioli RM (2001) Organic ion imaging of biological tissue with secondary ion mass spectrometry and matrix-assisted laser desorption/ionization. J Mass Spectrom 36: 355-369

Tohge T, Watanabe M, Hoefgen R, Fernie AR (2013) Shikimate and phenylalanine biosynthesis in the green lineage. Front Plant Sci 4: 62

Tran L, Nguyen H (2009) Future Biotechnology of Legumes. *In* Nitrogen Fixation in Crop Production, pp 265-307

Udvardi M, Poole PS (2013) Transport and metabolism in legume-rhizobia symbioses. Annu Rev Plant Biol 64: 781-805

Uhde-Stone C, Gilbert G, Johnson JMF, Litjens R, Zinn KE, Temple SJ, Vance CP, Allan DL (2003) Acclimation of white lupin to phosphorus deficiency involves enhanced expression of genes related to organic acid metabolism. Plant and Soil 248: 99-116

Valdes-Lopez O, Hernandez G (2008) Transcriptional regulation and signaling in phosphorus starvation: what about legumes? J Integr Plant Biol 50: 1213-1222

van Berkum P, Beyene D, Bao G, Campbell TA, Eardly BD (1998) Rhizobium mongolense sp. nov. is one of three rhizobial genotypes identified which nodulate and form nitrogen-fixing symbioses with Medicago ruthenica [(L.) Ledebour]. Int J Syst Bacteriol 48 Pt 1: 13-22

Vance CP (2001) Symbiotic nitrogen fixation and phosphorus acquisition. Plant nutrition in a world of declining renewable resources. Plant Physiol 127: 390-397

Vance CP, Uhde-Stone C, Allan DL (2003) Phosphorus acquisition and use: critical adaptations by plants for securing a nonrenewable resource. New Phytologist 157: 423-447

Vasse J, de Billy F, Camut S, Truchet G (1990) Correlation between ultrastructural differentiation of bacteroids and nitrogen fixation in alfalfa nodules. J Bacteriol 172: 4295-4306

Veerappan V, Jani M, Kadel K, Troiani T, Gale R, Mayes T, Shulaev E, Wen J, Mysore KS, Azad RK, Dickstein R (2016) Rapid identification of causative insertions underlying Medicago truncatula Tnt1 mutants defective in symbiotic nitrogen fixation from a forward genetic screen by whole genome sequencing. BMC Genomics 17: 141

Veereshlingam H, Haynes JG, Penmetsa RV, Cook DR, Sherrier DJ, Dickstein R (2004) nip, a symbiotic Medicago truncatula mutant that forms root nodules with aberrant infection threads and plant defense-like response. Plant Physiol 136: 3692-3702

Verma DP, Hong Z (1996) Biogenesis of the peribacteroid membrane in root nodules. Trends Microbiol 4: 364-368

Wang T, Zhao M, Zhang X, Liu M, Yang C, Chen Y, Chen R, Wen J, Mysore KS, Zhang WH (2017) Novel phosphate deficiency-responsive long non-coding RNAs in the legume model plant Medicago truncatula. J Exp Bot 68: 5937-5948

Wang TZ, Liu M, Zhao MG, Chen R, Zhang WH (2015) Identification and characterization of long non-coding RNAs involved in osmotic and salt stress in Medicago truncatula using genome-wide high-throughput sequencing. BMC Plant Biol 15: 131

Wang Y, Fan X, Lin F, He G, Terzaghi W, Zhu D, Deng XW (2014) Arabidopsis noncoding RNA mediates control of photomorphogenesis by red light. Proc Natl Acad Sci U S A 111: 10359-10364

Wang Z, Cai Y, Wang Y, Zhou X, Zhang Y, Lu H (2017) Improved MALDI imaging MS analysis of phospholipids using graphene oxide as new matrix. Sci Rep 7: 44466

Wang Z, Straub D, Yang H, Kania A, Shen J, Ludewig U, Neumann G (2014) The regulatory network of cluster-root function and development in phosphate-deficient white lupin (Lupinus albus) identified by transcriptome sequencing. Physiol Plant 151: 323-338

Watson RJ, Chan YK, Wheatcroft R, Yang AF, Han SH (1988) Rhizobium meliloti genes required for C4-dicarboxylate transport and symbiotic nitrogen fixation are located on a megaplasmid. J Bacteriol 170: 927-934

Whitehead LF, Day DA (1997) The peribacteroid membrane. Physiologia Plantarum 100: 30-44

Williamson LC, Ribrioux SP, Fitter AH, Leyser HM (2001) Phosphate availability regulates root system architecture in Arabidopsis. Plant Physiol 126: 875-882

Wilusz JE, Sunwoo H, Spector DL (2009) Long noncoding RNAs: functional surprises from the RNA world. Genes Dev 23: 1494-1504

Woodfield HK, Sturtevant D, Borisjuk L, Munz E, Guschina IA, Chapman K, Harwood JL (2017) Spatial and Temporal Mapping of Key Lipid Species in Brassica napus Seeds. Plant Physiol 173: 1998-2009

Wu P, Ma L, Hou X, Wang M, Wu Y, Liu F, Deng XW (2003) Phosphate starvation triggers distinct alterations of genome expression in Arabidopsis roots and leaves. Plant Physiol 132: 1260-1271

Xia J, Mandal R, Sinelnikov IV, Broadhurst D, Wishart DS (2012) MetaboAnalyst 2.0--a comprehensive server for metabolomic data analysis. Nucleic Acids Res 40: W127-133

Xu X-W, Zhou X-H, Wang R-R, Peng W-L, An Y, Chen L-L (2016) Functional analysis of long intergenic non-coding RNAs in phosphate-starved rice using competing endogenous RNA network. Scientific Reports 6: 20715

Yang WC, Katinakis P, Hendriks P, Smolders A, de Vries F, Spee J, van Kammen A, Bisseling T, Franssen H (1993) Characterization of GmENOD40, a gene showing

novel patterns of cell-specific expression during soybean nodule development. Plant J 3: 573-585

Young ND, Bharti AK (2012) Genome-enabled insights into legume biology. Annu Rev Plant Biol 63: 283-305

Young ND, Debellé F, Oldroyd GED, Geurts R, Cannon SB, Udvardi MK, Benedito VA, Mayer KFX, Gouzy J, Schoof H, Van de Peer Y, Proost S, Cook DR, Meyers BC, Spannagl M, Cheung F, De Mita S, Krishnakumar V, Gundlach H, Zhou S, Mudge J, Bharti AK, Murray JD, Naoumkina MA, Rosen B, Silverstein KAT, Tang H, Rombauts S, Zhao PX, Zhou P, Barbe V, Bardou P, Bechner M, Bellec A, Berger A, Bergès H, Bidwell S, Bisseling T, Choisne N, Couloux A, Denny R, Deshpande S, Dai X, Doyle JJ, Dudez A-M, Farmer AD, Fouteau S, Franken C, Gibelin C, Gish J, Goldstein S, González AJ, Green PJ, Hallab A, Hartog M, Hua A, Humphray SJ, Jeong D-H, Jing Y, Jöcker A, Kenton SM, Kim D-J, Klee K, Lai H, Lang C, Lin S, Macmil SL, Magdelenat G, Matthews L, McCorrison J, Monaghan EL, Mun J-H, Najar FZ, Nicholson C, Noirot C, O'Bleness M, Paule CR, Poulain J, Prion F, Qin B, Qu C, Retzel EF, Riddle C, Sallet E, Samain S, Samson N, Sanders I, Saurat O, Scarpelli C, Schiex T, Segurens B, Severin AJ, Sherrier DJ, Shi R, Sims S, Singer SR, Sinharoy S, Sterck L, Viollet A, Wang B-B, Wang K, Wang M, Wang X, Warfsmann J, Weissenbach J, White DD, White JD, Wiley GB, Wincker P, Xing Y, Yang L, Yao Z, Ying F, Zhai J, Zhou L, Zuber A, Dénarié J, Dixon RA, May GD, Schwartz DC, Rogers J, Quétier F, Town CD, Roe BA (2011) The Medicago genome provides insight into the evolution of rhizobial symbioses. Nature 480: 520-524

Young ND, Udvardi M (2009) Translating Medicago truncatula genomics to crop legumes. Curr Opin Plant Biol 12: 193-201

Yuan ZC, Zaheer R, Finan TM (2006) Regulation and properties of PstSCAB, a high-affinity, high-velocity phosphate transport system of Sinorhizobium meliloti. J Bacteriol 188: 1089-1102

Zavaleta-Pastor M, Sohlenkamp C, Gao JL, Guan Z, Zaheer R, Finan TM, Raetz CR, Lopez-Lara IM, Geiger O (2010) Sinorhizobium meliloti phospholipase C required for lipid remodeling during phosphorus limitation. Proc Natl Acad Sci U S A 107: 302-307

Zhang G, Ahmad MZ, Chen B, Manan S, Zhang Y, Jin H, Wang X, Zhao J (2020) Lipidomic and transcriptomic profiling of developing nodules reveals the essential roles of active glycolysis and fatty acid and membrane lipid biosynthesis in soybean nodulation. Plant J 103: 1351-1371

Zhao M, Wang T, Sun T, Yu X, Tian R, Zhang WH (2020) Identification of tissue-specific and cold-responsive lncRNAs in Medicago truncatula by high-throughput RNA sequencing. BMC Plant Biol 20: 99

Zheng L, Huang F, Narsai R, Wu J, Giraud E, He F, Cheng L, Wang F, Wu P, Whelan J, Shou H (2009) Physiological and transcriptome analysis of iron and phosphorus interaction in rice seedlings. Plant Physiol 151: 262-274

Zhou P, Silverstein KA, Ramaraj T, Guhlin J, Denny R, Liu J, Farmer AD, Steele KP, Stupar RM, Miller JR, Tiffin P, Mudge J, Young ND (2017) Exploring structural variation and gene family architecture with De Novo assemblies of 15 Medicago genomes. BMC Genomics 18: 261

Zhu QH, Stephen S, Taylor J, Helliwell CA, Wang MB (2014) Long noncoding RNAs responsive to Fusarium oxysporum infection in Arabidopsis thaliana. New Phytol 201: 574-584

Zoeller M, Stingl N, Krischke M, Fekete A, Waller F, Berger S, Mueller MJ (2012) Lipid profiling of the Arabidopsis hypersensitive response reveals specific lipid peroxidation and fragmentation processes: biogenesis of pimelic and azelaic acid. Plant Physiol 160: 365-378